

**Sedimentology and Stratigraphy of deep-water
reservoirs in the 9A to 14A Sequences of the
central Bredasdorp Basin, offshore South Africa**

By

Alain-Cédrique MEGNER-ALLOGO



Thesis presented in partial fulfillment of the requirements for the degree of

Master of Science

at the University of Stellenbosch,

South Africa

Study leader: **Dr. H. de V. Wickens**

December 2006

DECLARATION

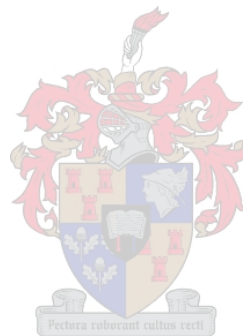
I, the undersigned, hereby declare that the work contained in this thesis is my own original work and has not previously in its entirety or in part been submitted at any other university for a degree or examination. Where use was made of the work of others it has been acknowledged in the text.



23/11/2006

Alain Cédrique MEGNER ALLOGO

Date



ABSTRACT

The Barremian to Albian siliciclastic deep-water deposits of the central Bredasdorp Basin were investigated primarily in terms of their stratigraphic evolution, depositional characteristics and facies distribution. Cores from the deep-water deposits reveal that the facies successions are composed of massive, ripple cross- to parallel-laminated sandstones, conglomerate, massive claystone, alternating laminated to interbedded sandstone/siltstone and claystone, laminated and clay-rich siltstone. These facies are grouped into channel-fill, sheet-lobe, overbank and basin plain deposits, by inference.

The application of sequence stratigraphy, based on gamma ray and resistivity log patterns, reveals that all 3rd-order depositional sequences comprise 4th-order cycles. The latter are subdivided into three components (lowstand, transgressive and highstand systems tracts), based on vertical facies changes and internal stratigraphic key surfaces.

Taking the 13Amfs as the stratigraphic datum for each well, correlation was possible on a regional basis. Lowstand deposits, comprising thick amalgamated massive sandstones, were interpreted to represent channel-fills. Their vertical and horizontal stacking forms channel-fill complexes above Type 1 unconformities. Adjacent thin-bedded intervals, comprising parallel- to ripple cross-laminated sandstones, were interpreted as levee/overbank deposits, whereas clay-rich intervals were interpreted to represent basin plain deposits of hemipelagic origin.

Facies associations and their distribution have revealed that channel-fills are associated with overflow deposits and sheet sand units. These deposits, as well as downdip sheet sands associated with small channel-fills within the 9A, 11A/12A, 13A Sequences and the 14A Sequence were interpreted to have been deposited in a middle fan to upper fan setting. A similar association occurs in the 10A Sequence, except that thick conglomerate units are present at the base of proximal channel-fills. This led to interpret the 10A Sequence as being deposited in a base-of-slope to upper fan setting.

The thickness of each sequence, as revealed by isochore maps, shows sinuous axial flow path which corresponds to channel-fill conduit. The continuous decrease of this sinuosity upward in the succession was interpreted as being related to basin floor control along the main sand fairways. Successive flows result in erosion-fill-spill processes, which locally favour connectivity of reservoirs over large areas.

Recognition of higher-order sequences and key stratigraphic surfaces helps to understand internal stratigraphic relationships and reveals a complex and dynamic depositional history for 3rd-order sequences. However, sparse well control and uneven distribution of boreholes, as well as lack of seismic and other data, limited the models derived for this study.

UITTREKSEL

Die Barremiaanse tot Albiaanse silisiklastiese diepwater afsettings van die sentrale Bredasdorp Kom is hoofsaaklik in terme van stratigrafiese evolusie, afsettingskarakteristieke en fasies distribusie ondersoek. Kerne van die diepwater afsettings toon dat die fasies opeenvolgings uit massiewe, riffelkruis- tot parallel-gelamineerde sandstene, konglomerate, massiewe kleistene, afwisselende gelamineerde tot intergelaagde sandstene/slikstene en kleistene, sowel as gelamineerde en klei-ryke sliksstene bestaan. Hierdie fasies word onderverdeel in kanaalopvulsel, plaatlob, oewerwal en komvlakke afsettings.

Die toepassing van opeenvolgingsstratigrafie gebaseer op gammastraal en resistiwiteit log patrone toon dat alle 3^{de}-orde afsettingsopeenvolgings uit 4^{de}-orde siklusse bestaan. Laasgenoemde word onderverdeel in drie komponente (lae-stand, transgressie en hoë-stand sisteemgedeeltes), gebaseer op vertikale fasies veranderinge en interne stratigrafiese sleutel vlakke.

Korrelasie op 'n regionale basis is moontlik gemaak deur die 13Amfs as die stratigrafiese verwysing vir elke boorgat te neem. Lae-stand afsettings, wat uit dik saamgevoegde massiewe sandstene bestaan, word geïnterpreteer as kanaalopvulsels. Die vertikale en horisontale stapeling van die sandstene vorm kanaalopvulsel komplekse bo Tipe 1 diskordansies. Naasliggende dun-gelaagde intervalle, wat uit parallel- tot kruisgelaagde sandstene bestaan, word geïnterpreteer as oewerwal afsettings, terwyl klei-ryke intervalle

geïnterpreteer word as verteenwoordigend van komvlakte afsettings van hemipelagiese oorsprong.

Fasies assosiasies en hul verspreiding toon dat kanaalvul geassosieër word met oorfloei afsettings en plaatsand eenhede. Hierdie afsettings, sowel as distale plaatsande geassosieër met klein kanaalopvulsels binne die 9A, 11A/12A, 13A en die 14A Opeenvolgings, word geïnterpreteer as afgeset in 'n middelwaaier tot bo-waaier omgewing. 'n Soortgelyke assosiasie bestaan in die 10A Opeenvolging, behalwe dat dik konglomeraat eenhede teenwoordig is by die basis van proksimale kanaalopvullings. Dit het gelei tot die interpretasie van die 10A Opeenvolging as afgeset in 'n basis-van-helling tot bo-waaier omgewing.

Die dikte van elke opeenvolging, soos verkry vanaf isochoor kaarte, toon 'n kronkelende aksiale vloepad wat ooreenkom met 'n kanaalopvulling toevoerkanaal. Die aaneenlopende afname van hierdie kronkeling na bo in die opeenvolging word geïnterpreteer as verwant aan komvloer-beheer langs die hoof sand roetes. Opeenvolgende vloei veroorsaak erosie-opvul-oorspoel prosesse, wat lokaal die konektiwiteit van reservoirs oor groot areas bevoordeel.

Herkenning van hoër-orde opeenvolgings en sleutel stratigrafiese vlakke dra by tot 'n goeie begrip van die interne stratigrafiese verhoudings en ontbloot 'n komplekse en dinamiese afsettingsgeskiedenis vir 3^{de}-orde opeenvolgings. Beperkte boorgatbeheer en 'n tekort aan seismiese en ander data het egter 'n beperkende rol gespeel in die daarstel van modelle vir hierdie studie.

ACKNOWLEDGEMENTS

Firstly, I would like to thank my Heavenly Father, without whom none of this work would be possible.

I wish to express my deepest gratitude to my supervisor Dr. H. de V. Wickens for his patience, assistance, and guidance throughout this study. I thank him, most of all, for giving me the opportunity to do this research via his close relationship with PetroSA and the Petroleum Agency of South Africa (PASA); also for his support during my various communications with the *Bourses et Stages* of Gabon.

My sincere thanks are due to the Gabonese government for funding this study and allowing me to complete it, despite the delay in the schedule. Special thanks to Dr. Guillaume Moutou (Managing Director of the *Bourses et Stages*) for his comprehension and indulgence.

I would like to thank Mr. Jean Malan (Project Manager, Western Africa, PetroSA) for giving permission to access the data at PetroSA and facilitating access to cores at PASA. I thank him also for his availability and continued support during this study. Very special thanks and gratitude to Mr. Jeff Aldrich (Chief Geologist, PetroSA) for his fruitful contribution to this study, indefinable availability and precious advices during the study. Thanks to all staff members of PetroSA and PASA who helped me directly and indirectly throughout my studies.

I would like to thank also Dr. R. Van den Berg for the translation of my Abstract in Afrikaans. I can not forget to thank my colleagues at the Department of Geology for their kindness and support.

Special thanks also to my fellow Gabonese students in Stellenbosch for their encouragement and support. I give my heart felt thanks to N. NDEMBI BOUANGA MAMBUNDU, Dr. B. NYANGONE ASSAM, D. NKOGHE OBAME, B.S. EWOUBA-BITEGHE, G.M. EKWA-EBANEGA, L.S. SOAMI and my colleague O.P. NGUEMA MVE and T. BAHISSY-MOUSSOUAMI for the very supportive role they have played during my study in Stellenbosch.

I am particularly grateful to my parents, i.e. my mother Blanche-Marie ASSENGONE NNANG, my father Michel ONGONE-ONDO, Aunties ANGUEZOME NNANG Pauline, Marie-Claire MENGUE M'OBIANG and G n vieve OBONE-OBIANG, Uncles Simplicie OBIANG-EYI, C lestin NANG-OBIANG and Jean-Jacques OBAME-OBIANG, for their unending love, support and advice. Thank you for your trust in me.

Lastly, I thank all other people that I did not name here but who have contributed to some extent to the completion of this thesis.

DEDICATION

I dedicate this work to my grandmother, **Jeanne NSEGUE MENGUE**, the corner stone of my family, who has never failed to encourage and motivate her progeny whenever there were difficulties.

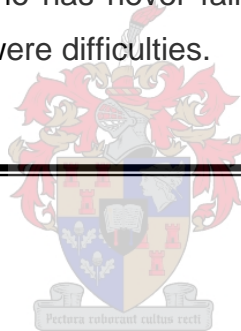


TABLE OF CONTENTS

DECLARATION.....	i
ABSTRACT	ii
UITTREKSEL	iv
ACKNOWLEDGEMENTS	vi
DEDICATION.....	viii
TABLE OF CONTENTS	ix
LIST OF FIGURES	xiii
LIST OF TABLES.....	xxiv

Chapter 1	Introduction	1
1.1	General	1
1.2	Previous work	6
1.3	Aims and objectives	7
1.4	Methodology	8
1.4.1	Database	8
1.4.2	Nomenclature	11
1.4.3	Data analysis	14
Chapter 2	Geological Setting	20
2.1	Introduction	20
2.2	Pre-Outeniqua Basin	20
2.2.1	Cape Fold Belt (CFB)	20
2.2.2	Break-up of Gondwana	22
2.3	Bredasdorp Basin	23



2.3.1	Structural geology	23
2.3.2	Stratigraphy	26
2.3.2.1	Syn-rift succession	26
2.3.2.2	Drift succession	29
Chapter 3	Brief review of deep-water deposits	31
3.1	Introduction	31
3.2	Characteristics of sediment gravity flows	32
3.2.1	Grain flows	32
3.2.2	Fluidized flows	34
3.2.3	Debris flows	34
3.2.4	Turbidity currents	34
3.3	Models for turbidity current deposits	35
3.3.1	Origin of turbidity currents	35
3.3.2	Morphology and models of turbidite deposits	35
3.4	Submarine fan models	40
Chapter 4	Facies and Facies Associations	46
4.1	Introduction	46
4.2	Sedimentary facies	48
4.2.1	Facies A: Massive sandstone	48
4.2.2	Facies B: Ripple cross-laminated sandstone	54
4.2.3	Facies C: Parallel-laminated sandstone	56
4.2.4	Facies D: Conglomerates	59
4.2.5	Facies E: Massive claystone	63

4.2.6	Facies F: Alternating laminated to interbedded sandstone/siltstone and claystone	66
4.2.7	Facies G: Laminated siltstone	69
4.2.8	Facies H: Clay-rich siltstone	72
4.3	Facies associations and depositional elements	73
Chapter 5	Application of sequence stratigraphy	81
5.1	Introduction	81
5.2	Sea-level and accommodation	82
5.3	Types of sequences and hierarchy within sequences	84
5.4	Key surfaces	87
5.4.1	Sequence boundaries	87
5.4.2	Transgressive surfaces	92
5.4.3	Maximum flooding surfaces	95
5.5	Systems tracts	95
5.5.1	Lowstand systems tract	96
5.5.2	Transgressive systems tract	97
5.5.3	Highstand systems tract	97
Chapter 6	Stratigraphy and sedimentology	98
6.1	Introduction	98
6.2	Correlation criteria	98
6.3	Stratigraphic evolution of sequences	103
6.3.1	9A Sequence	109
6.3.2	10A Sequence	114
6.3.3	11A/12A Sequence	118

6.3.4	13A Sequence	120
6.3.5	14A Sequence (lower sandstone unit)	124
6.4	Depositional architecture	130
6.5	Influence of basin floor topography on deposition	133
Chapter 7	Depositional model	137
7.1	Depositional model for sequences	137
7.2	Prediction of reservoir distribution and development	142
7.2.1	Characteristics of channel-fill reservoirs	142
7.2.2	Characteristics of interchannel reservoirs	143
7.2.3	Connectivity of reservoirs	144
Chapter 8	Conclusions	145
References		149
Appendix	Whole core photographs and their stratigraphic positions in the wells.	165



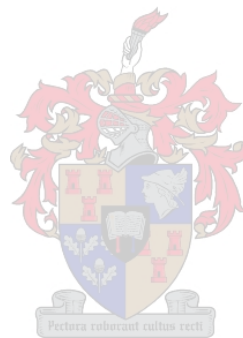
LIST OF FIGURES

CHAPTER 1

Figure	Page
<p>Figure 1.1 Seafloor depths and land topography of southern Africa. The continental margin, on which the Outeniqua Basin lies, is off the south coast of South Africa. The Agulhas-Falkland Fracture Zone forms the southern limit of the continental margin. Locality map in Figure 1.2 is indicated by the dotted line (National Geophysical Data Centre, [www.ngdc.noaa.gov/image/]).</p>	2
<p>Figure 1.2 Locality map of the Outeniqua Basin and onshore Mesozoic sedimentary basins in South Africa (from Van der Spuy, 2003).</p>	3
<p>Figure 1.3 Locality map showing the Bredasdorp Basin and adjacent basins, including the Southern Outeniqua Basin to the south of them. The study area (red dashed line) and borders of Block 9 are indicated (from Burden and Davies, 1997b).</p>	5
<p>Figure 1.4 Study area and locations of the investigated boreholes (from Burden and Davies, 1997b).</p>	9
<p>Figure 1.5 Summary of sequence nomenclature and chronostratigraphy of the drift succession in the Bredasdorp Basin (from Brown et al., 1995).</p>	15
<p>Figure 1.6 Legend of symbols used in core analysis.</p>	16
<p>Figure 1.7 Outline of the methodology used in this investigation.</p>	19

CHAPTER 2

Figure	Page
Figure 2.1 Detailed map showing the major structural elements of the Bredasdorp Basin. These structural elements roughly follow the regional WNW-ESE structural trend of the Swartberg Branch (after McLachlan and McMillan, 1976; McMillan et al., 1997).	24
Figure 2.2 Schematic cross-sections across the Bredasdorp Basin. Section A-A', Section B-B' and Section C-C' represents respectively an oblique section, dip section and strike section of the basin (from Thomson, 1998).	25
Figure 2.3 Stratigraphic chart of the Bredasdorp Basin (from Burden, 1992).	27



CHAPTER 3

Figure	Page
Figure 3.1 Diagram illustrating the sedimentary characteristics of the four types of gravity flows (from Middleton and Hampton, 1976).	33
Figure 3.2 Ideal Bouma Sequence showing the sedimentary features of the different divisions of turbidity current deposits (from Shanmugam, 1997).	37
Figure 3.3 Different models of turbidites. (A) Coarse-grained turbidites (Lowe, 1982), (B) Classic turbidites (Bouma, 1962), and (C) Fined-grained turbidites (Stow and Shanmugam, 1980).	38
Figure 3.4 Model of modern sand-rich submarine fan system (from Normark, 1970).	41

Figure 3.5 Illustration of the three distinct intervals along a submarine fan system and respective facies succession within each interval (from Mutti and Ricci Lucchi, 1972). **43**

Figure 3.6 Depositional models for single-sourced submarine fans, (A) mud-rich system, and (B) mixed sand/mud-rich system (from Reading and Richards, 1994). **44**

CHAPTER 4

Figure	Page
Figure 4.1 Virtual sedimentary log representing the sedimentary facies observed.	47
Figure 4.2a Illustration of massive sandstone facies. It displays various primary and secondary sedimentary structures such as bioturbation, fluid escape features, clay laminae and clay clasts.	49
Figure 4.2b Illustration of massive sandstone facies. Loading structures occur associated with clay intervals. Clay clasts are seen above possible amalgamated surfaces.	50
Figure 4.3 Illustration of ripple cross-laminated sandstone facies. Faint parallel laminations are associated with ripple laminations. Note that the facies shares sharp bounding surfaces with the alternating laminated to interbedded sandstone/siltstone and claystone facies.	55
Figure 4.4 Illustration of parallel-laminated sandstones with secondary structures such as bioturbation, water escape features and distortions.	58
Figure 4.5a Illustration of polymictic conglomerate facies with sandy matrix. Conglomerate show organized and disorganized	

structures form left to right. Note that the thicker conglomerate unit displays an upward-fining pattern. 60

Figure 4.5b Illustration of polymictic conglomerate facies, with a silty matrix showing soft-sediment deformation. The facies shares sharp irregular contacts with the parallel- to ripple cross-laminated sandstone. 62

Figure 4.6 Illustration of massive claystone facies. Note the blocky appearance of this facies. 65

Figure 4.7a Illustration of alternating laminated to interbedded sandstone/siltstone and claystone facies. Beds appear slightly parallel to wavy and display a rhythmic alternation. 67

Figure 4.7b Illustration of alternating laminated to interbedded sandstone/siltstone and claystone facies. Rhythmic alternation of beds is remarkable. Irregular contact surfaces as well as internal convolute laminations are frequent. Burrows are also present. 68

Figure 4.8 Example of laminated siltstone facies and clay-rich siltstone facies. (A) Clay-rich siltstone with no apparent structures. (B) Clay-rich siltstone unit is overlain by laminated siltstone unit displaying overturned bed at the base. This overturning feature results probably from small-scale slumping. (C) Dipping beds within laminated siltstone unit with reactivated surface (dotted line). (D) Interbedding of clay-rich siltstone and laminated siltstone. The dotted line indicates the sharp boundaries between the two facies. Note the presence of small-scale slump in the upper laminated siltstone. (E) Dipping laminations within laminated siltstone facies. (F) Clay-rich siltstone displaying micro normal faults. 70

Figure 4.9 Example of stacked channel-fill deposits. Cliff section is 35 m. Ongeluks River channel-fills comprise massive sandstone units, Fan 3, Tanqua subbasin. Note multiple erosional surfaces. 75

Figure 4.10 Example of overbank deposits. Thin, ripple-cross laminated sandstone beds of Fan 3, Tanqua subbasin. Note extreme lateral continuity of beds. **77**

Figure 4.11 Example of sheet deposits. A) Fan A of the Laingsburg Fan Complex, Karoo Basin, Grootkloof, Laingsburg. B) Fan 3, Tanqua Fan Complex, Karoo Basin. **79**

Figure 4.12 Example of basin plain deposits representing interfan unit between Fans 3 and 4, Tanqua subbasin, and comprising finely laminated shale. Note overlying sandstone beds. **80**

CHAPTER 5

Figure **Page**

Figure 5.1 Difference between eustatic sea level and relative sea level. The datum is an imaginary, reference horizon taken just beneath the sea floor to monitor the magnitude of vertical tectonics relative to the centre of the earth (Catuneanu, 2002). **83**

Figure 5.2 Hierarchical organization of turbidites by sub-dividing a turbidite fan sequence into a turbidite complex, system, stage and sub-stages based on physical scale of deposits (from Mutti and Normark, 1987). **86**

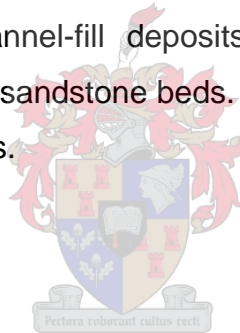
Figure 5.3 The idealised stratigraphy in a basin coupled with a relative sea-level curve. Position of systems tracts and key surfaces are given on the curve. The LST is recognised by erosional surfaces. Deposition of TST and HST is concentrated on the shelf and is represented in the deep basin within a condensed section (from Sixsmith, 2000). **89**

Figure 5.4 Application of sequence stratigraphy on well E-BE1, supported by core interpretation. Stratigraphic key surfaces,

respective systems tracts and possible sedimentological interpretation of the intervals between these surfaces are given. Boundaries with solid lines are low-order (3rd-order) boundaries whereas dashed lines are high-order (4th-order) boundaries. **90**

Figure 5.5 Example of stratigraphic key surfaces and respective systems tracts in wells E-CA1 and E-AA1, supported by a sedimentological interpretation of the intervals between these surfaces. Third-order sequence boundaries (unconformities) are in solid lines whereas fourth-order stratigraphic surfaces are in dashed lines. **91**

Figure 5.6 Example of two distinct surfaces, named here lower and upper surfaces within the lowstand deposits. The upper surface separates the lower deposits which are interpreted as a by-pass package underlying the channel-fill deposits. By-pass deposits consist of siltstone with minor sandstone beds. Channel-fill deposits consist of massive sandstones. **93**



CHAPTER 6

Figure	Page
---------------	-------------

Figure 6.1 Well locations and correlation sections over the study area. S1, S2, S3 and S4 indicate sections 1-4, respectively.	99
---	-----------

Figure 6.2 Depositional elements and generalized log response of channel/lobe complex. (A) Bounding upper slope slump and cohesive debris flow deposits. (B) Erosional channel-fill of sandy to muddy debris flow. (C) Amalgamated channel-fill. (D) Interbedded levee deposits. (E) Overbank deposits, muddy interchannel mud flow, fine-grained turbidites. (F) Channel/lobe transition. (G) Stacked turbidites of the proximal lobe. (H) Interbedded turbidite of	
---	--

the middle lobe. (l) Basin plain deposits (after Galloway and Hobday, 1996). **101**

Figure 6.3 Typical vertical facies associations and log responses for deep-water deposits. Note that similar facies associations can occur in more than one environment. Each log segment may range from tens to a few hundred meters (after Galloway and Hobday, 1996). **102**

Figure 6.4 Cross-section 1 is orientated NW-SE and is approximately parallel to the depositional profile. Its location is shown on the inset map. Note that highstand deposits consist frequently of thick amalgamated sands interpreted to represent channel-fill complexes. Their direct correlation is not obvious between the major stratigraphic unconformities. **104**

Figure 6.5 Cross-section 2, orientated NW-SE, is approximately parallel to the depositional profile. Its location is shown on the inset map. **105**

Figure 6.6 Cross-section 3, oriented North-South, is normal to the depositional profile. Its location of the correlation section is shown on the inset map on the inset map. **106**

Figure 6.7 Cross-section 4, orientated North-South, is normal to the depositional profile. Its location of the correlation section is shown on the inset map. **107**

Figure 6.8 Isochron map of the 9A to 13A Sequence. Investigated wells and the 280 ms contour line, which is used for guidance of the general depositional trend, are outlined in red (unpublished map from PetroSA, Turner, 2006). **108**

Figure 6.9 Isochore map of the 9A Sequence based on drilled thickness of the sequence in each well. Contours reflect the interpretation of the thickness variation. Colours are assigned to

contour intervals for a better illustration of thickness variation. The axial area indicates the main route followed by density flow currents. The sinuous pattern suggests topographic influence on routing of flows and therefore on deposition. **111**

Figure 6.10 Net-sand interval map of the 9A Sequence. Contours reflect the interpretation of net-sand thickness. Colours are assigned to contour intervals for a better illustration of thickness variation. Corresponding GR logs of the interval is given. The net-sand displays a sinuous pattern fairly parallel to the axial part of the corresponding 9A isochore map. **112**

Figure 6.11 Schematic illustration of facies in the 9A Sequence. Contours reflect a great deal of interpretation of facies distribution. The main channel-fill facies follows a fairly straight fairway. Secondary channel-fills seem to be present within overflow areas which could be interpreted as crevasse splays. **113**

Figure 6.12 Isochore map of the 10A Sequence based on drilled thickness of the sequence in each well. Contours reflect the interpretation of the thickness variation. Colours are assigned to contour intervals for a better illustration of thickness variation. Deposition defines a sinuous trend that may suggest a topographic influence on routing of flows and therefore on deposition. The distribution of wells does not allow prediction of the axial area to the west. **115**

Figure 6.13 Net-sand map of the 10A Sequence. Contours reflect the interpretation of net-sand. Colours are assigned to contour intervals for a better illustration of thickness variation. Corresponding GR logs of the interval is given. The sand trend displays a sinuous channel axis with minor off-axis deposition. **116**

Figure 6.14 Schematic illustration of facies in the 10A Sequence. Contours reflect a great deal of interpretation of facies distribution. The channel-fill trend may be more complex than illustrated. It

displays a sinuous pattern that suggests compensation for topography during deposition. Secondary channel-fills intersecting the main channel to the north-western part may suggest a subordinate source for sediment gravity flows. Crevasse splays predominantly comprise sheet sands.

117

Figure 6.15 Schematic illustration of different elements within the 10A Sequence and their possible location on a submarine fan. A) Slope channel complexes erode deeply into underlying deposits and are associated with overbank deposits, which consist of sheet sands and possible small-scale channel-fills. B) Aggradational channel complexes are confined to a broad conduit and are associated with overbank deposits, sometimes well preserved between the channels. C) Distal sands of this sequence are predominantly sheet-like but comprise some channel-fills. Note that scale was not applied to any illustration.

119

Figure 6.16 Isochore map of the 11A / 12A Sequence based on drilled thickness of the sequence in each well. Contours reflect the interpretation of the thickness variation. Colours are assigned to contour intervals for a better illustration of thickness variation. Thickness of the sequence seems to increase toward the north and shows a less pronounced sinuous trend in contrast to older sequences.

121

Figure 6.17 Net-sand map of the 11A / 12A Sequence. Contours reflect the interpretation of drilled net-sand. Colours are assigned to contour intervals for a better illustration of thickness variation. Corresponding GR log of the interval is given. Channel-like patterns display a fairly straight pattern.

122

Figure 6.18 Schematic illustration of facies in the 11A / 12A Sequence. Contours reflect the interpretation of facies distribution. Channel-fills are small but are complex in the sequence. They appear fairly straight compared to the lower sequences.

123

Figure 6.19 Isochore map of the 13A Sequence based on drilled thickness of the sequence in each well. Contours reflect the interpretation of the thickness variation. Colours are assigned to contour intervals for a better illustration of thickness variation. The sequence is more extensive compared to the older sequences. A sinuous trend is still observable. The axial area seems to present a southeast orientation, which is different from the underlying sequences. **125**

Figure 6.20 Net-sand map of the 13A Sequence. Contours reflect the interpretation of net-sand thickness. Colours are assigned to contour intervals for a better illustration of thickness variation. Corresponding GR logs of the interval is given. In places, net-sand displays a sinuous pattern trending in a west-east direction. **126**

Figure 6.21 Schematic illustration of facies in the 13A Sequence. Contours reflect the interpretation of facies distribution. Deposits intersected in the valley are massive amalgamated sandstones. Overflow deposits seem not to be present. **127**

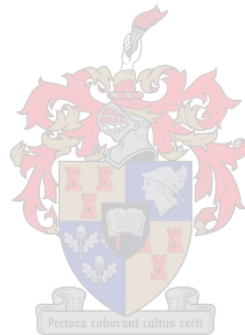
Figure 6.22 Net-sand interval map of the 14A sand. Contours reflect the interpretation of the net-sand drilled thickness. Colours are assigned to contour intervals for a better illustration of thickness variation. Corresponding GR logs of the interval is given. Distribution of sand suggests two distinct conduits, with less sinuosity compared to the underlying sequences. The pattern of net-sand in the conduit suggests that E-CR1 and E-AJ1 intersected the marginal part of the conduit. The axial part of this conduit may trend as shown by the dotted yellow line. **129**

Figure 6.23 Schematic diagrams of the main channel types observed in the Tanqua depocentre (from Johnson et al., 2001) **131**

Figure 6.24 Schematic diagrams of two contrasting types of turbidity flow confinement. A) Subtle-topography control and B) Erosion control (from Grecula, 2000). **136**

CHAPTER 7

Figure 7.1 Schematic illustration of sequence evolution. Only the proximal and distal wells are indicated on illustrations. See text for explanations.

139

List of Tables

CHAPTER 1

Table	Page
<p>Table 1.1 Borehole co-ordinates and various depths involved during drilling. Kelly Bushing (KB) refers to the vertical distance from the rotary table or Kelly bushing device on rigs to sea level. Water depth refers to the distance between sea surface and sea floor. Total drilling depth indicates the distance from Kelly Bushing to the bottom of the well. Cores (C) are pieces of rock formation collected from drilling. Core depths are in meter below KB.</p>	10
<p>Table 1.2 Primary and secondary reservoirs targeted in each borehole. Well logs available in targeted intervals are gamma ray (GR), sonic (S), density (D), resistivity (R), spontaneous potential (SP), caliper (C), multi-spherical focused log (MSFL), lateral log deep (LLD), lateral log medium (LLM), lateral log shallow (LLS). The last three are resistivity logs as applied to three sets of resistivity reading in the formation, away from the borehole wall.</p>	12

CHAPTER 5

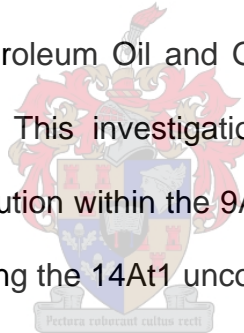
Table	Page
<p>Table 5.1 Depth, in meter, of major unconformities in the investigated wells. Value with (*) are locations of unconformities proposed in this investigation, after further analysis of well logs.</p>	88

CHAPTER 1

INTRODUCTION

1.1 General

This project investigates the Barremian to Albian deep-water sandstone deposits of the central Bredasdorp Basin located offshore the south coast of South Africa, where the best hydrocarbon accumulations were found on the South African south coast so far. The project forms part of the ongoing deep-water exploration research programme of the Petroleum Oil and Gas Corporation of South Africa (Pty) Ltd., known as PetroSA. This investigation focuses on the depositional characteristics and facies distribution within the 9A and 14A Sequences, including the sand-rich succession overlying the 14At1 unconformity.



The Bredasdorp Basin is one of five sub-basins, which together with Pletmos (20 000 km²), Gamtoos (3 000 km²), Algoa (4 000 km²) and the Southern Outeniqua (22 000 km²) constitute the large Outeniqua Basin that developed along the south coast of South Africa, in response to rift tectonics during the break-up of Gondwana (Figs. 1.1 and 1.2). Figure 1.1 gives an indication of the seafloor depths and land elevations of southern Africa and highlights the limits of the continental margin on which the Outeniqua Basin lies. Figure 1.2 illustrates the exact extension of the Outeniqua Basin, but gives the location of the onshore Mesozoic basins in South Africa. The Bredasdorp Basin, filled with Jurassic and

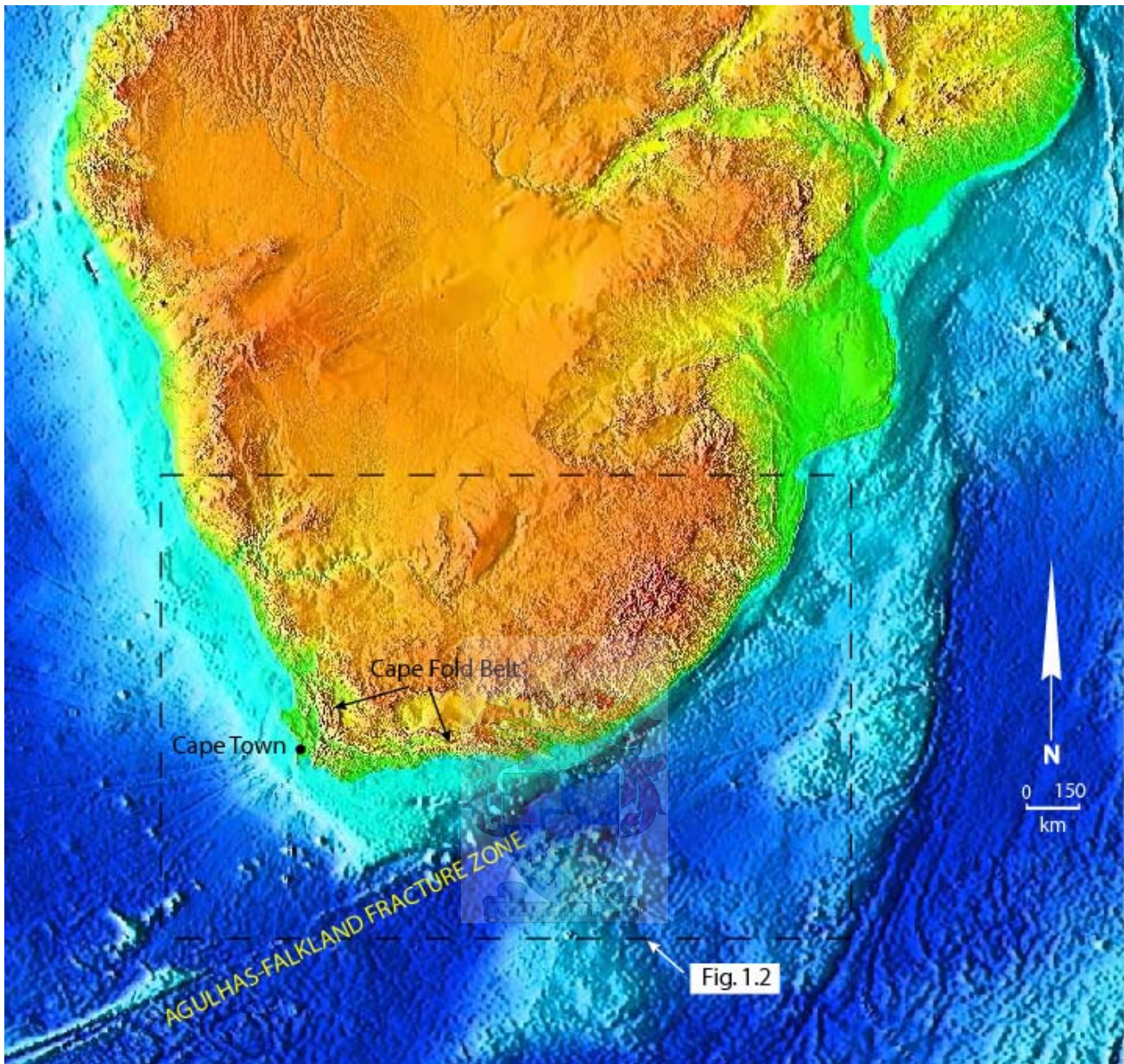


Figure 1.1 Seafloor depths and land topography of southern Africa. The continental margin, on which the Outeuqua Basin lies, is off the south coast of South Africa. The Agulhas-Falkland Fracture Zone forms the southern limit of the continental margin. Locality map in Figure 1.2 is indicated by the dotted line (from National Geophysical Data Centre, [www.ngdc.noaa.gov/image/]).

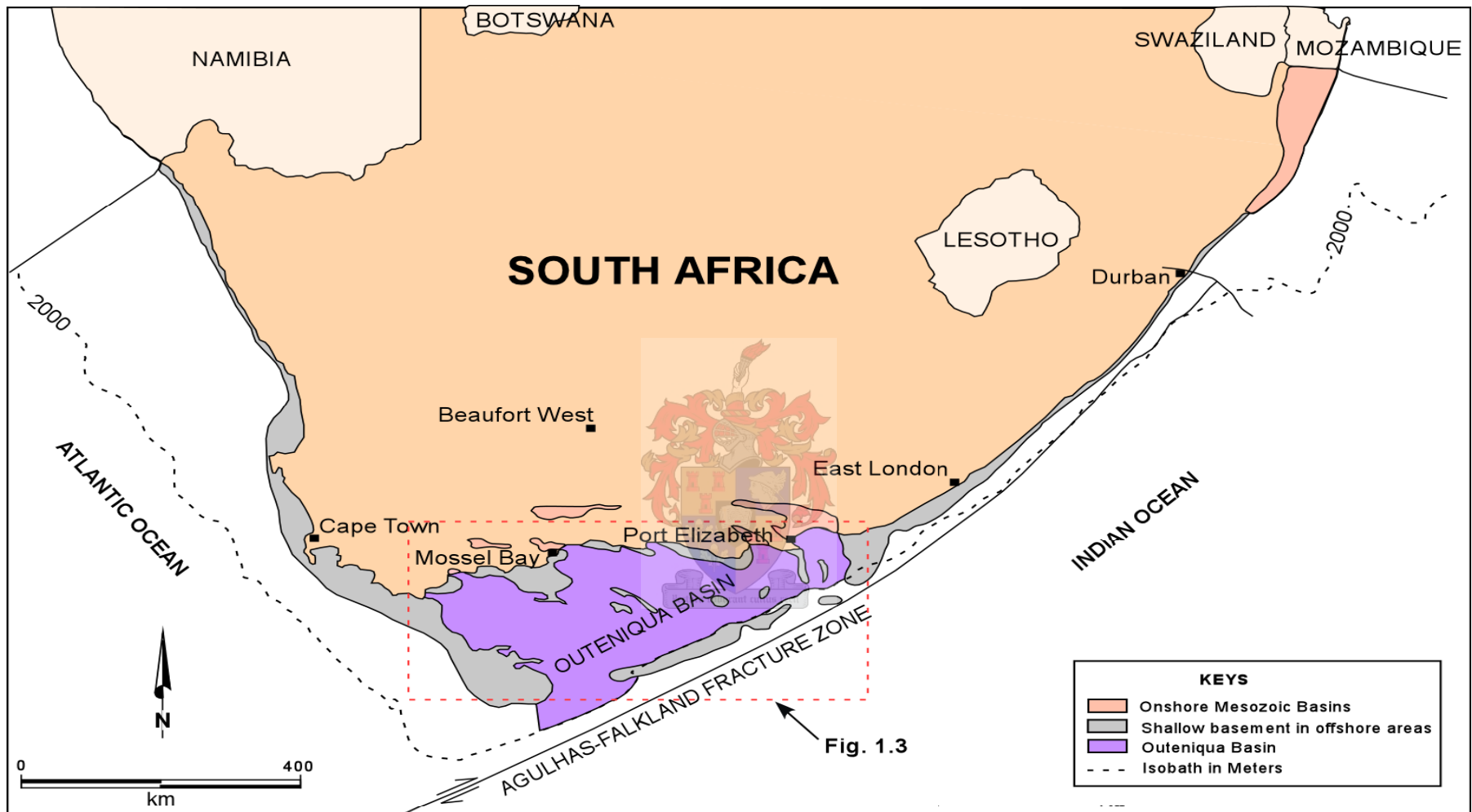


Figure 1.2 Locality map of the Outeniqua Basin and onshore Mesozoic sedimentary basins in South Africa (from Van der Spuy, 2003).

Cretaceous continental and marine sediments, covers an area of about 15 000 km² which is approximately 100 km long and 150 km wide (Davies, 1997).

Geographically, the Bredasdorp Basin is bounded on the western and southwestern side by the Columbine-Agulhas Arch and on the northeastern side by the Infanta Arch. The latter physically separates the Bredasdorp Basin from the Pletmos Basin (Fig. 1.3). Geologically, the tectono-sedimentary history of the Bredasdorp Basin can be traced back to the Permo-Triassic Cape Orogeny. Most of the structural features of the basin, i.e. faults, horst and grabens, display a strong parallelism with the regional structural trend of the Swartberg Branch of the Cape Fold Belt (CFB) (Dingle *et al.* 1983).

The area of investigation is located in the southeast central part of the Bredasdorp Basin, between 35°00'S - 35°30'S and 21°30'E - 22°00'E. It is situated southwest of Mossel Bay on the Agulhas Bank, i.e. approximately 80-120 km offshore, in a water depth ranging between 100 m and 120 m. Block 9, which is 23 000km² in size, is the offshore exploration license block that covers most of the Bredasdorp Basin (Fig.1.3).

Hydrocarbon exploration started in South Africa in 1965 when Soekor (Pty.) Ltd., the State Petroleum Company and predecessor to PetroSA, began to explore the onshore Permian Karoo Basin and the Mesozoic Algoa Basin. Exploration was extended to the offshore in 1973, particularly in the Bredasdorp Basin where the first exploration well, F-1, was drilled. This well is located on the northern flank of the basin and targeted shallow marine sandstones of synrift origin, just below the

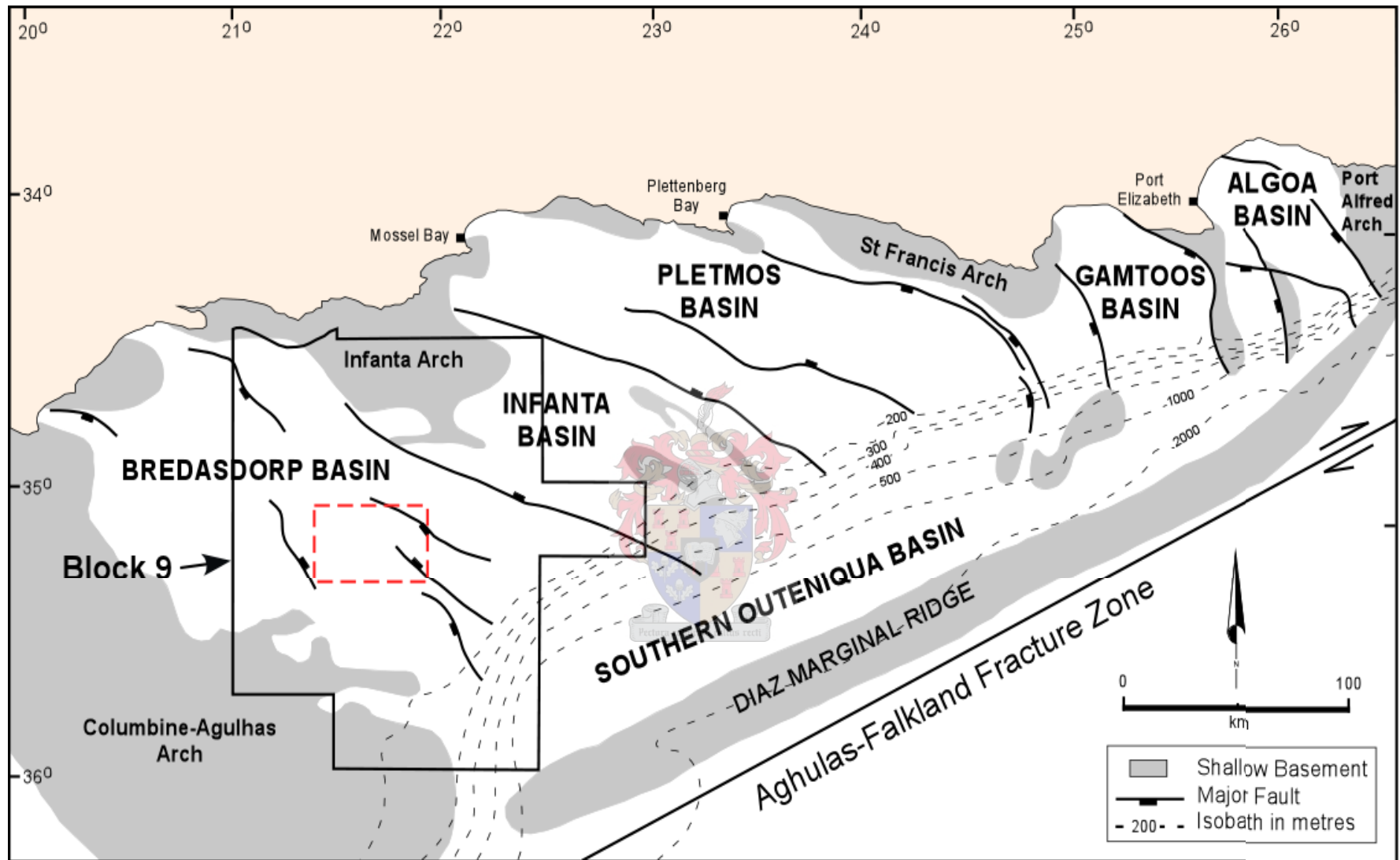
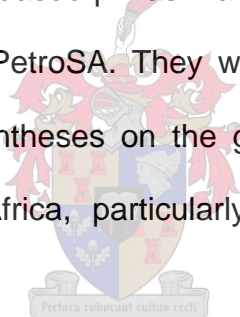


Figure 1.3 Locality map showing the Bredasdorp Basin and adjacent basins, including the Southern Outeniqua Basin. The study area (red dashed line) and borders of Block 9 are indicated (from Burden and Davies, 1997b).

drift onset unconformity (Brown *et al.*, 1995). Reservoirs were however, of poor quality due to secondary porosity (Burden, 1992). Extensive local studies that flowed from the ongoing exploration program led to the discoveries of oil and gas accumulations in Block 9 in the Bredasdorp Basin, e.g. the F-A and E-M gas fields, and the Oribi, Sable and Oryx oil fields. The latter discoveries shifted the interest to the deep-water stratigraphic successions of the drift succession of the basin.

1.2 Previous work

Most studies related to the Bredasdorp Basin are in the form of internal reports which remain the property of PetroSA. They were not made available for this study. To date, only a few syntheses on the geology and stratigraphy of the southern offshore of South Africa, particularly the Bredasdorp Basin, were published.



The work of Dingle *et al.* (1983) gives a good relationship between the current morphology of southern Africa and the complex tectonic regime that developed in southern Gondwana, including the CFB and later the breakup between South America and Africa. Dingle *et al.* (1983) observed that the offshore basins along the east coast of South Africa were formed as a result of the shearing movement between the two continents and that the overall offshore basin geometry was influenced by the Cape Orogeny. They also describe the stratigraphy of the Bredasdorp Basin. Burden (1992) summarizes this stratigraphy and emphasizes the hydrocarbon potential of individual sequences.

Burden and Davies (1997a) interpreted the 14A sand unit as channelized deposits comprising three distinct sub-units, which are a lower siltstone unit, a middle massive amalgamated sandstone unit interpreted as fan-lobe deposits and an upper interbedded sandstone and claystone unit interpreted as abandonment channel-fill deposits.

Brown *et al.* (1995) and McMillan *et al.* (1997) discuss the stratigraphy of the Mesozoic sedimentary basins along the south coast of South Africa. Their description of the offshore stratigraphy provides insight on the occurrence of good reservoirs in the drift succession, particularly between the 1A and 14A Sequences.

Albeit an extensive exploration program in the basin, and particularly in the central area, there are still uncertainties concerning sandstone fairways and distribution of facies.



1.3 Aims and Objectives

The primary aim of this investigation is to develop a better understanding of the stratigraphy and sedimentology of the turbidite succession in the central Bredasdorp Basin in the 9A to 14A Sequences, including the 14A sand-rich succession overlying the 14At1 unconformity.

The main objectives of this study are to:

- identify and describe all the sedimentary facies present that characterise the deep-water deposits in the study area.

- identify and interpret the depositional processes responsible for the origin of these facies.
- place the identified facies and facies assemblages into a high-resolution sequence stratigraphic framework by defining key surfaces and systems tracts.
- document the development, distribution, and vertical and horizontal relationship of channelized and non-channelized depositional elements.
- construct a working model for the emplacement of sand in the central Bredasdorp Basin, based on sedimentary features such as primary sedimentary structures, key surfaces, facies and facies assemblages, stacking patterns, facies distribution and stratigraphy.

1.4 Methodology

1.4.1 Database



To date more than 150 wells have been drilled in the Bredasdorp Basin of which only eighteen boreholes are available for this investigation. The location map of the investigated boreholes is given in Figure 1.4. Additional information regarding location and depth of these wells is given in Table 1.1. Data available from these wells include a suite of geophysical logs, drilling reports, geological well completion reports, coregraphs, composite logs, sidewall core descriptions and conventional cores. PetroSA provided all the paper-based data.

Nineteen slabbed and lapped cores with a cumulative length of 285.9 m were

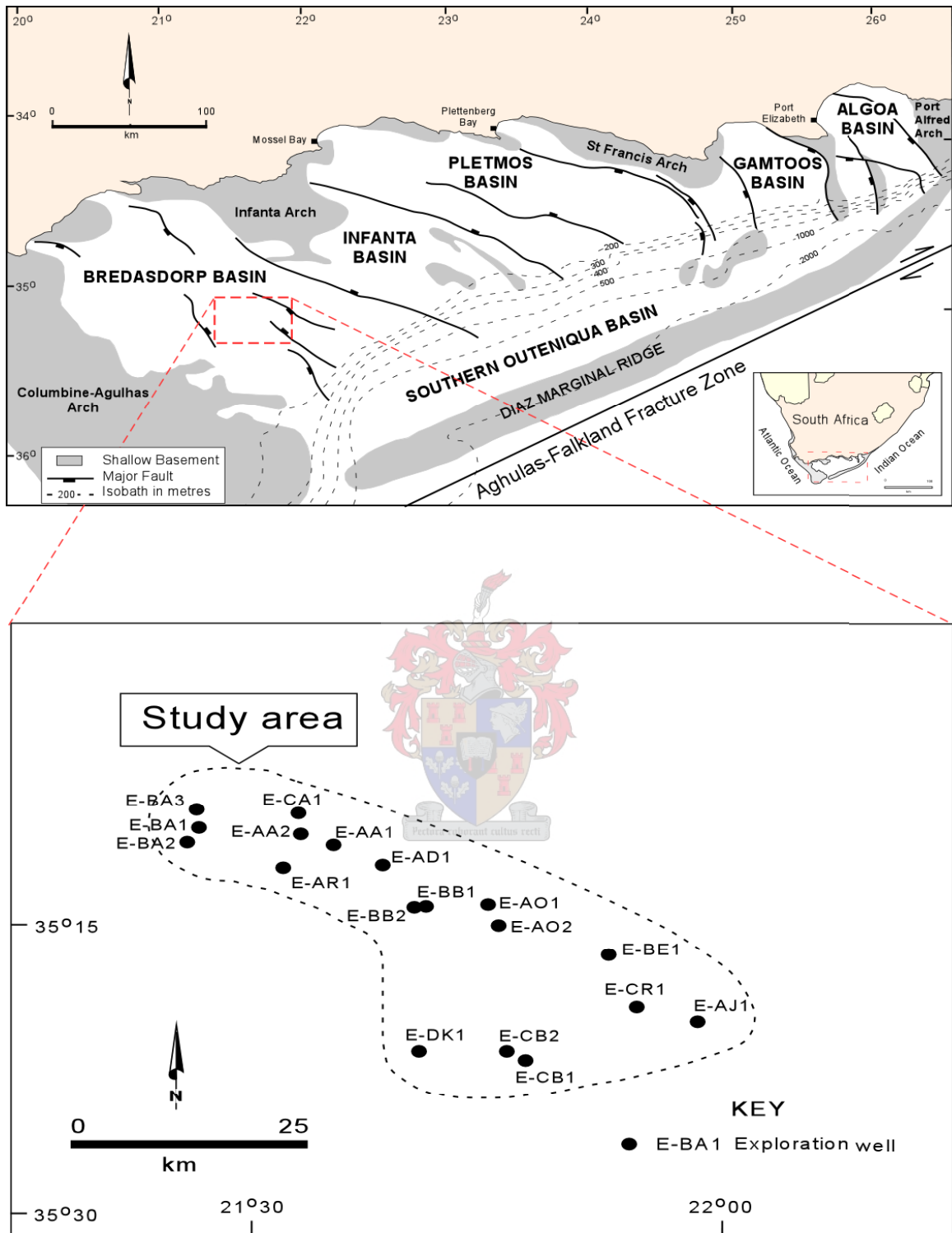


Figure 1.4 Study area and locations of the investigated wells (from Burden and Davies, 1997b).

Wells	E-AA1	E-AA2	E-AD1	E-AJ1	E-AO1	E-AO2	E-AR1	E-BA1
Co-ordinates	Lat. 35°11'8.8"S Long. 21°35'36.18"E	Lat. 35°10'23.78"S Long. 21°33'32.73"E	Lat. 35°11'59.08"S Long. 21°38'58.25"E	Lat. 35°20'09.15"S Long. 21°58'37.45"E	Lat. 35°14'15.66"S Long. 21°45'41.89"E	Lat. 35°15'12.77"S Long. 21°46'27.53"E	Lat. 35°12'13.67"S Long. 21°32'41.86"E	Lat. 35°09'29.67"S Long. 21°28'31.19"E
KB to sea level (m)	26	22	26	26	26	26	22	22
Water depth (m)	121	120	123	142	124	129	120	115
Total drilling depth (m)	3920	3117	3862	3490	3350	3183	3455	3130
Cores described	C1 (2509-2524 m) C4 (3060.5-3072 m)	C4 (3013-3031 m)	C1 (2500-2513.5 m) C6 (2945-2959 m)	C4 (3037-3043 m)	C2 (3000-3018 m)	C2 (2928-2935 m)	C1 (2455-2473.5 m)	C2 (2828-2848 m)

Wells	E-BA2	E-BA3	E-BB1	E-BE1	E-CA1	E-CB1	E-CB2	E-CR1	E-DK1
Co-ordinates	Lat. 35°10'00.19"S Long. 21°27'36.97"E	Lat. 35°08'34.05"S Long. 21°28'50.22"E	Lat. 35°14'51.32"S Long. 21°41'41.088"E	Lat. 35°16'45.34"S Long. 21°53'11.83"E	Lat. 35°09'20.09"S Long. 21°33'34.96"E	Lat. 35°22'25.16"S Long. 21°47'55.99"E	Lat. 35°21'53.25"S Long. 21°46'47.38"E	Lat. 35°19'25.00"S Long. 21°54'54.00"E	Lat. 35°21'55.45"S Long. 21°41'59.82"E
KB to sea level (m)	22	22	22	25	22	22	22.5	22	25
Water depth (m)	114	112	122	126	120	135	133	140	130
Total drilling depth (m)	2950	3023	3320	3050	3288	3100	2793	2825	2620.5
Cores described	C1 (2755-2783 m) C2 (2783-2789 m)	C1 (2871-2884 m)	C2 (2537.5-2556.42 m)	C2 (3026-3038.5 m)	C1 (2784-2802 m) C5 (2949-2961 m)	No core described	C1 (2498-2515.98 m)	C1 (2674-2691.5 m)	No core described

Table 1.1 Well co-ordinates and various depths involved during drilling. Kelly Bushing (KB) refers to the vertical distance from the rotary table or Kelly bushing device on rigs to sea level. Water depth refers to the distance between sea surface and sea floor. Total drilling depth indicates the distance from Kelly Bushing to the bottom of the well. Cores (C) are pieces of rock formation collected from drilling. Core depths are in meter below KB.

made available by PASA.

From the geological well completion reports, it appears that all investigated boreholes targeted specific reservoir intervals (Table 1.2). The 14A reservoirs generally constitute the primary target of most boreholes.

1.4.2 Nomenclature

The sequence stratigraphic nomenclature used in this investigation respects the original nomenclature developed for the Outeniqua Basin by geoscientists from PetroSA. The sequence stratigraphic framework outlined in Brown *et al.* (1995), shows that the Bredasdorp Basin can be subdivided into seventeen depositional sequences separated by regionally extensive Type 1 unconformities. These depositional sequences are referred to as third-order sequences (Brown *et al.*, 1995). A Type1 unconformity is defined as a surface that exhibits subaerial exposure or submarine erosion that forms as a result of rapid fall of sea level (Vail, 1987; Van Wagoner *et al.*, 1990). Depositional sequences of the Bredasdorp Basin were named following an alphanumerical nomenclature. Thus, the seventeen sequences were called sequences 1 to 17, from the oldest to the youngest, respectively. Capital alphabetical letters (A-E) were subsequently assigned to sub-sequences within these third-order sequences. As a result, 1A designates, for example, the first third-order sequence within the first third-order

Table 1.2 Primary and secondary reservoirs targeted in each well. Well logs available in targeted intervals are gamma ray (GR), sonic (S), density (D), resistivity (R), spontaneous potential (SP), caliper (C), multi-spherical focused log (MSFL), lateral log deep (LLD), lateral log medium (LLM), lateral log shallow (LLS). The last three are resistivity logs as applied to three sets of resistivity reading in the formation, away from the borehole wall.

Wells	E-AA1	E-AA2	E-AD1	E-AJ1	E-AO1	E-AO2	E-AR1	E-BA1	E-BA2
Year of drilling	1987	1995	1988	1989	1988	1990	1988	1990	1992
Primary target (sandstones)	5A to 13A	14A	14A	9A to 10A	14A	14A	14A and 9A to 13A	14A	10A
Secondary target (sandstones)	1A to 5A	10A	All sandstones below 13Amfs	Above 15At1 and below 9At1	13A	13A	below 9At1	9A	9A
Well logs	SP, GR, LLD, MSFL, D	GR, LLD, S, MSFL, D, C	GR, SP, LLD, LLM, MSFL, D	GR, SP, LLD, LLS, LLM, D	GR, SP, LLD, MSFL, D, S, C	GR, LLD, LLS, S, C	SP, GR, LLD, MSFL, D	GR, C, MSFL, LLD, LLS, S	GR, LLD, LLS, S, D, C

Table 1.2 (continued)

Wells	E-BA3	E-BB1	E-BE1	E-CA1	E-CB1	E-CB2	E-CR1	E-DK1
Year of drilling	1994	1991	1991	1993	1993	1995	1995	1998
Primary target (sandstones)	10A	9A to 14A	14A	10A	14A	14A	14A	14A
Secondary target (sandstones)	9A	6A and some 9A	9A to 13A	14A	Not	Not	Not	Not
Well logs	GR, LLD, LLS, S, D, C	GR, LLD, S, LLS	GR, LLD, S	GR, LLD, LLS S, D, C		GR, LLD, S, D, LLS, C	GR, LLD, S, D, LLS, C	

sequence-set, of which the basal unconformity is 1At1. Similarly, 13B is the second third-order sequence of the thirteenth third-order sequence set, of which its basal unconformity is 13At1. Figure 1.5 provides a detailed sequence nomenclature chart for the Bredasdorp Basin.

1.4.3 Data analysis

Methods used in this investigation aim to provide a high-resolution characterisation of the stratigraphy and sedimentology of the central Bredasdorp Basin.

The sedimentological analysis primarily involved identification, description and interpretation of sedimentary facies and facies associations from cores. The latter were visually described as objectively as possible, focusing on grain-size, bed thickness trends, bed contacts and sedimentary structures, both primary and secondary. Sedimentary structures were particularly useful for identifying changes in sedimentary style, depositional trends, and possible sequence boundaries. Sedimentary structures also reveal useful information concerning depositional and diagenetic events in the rocks. Figure 1.6 presents the symbols used for core analysis.

Colour assisted to differentiate between the major rock types, i.e. claystone, sandstone and siltstone. Claystones are generally dark grey to black in colour, whereas sandstones and siltstones are usually light grey. It is assumed that change of colour during aerial exposure of cores have had a minor effect on the overall

Standard chronostratigraphy	Age of unconformity (Ma)	Chronostratigraphy and sequence stratigraphy of the drift succession of the Bredasdorp Basin	
		Sequence / Set	
		Type	No
66.5			
MAASTRICHIAN			
74			
CAMPANIAN	-77.5 ----- 18At1	3rd-order seq. set	17B 17A
84	-80 ----- 17At1		
SANTONIAN		3rd-order	16C
88		3rd-order	16B
CONIACIAN		3rd-order	16A
89	-90 ----- 16At1		
TURONIAN			
92	-93 ----- 15At1	3rd-order	15A
CENOMANIAN		3rd-order seq. set	14H
96			
ALBIAN		3rd-order	14B
	-103 ----- 14At1	3rd-order	14A
108			
APTIAN		3rd-order?	13B
	-112 ----- 13At1	3rd-order	13A
113			12B 12A
BARREMIAN		3rd-order seq. and 4th-order paraseq. sets	11 9-10 7-8
	-113.5 ----- 11At1		
	-115 ----- 9At1		
	-116 ----- 7At1		
116.5	-117.5 ----- 6At1	3rd-order seq.	6
HAUTERIVIAN		3rd-order seq. and 4th-order paraseq. sets	5 4 3
	-118.5 ----- 5At1		
	-119.5 ----- 4At1		
121	-120.5 ----- 3At1		2
VALANGINIAN		3rd-order composite seq.	1
	-121.5 ----- 2At1		
	-126 ----- 1At1		
		RIFT-DRIFT UNCONFORMITY	

Figure 1.5 Summary of sequence nomenclature and chronostratigraphy of the drift succession in the Bredasdorp Basin (from Brown *et al.*, 1995).

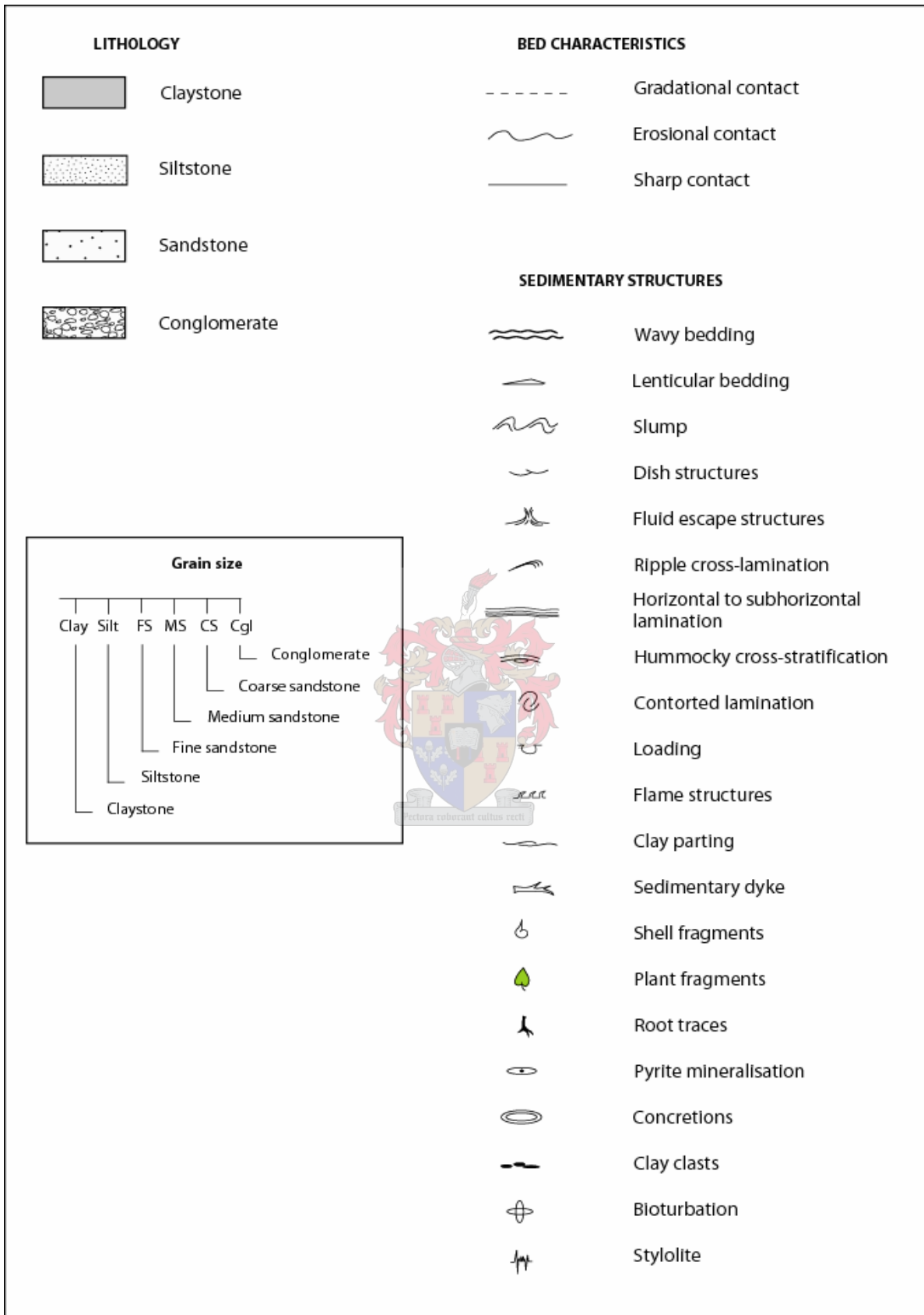


Figure 1.6 Legend of symbols used in core analysis.

colour of the rocks.

Thickness of beds was carefully recorded and described in the context of lithology and grain-size. It primarily reflects energy conditions during deposition.

Information was compiled in coregraphs that were integrated with gamma ray logs in order to define facies signatures. Except for single photographs of entire cores, contact surfaces and sedimentary structures were photographed where necessary for illustration. Sidewall core descriptions were also integrated with facies signatures displayed by geophysical logs in order to predict lithology within uncored intervals; the purpose being to have fair representation of facies distribution in the investigated interval.

A stratigraphic analysis was done by mainly using conventional well logs, such as gamma ray, resistivity and sonic logs. Paper copies of these well logs were digitized for computer manipulation. Methods outlined by Van Wagoner *et al.* (1990), and explained by Tearpock and Bischke (2003) were used for identification of stratigraphic surfaces on well logs. Additionally, methods of identification of key surfaces in outcrop from Sixsmith (2000) and Van der Merwe (2005) have also been considered.

A first step in stratigraphic analysis consists of choosing a regionally developed stratigraphic marker horizon. Previous work on Bredasdorp Basin stratigraphy suggests that the interval overlying the 13At1 unconformity comprises organic-rich claystones distinguished by high gamma ray (Brown *et al.*, 1995, and McMillan *et al.*, 1997). It is assumed that the 13A maximum flooding surface

(13Amfs), which is present on all well logs, was a topographically fairly flat surface during deposition of the 13A Sequence. This motivated the pick of this surface as the stratigraphic datum for the investigated succession. The 13Amfs was commonly fixed, in the previous work, where the gamma ray log presents very high values (about 75-130 API), and the resistivity log presents very low values (about 4-6 Ohms) directly above the 13At1 unconformity. By considering this surface as a stratigraphic datum for the investigated succession, it is assumed that the surface was a topographically fairly flat surface during the 13A Sequence. Van Wagoner *et al.* (1990), Danielsen *et al.* (1997) and Tye *et al.* (1999) picked their maximum flooding surfaces in the same way. Identification of stratigraphic surfaces and stacking patterns within sequences is also included in this first step.

A second step consists of identifying and correlating different key surfaces, such as flooding surface unconformities, and different vertical stacking patterns of sand-rich packages within sequences. These vertical stacking patterns define depositional cycles, which may be attributed to allocyclic sea level fluctuations.

Gamma ray logs were used to construct isochore, net-sand, and facies maps for creating models of deposition for the different sequences.

A flow chart showing steps of the methodology is presented in Figure 1.7

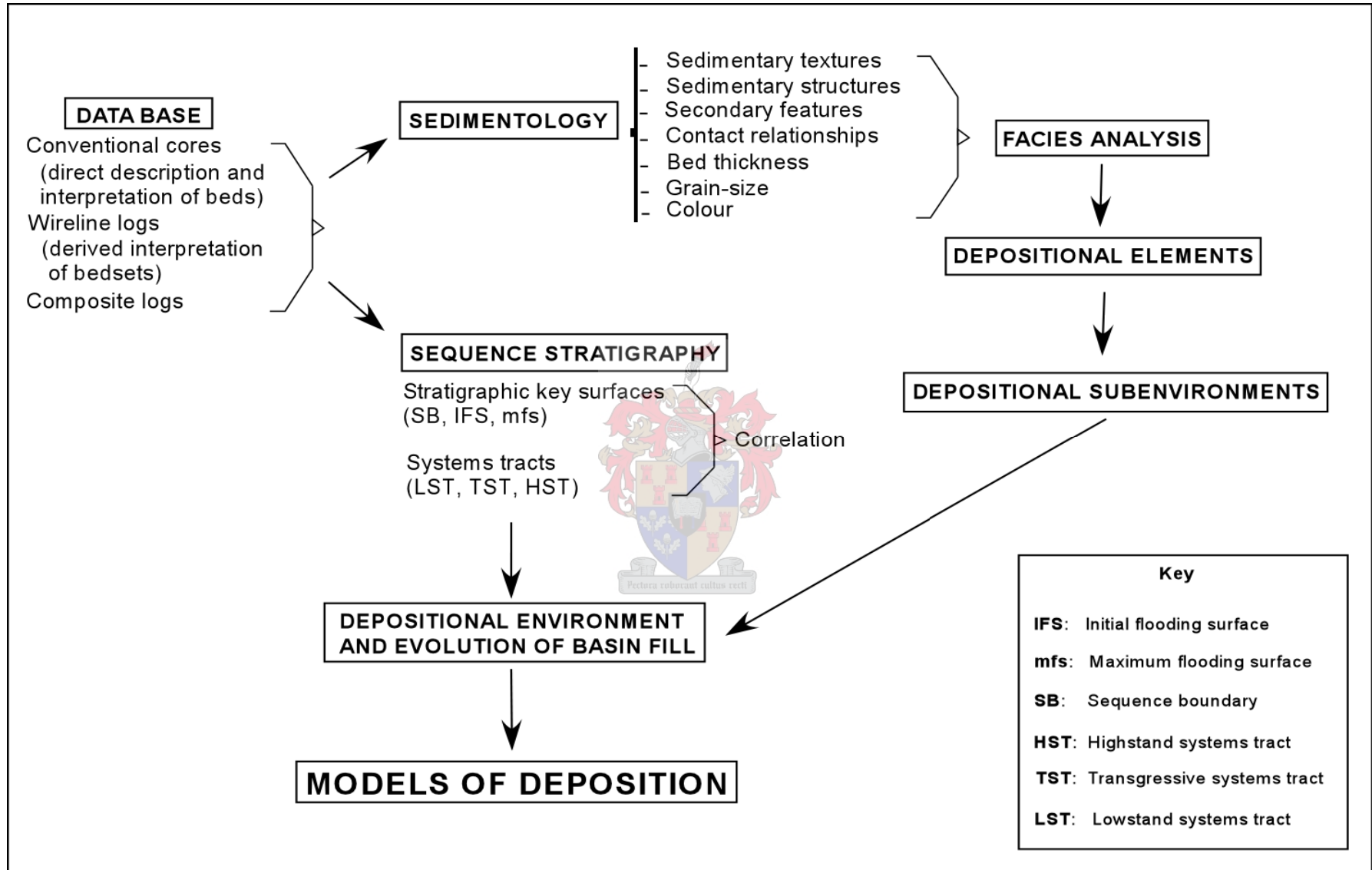


Figure 1.7 Outline of the methodology used in this investigation.

CHAPTER 2

GEOLOGICAL SETTING

2.1 Introduction

The continental margin off the south coast of South Africa developed during the Mesozoic, in response to the separation of the southern Africa and South America. This continental margin, a passive margin that underwent several rift phases during the break-up, forms the Outeniqua Basin and its sub-basins.

Structural trends of the Outeniqua Basin followed ancient weak zones created during thrust tectonics of the Permo-Triassic Cape Fold Belt. Detailed information concerning the regional geology of the Outeniqua Basin is given by Dingle *et al.* (1983), Brown *et al.* (1995) and McMillan *et al.* (1997). Only a brief summary of this work is given in this section, with emphasis on the influence of the tectonic events on the structural development and stratigraphy of the Bredasdorp Basin.

2.2 Pre-Outeniqua Basin

2.2.1 Cape Fold Belt (CFB)

The Permo-Triassic CFB is a low-pressure and low-temperature orogen, which formed part of the Gondwanide orogenic belt that affected South America, southern Africa, Antarctica and Australia. The CFB was a major the major pre-break-up event related to the subsequent formation of the

Outeniqua Basin off the south coast of South Africa. Dingle *et al.* (1983) pointed out that the Cape Orogeny developed when the Gondwana landmass started to override the Pacific Plate. Other researchers termed this plate movement Andean-type subduction of the Pacific Plate under the Gondwana Plate (Martini, 1974; Rhodes, 1974; De Wit and Ransome, 1992; Visser, 1995; Lock, 1980; Smellie, 1981; Johnson, 1991; Cole, 1992).

The CFB consists of two structural branches, namely the Cedarberg Branch and the Swartberg Branch. The Cedarberg or Western Branch trends northwest-southeast and constitutes gentle open folds, whereas the Swartberg or Southern Branch trends east-west and is intensely deformed with thrusting and overturned beds (Lock, 1978, Hälbich *et al.*, 1983). Both branches merge in the Ceres area to form the Cape Syntaxis with a southwest-northeast trend (Hälbich *et al.*, 1983; Johnston, 2000). The Swartberg Branch, which extends more than 600 km from the Cape Syntaxis to Port Elizabeth on the east coast, forms the bulk of the CFB (Johnston, 2000). This suggests that the major stress direction was oriented north-south.

The CFB affected mainly the Cape Supergroup and subordinately the Karoo Supergroup (Hälbich, 1992). The Cape Supergroup is a siliciclastic succession of sandstones and shales deposited to the south of the Kaapvaal Craton during the Late Palaeozoic. It is overlain by the Karoo Supergroup. The deformational trends of the Swartberg Branch are well defined onshore along the south and east coast of South Africa, but can also be followed off the south coast of South Africa where it forms the basement rocks of the younger offshore basins (De Beer, 1989).

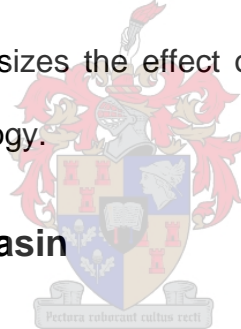
Dating of the orogen revealed five major paroxysmic events at 278 ± 2 Ma, 258 ± 2 Ma, 247 ± 3 Ma, 230 ± 3 Ma and 215 ± 5 Ma (Hälbich *et al.*, 1983). These different ages are interpreted as ages of deformation, likely related to episodic compression caused by subduction of the Pacific Plate under the Gondwana Plate. The 215 Ma age marks the cooling age of the CFB orogenesis (Hälbich *et al.*, 1983).

2.2.2 Break-up of Gondwana

Reconstruction of the Gondwana supercontinent shows that it constituted the present landmasses: South America, Africa, India, Madagascar, Australia, New Zealand and Antarctica (www.en.wikipedia.org/wiki/Gondwana). Although there are still uncertainties about the reasons that caused the sudden disintegration of Gondwana into smaller continental plates, the timing and evolution of break-up is however known. Break-up developed into four main extensional episodes. The initial rifting stage commenced in Early Jurassic (180 million years ago), with the separation of West Gondwana (South America and Africa) and East Gondwana (Antarctica, Australia, India and New Zealand). The second stage occurred in Early Cretaceous times (130 million year ago) when South America separated from the Africa-India plate, and the African-Indian plate from Antarctica. The third stage occurred during the Late Cretaceous times (90-100 million year ago), with the separation of Australia and New Zealand from the Antarctica, as well as separation of Madagascar and Seychelles from India. Break-up was completed in mid-Tertiary (25 million year ago), with the separation of the tip of the Antarctic Peninsula from South America (www.antarctica.ac.uk).

The continental margin, extending along the south coast and on which lies the Outeniqua Basin, formed as a result of the separation of South America, Africa and the Falkland Plateau (McMillan *et al.*, 1997; Liro and Dawson, 2000). The detachment followed ancient thrust faults of the CFB that were reactivated during Gondwana break-up. Normal faults present within the Cretaceous offshore basins represent these reactivated weak zones (Johnston, 2000). A remarkable feature of this rifting is the shear movement that developed along the Agulhas-Falkland Fracture Zone (AFFZ). This tectonic feature separated the great Falkland Plateau from the Outeniqua Basin. The perfect match of the structural trend between the Outeniqua Basin and the Falkland Islands, after a rotation of 180° of the latter (Marshall, 1994, and Johnston, 2000), emphasizes the effect of the AFFZ on the change of southern Gondwana morphology.

2.3 The Bredasdorp Basin



2.3.1 Structural geology

Prominent structural features of the Bredasdorp Basin are normal faults. The latter present a WNW-ESE trend inherited from the Swartberg Branch of the CFB (Figs. 2.1 and 2.2) (De Wit and Ransome, 1992; Davies, 1997, Johnston, 2000). These normal faults bound half-grabens and structural highs throughout the basin.

Most of the faults are confined to the rift sequence, but there are some that extend into the post-rift succession (Davies, 1997). Another group of faults displaying a NNW-SSE trend, identified by Ziegler and Cloetingh (2004), was

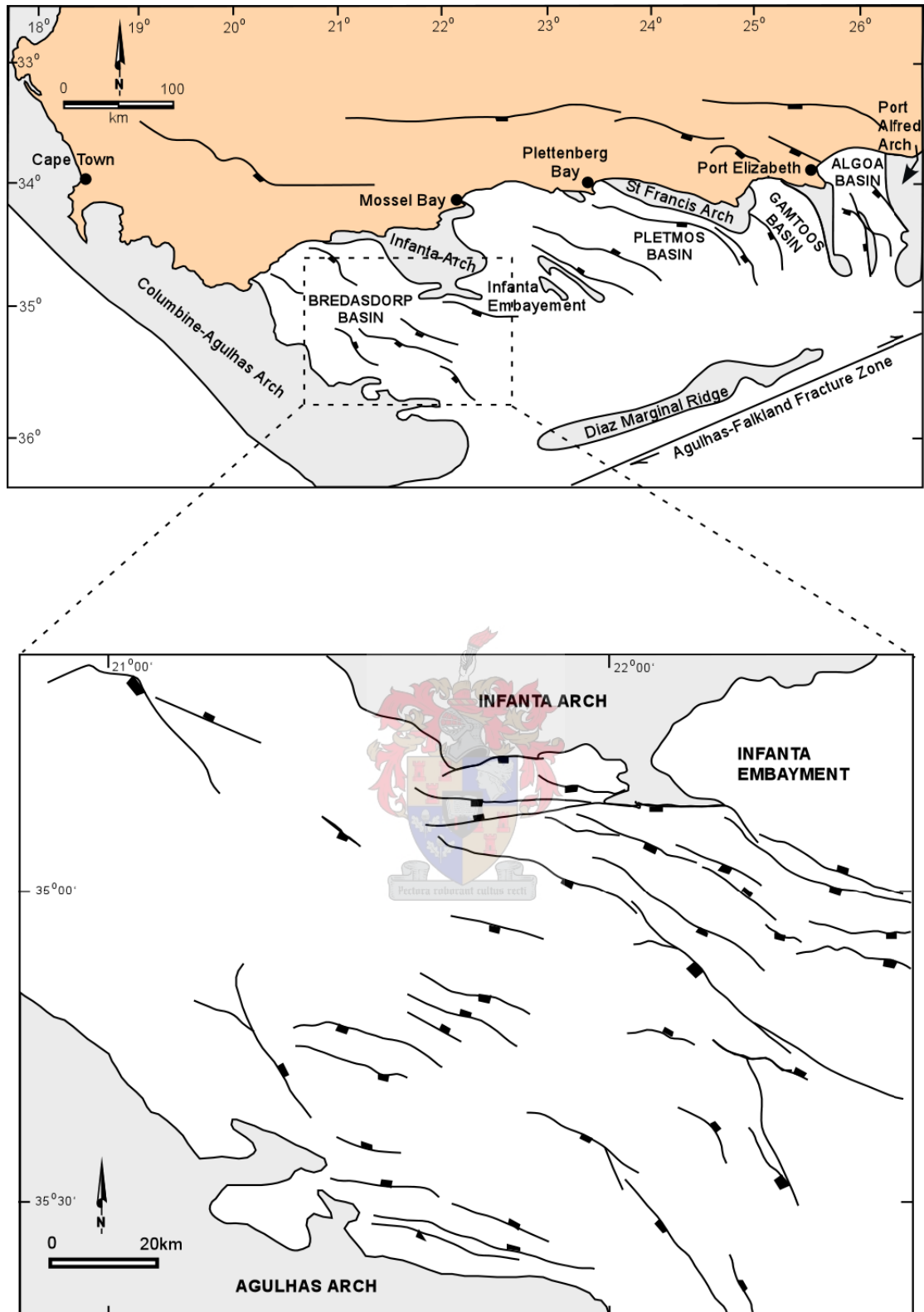


Figure 2.1 Detailed map showing the major structural elements of the Bredasdorp Basin. They roughly follow the regional WNW-ESE structural trend of the Swartberg Branch (after McLachlan and McMillan, 1976; McMillan *et al.*, 1997).

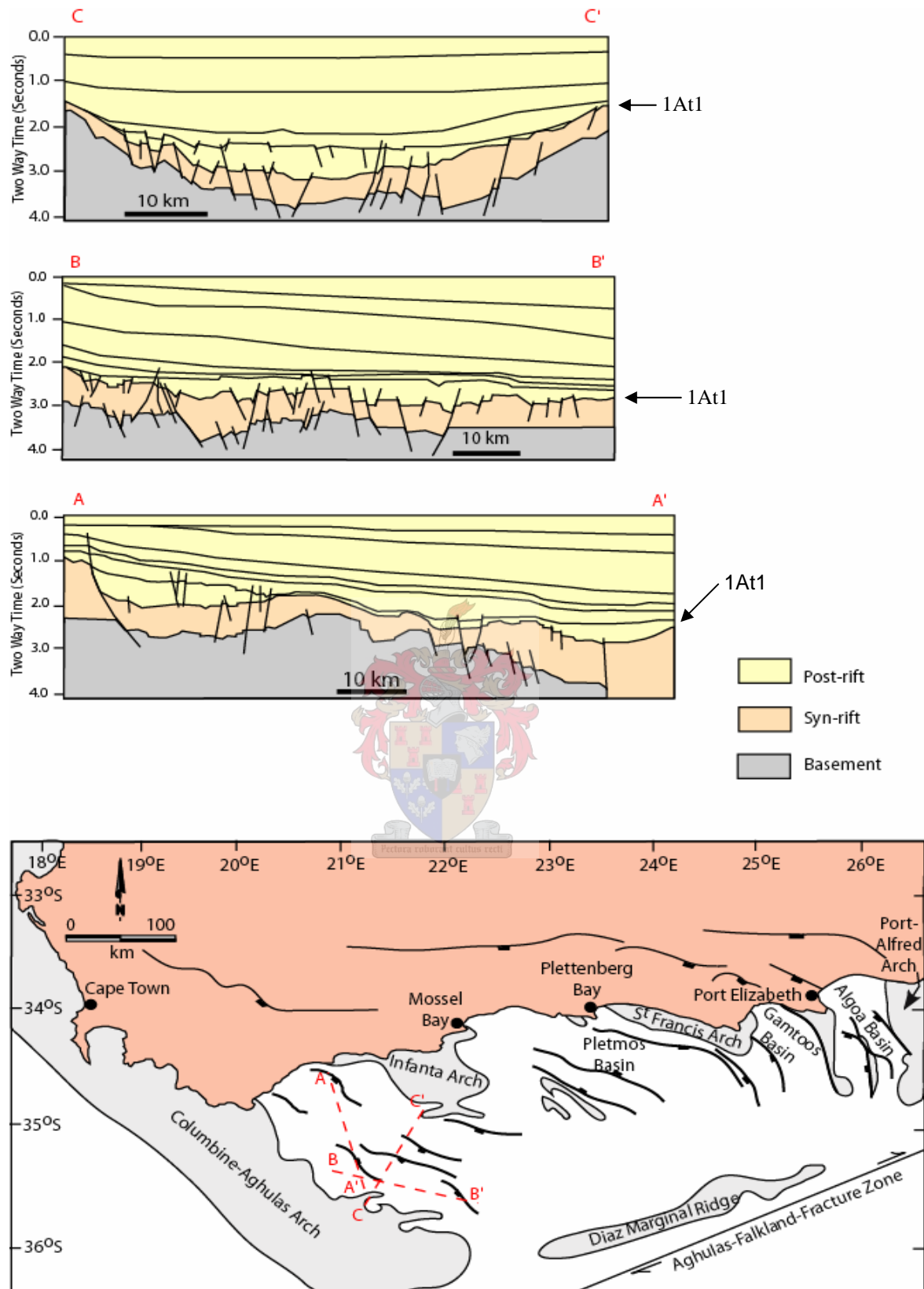


Figure 2.2 Schematic cross-sections across the Bredasdorp Basin. Section A-A', Section B-B' and Section C-C' represents respectively a dip section, oblique section and strike section of the basin (from Thomson, 1998).

ascribed to subsequent shear movement along the Agulhas-Falkland Fracture Zone to the south of the basin (Du Toit, 1976; Fouché *et al.*, 1992; Johnston, 2000).

2.3.2 Stratigraphy

The Outeniqua Basin-fill succession is divided into two major sequences namely a syn-rift sequence and a drift sequence, typical of passive margin settings. These two sequences are separated by a regionally developed unconformity called 1At1. Figure 2.3 present the stratigraphic chart of the sedimentary Bredasdorp Basin, which is detailed hereafter.

2.3.2.1 Syn-rift succession

This sequence is bounded by Horizon D and “1At1”, the rift-drift unconformity, at the base and top respectively and consists of Late Jurassic - Early Cretaceous-aged sediments that rest unconformably on faulted basement. These sediments, which filled half-grabens that developed as a result of extensional tectonics during initial rifting, comprise alluvial fan conglomerates, braided and meandering channel fluvial deposits that accumulated contemporaneously with faulting (Burden, 1992; McMillan *et al.*, 1997; Davies, 1997). Syn-rift sediments consist of continental clastic deposits eroded from orthoquartzites and slates of the Cape Supergroup and sandstones and shales of the Karoo Supergroup, which constituted the Cape Mountains at that time (McMillan *et al.*, 1997). These continental clastic sediments were intercalated with shallow marine sediments. McMillan *et al.* (1997) recognised

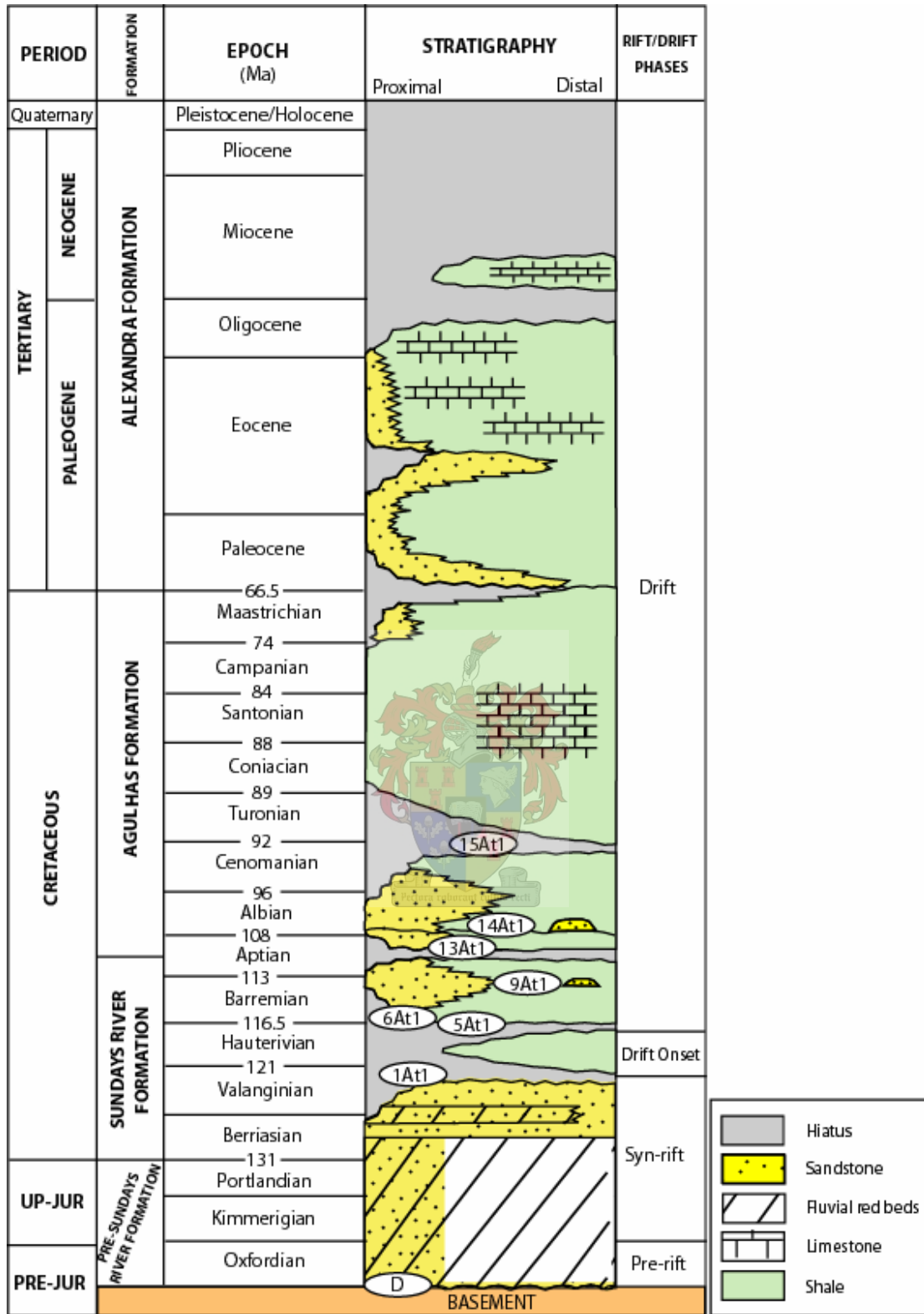


Figure 2.3 Stratigraphic chart of the Bredasdorp Basin (from Burden, 1992).

four distinct intervals in the rift sequence:

- i. a *lower fluvial interval* consisting of red and minor green argillite with subordinate reddish sandstones and rare conglomerates,
- ii. a *lower shallow marine* interval that resulted from the first marine incursion in the basin. It occurred at “Horizon V” and is marked by the appearance of glauconitic sandstones. These sandstones reflect tidally influenced shallow marine deposits.
- iii. an *upper fluvial* interval overlying marine sediments that consists of interbedded non-glauconitic sandstones, red and green claystones, and siltstones.
- iv. an *upper shallow marine* interval marked by the second appearance of glauconitic sandstones. The latter are rich in quartz grains and poor in lithics compared to the lower shallow marine sandstones. However, the upper shallow marine sandstones contain shell fragments similarly to the lower shallow marine sandstones.

The shallow marine sandstones constitute the reservoir rocks of the rift sequence. The F-A gas field exploits hydrocarbons from these reservoirs.

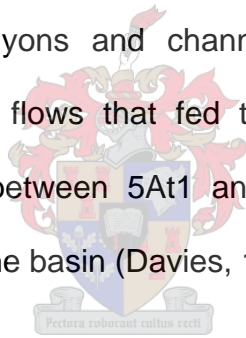
Rifting ceased at end Valanginian and was followed by a major marine transgression which resulted in the rift/drift unconformity (1At1).

2.3.2.2 Drift succession

Based on tectonic development and depositional history, McMillan *et al.* (1997) divided the drift sequence into two major intervals, namely a) transitional to early drift sequence and b) late drift sequence.

a. Transitional to early drift sequence (1At1-13At1)

The first sediments of this sequence rest directly on the rift/drift unconformity (1At1). Following the marine transgression, the increase in water depth resulted in a deep-water environment with a strong shelf progradation. The latter favoured the deposition of deep marine sediments subsequent to the formation of submarine canyons and channels. Both types of conduits provided routes for turbidity flows that fed the lowest part of the basin, particularly the succession between 5At1 and 13At1 (Barremian to Early Aptian) in the central part of the basin (Davies, 1997 and Burden, 1992).



Subsidence followed and marked a stable depositional environment in the Bredasdorp Basin, characterised by low sedimentation rates and a sediment starvation that favoured the deposition of organic-rich mud (Davies, 1997). The deposition of mud was particularly intermittent between 1At1 and 13At1.

b. Late drift sequence (13At1 to present)

During Early Aptian, a major marine regression took place that caused significant erosion in the Bredasdorp Basin resulting in the regional 13At1 unconformity. A major marine transgression followed and introduced severe low oxygen conditions, which favoured deposition of organic-rich mud,

particularly in the central and southern Bredasdorp Basin (McMillan *et al.*, 1997). These marine claystones form the best source rocks in the basin.

Renewed active turbidity deposition occurred intermittently during the earlier marine transgression and favoured the deposition of isolated high-order lowstand sandstones near the base of the 13A Sequence, but particularly within the 14A Sequence.

Another period of sediment starvation occurred after the 15At1 unconformity (Late Cenomanian). Organic-rich muds were deposited during this period, yet they remain too immature to generate hydrocarbons (McMillan *et al.*, 1997). In general, deposition that followed the 15At1 surface was controlled by the shelf progradation. Common sediments found in the succession are marine claystones, calcareous sandstones and limestones.



CHAPTER 3

BRIEF REVIEW OF DEEP-WATER DEPOSITS

3.1 Introduction

Deep-water deposits represent sediments transported by sediment gravity flow processes from the shelf and deposited on continental slope and basin floor as submarine fans. These gravity flow processes induce turbidity currents such as debris flows, slumps, liquefied or fluidized flows, initiated after a failure of equilibrium between shelfal and basinal sedimentation (Vail *et al.*, 1977; Mutti, 1985; Van Wagoner *et al.*, 1990).

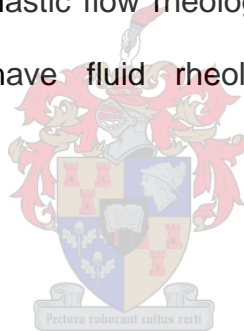
The complexity of flow processes, including transport and deposition (Stow and Johannson, 2000) has resulted in a controversial debate on deep-water deposits. Consequently, many turbidite facies models have been proposed over the last 50 years, including Bouma (1962), Mutti and Ricci Lucchi (1972 and 1975), Walker (1978), Stow and Shanmugam (1980), Lowe (1982), Howell and Normark (1982), Bouma *et al.* (1986), Reading and Richards (1994), and Johnson *et al.* (2001).

This chapter provides brief background information on deep-water deposits that will clarify the meaning of terminology used in this study. It focuses mainly on passive margin settings, similar to the Bredasdorp Basin.

3.2 Characteristics of sediment gravity flows

Sediment gravity flows are broadly defined as sediment-water mixtures that flow downslope under the influence of gravity. They play an important role in transporting and depositing sediments from the shelf to the deep-water settings.

Lowe (1979) recognised five types of gravity flows based on their rheology or the behaviour of fluid material within a flow and over time. To date, sediment gravity flows are grouped into four end-members: grain flows, fluidized or liquefied flows, debris flows, and turbidity currents. Practically, grain flows, fluidized flows and debris flows (GFD) display a plastic flow rheology, also termed non-Newtonian, whereas turbidity currents have fluid rheology, also termed Newtonian (Shanmugam *et al.*, 1994).



3.2.1 Grain flows

Lowe (1976) defines grain flows as gravity flow of cohesionless solids, maintained in a dispersed state against the force of gravity by an intergranular dispersive pressure arising from grain interaction within the shearing sediments. Deposition from grain flows results from a quick “freezing” process. Deposits commonly form massive-bedded units, with few to no primary structures, except for inverse grading, scouring and injection structures near the base (Fig. 3.1).

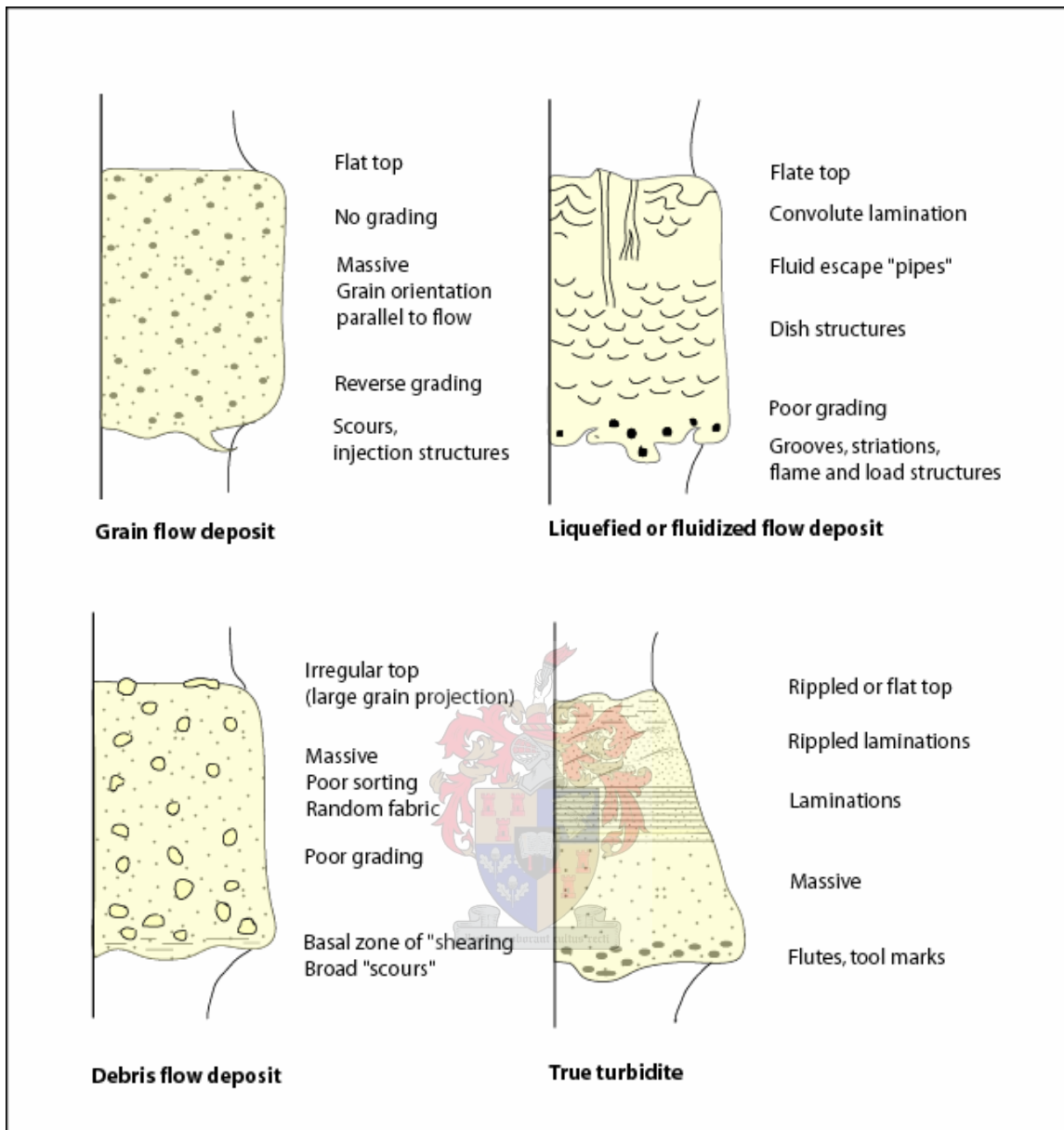



Figure 3.1 Diagram illustrating the sedimentary characteristics of the four types of gravity flows (from Middleton and Hampton, 1976).

3.2.2 Fluidized flows

Fluidization occurs when fluid, trapped in pore spaces, escapes upward as settling takes place downward by gravity. Fluidized sediment flows are therefore characterized by the presence of pore water between the grains. Deposits are typically thick, poorly sorted sand units that are characterized by fluid escape structures such as dish structures and fluid escape pipe structures (Dasgupta, 2003). Load, flame, and convoluted structures are also common in these deposits (Fig. 3.1). As soon as grains settle out of the fluid, grain-to-grain contact is re-established resulting in “freezing” of sediments and ending the flow motion.

3.2.3 Debris flows

The image shows a watermark of a university crest, likely from the University of Jammu, featuring a shield with various symbols, a crown on top, and a banner at the bottom with the motto 'Pectus roburant cultus ceet'.

Debris flows are usually matrix-supported flows, in which the matrix can be muddy or sandy. Muddy debris flows have enough cohesive strength to maintain large clasts, reaching boulder size, in suspension. Sandy debris flows have a sand portion falling between 25% and 30%. Their deposits are characterised by ungraded massive sand with a sheared basal interval, rafted mudstone clasts near the top, occasional inverse grading, and floating quartz pebbles and granules in fine-grained sandstone (Shanmugam, 1997). Resulting deposits are thick and poorly sorted, with no internal bedding or structures (Fig. 3.1).

3.2.4 Turbidity currents

Shanmugam (1997) defines a turbidity current as a sediment-gravity flow, with fluidal rheology and turbulent state in which sediment is held in suspension by

fluid turbulence. Deposition from true turbidity currents results from fall-out of suspension when turbulence, the main grain-supporting mechanism, begins to diminish. Grading, which results from deposition of coarse grains followed by deposition of finer grains, is very common and displays a well-defined fining-upward succession (Fig. 3.1).

3.3 Models for turbidity current deposits

3.3.1 Origin of turbidity currents

Two types of mechanisms are suggested for the origin of turbidity currents. The first mechanism is slumping that evolves downslope into turbulent sediment gravity flows. The second mechanism occurs at the mouth of large rivers where large amounts of sediments are discharged into the sea as hyperpycnal flows.

3.3.2 Morphology and models of turbidite deposits

A turbidity current usually presents three distinct parts namely head, body and tail (Middleton, 1967). The head is usually thicker than the rest of the flow and is characterised by intense turbulence commonly associated with erosion. The body is relatively thinner than the head and is characterised by a uniform thickness, which may result from the occurrence of a steady or uniform flow. The tail forms the dilute portion of the flow (Gardner *et al.*, 2003).

Two main types of turbidity currents, usually termed short-lived surge-type flows and long-lived steady flows have been identified. Lowe (1982) called them high-

density and low-density turbidity currents. High-density turbidity currents form thick-bedded and coarse-grained deposits with poor internal laminations. Basal scouring may be present or not. Low-density turbidity currents, however, form thin-bedded and fine-grained deposits with well-developed grading and laminations. Scours are often present at the base of beds (Lowe, 1982; Gardner *et al.*, 2003).

Several turbidite facies models have been proposed over time but the ideal model was proposed by Bouma (1962). He defined the individual flow units of true turbidites in terms of internal sedimentary structures associated with different flow regimes of sediment transport. This standard sequence is commonly called the “Bouma Sequence” and consists of five divisions, namely T_a , T_b , T_c , T_d , and T_e (Fig. 3.2).

The basal division (T_a) consists of a massive, poorly sorted and graded sandstone interval. This is successively overlain by T_b (parallel-laminated sandstone) interval, T_c ripple cross-laminated and/or convolute interval and T_d (parallel-laminated fines, i.e. siltstone and claystone) interval. The top division (T_e) represents hemipelagic mud deposits. The T_a interval was deposited from rapid fall-out of suspension compared to the other intervals that originated from traction and suspension (Shanmugam, 1997).

Similar turbidite models were proposed lately by Stow and Shanmugam (1980) and Lowe (1982). These models focus on the fine-grained part and coarse-grained part of turbidites, respectively (Fig. 3.3). In the Stow and Shanmugam

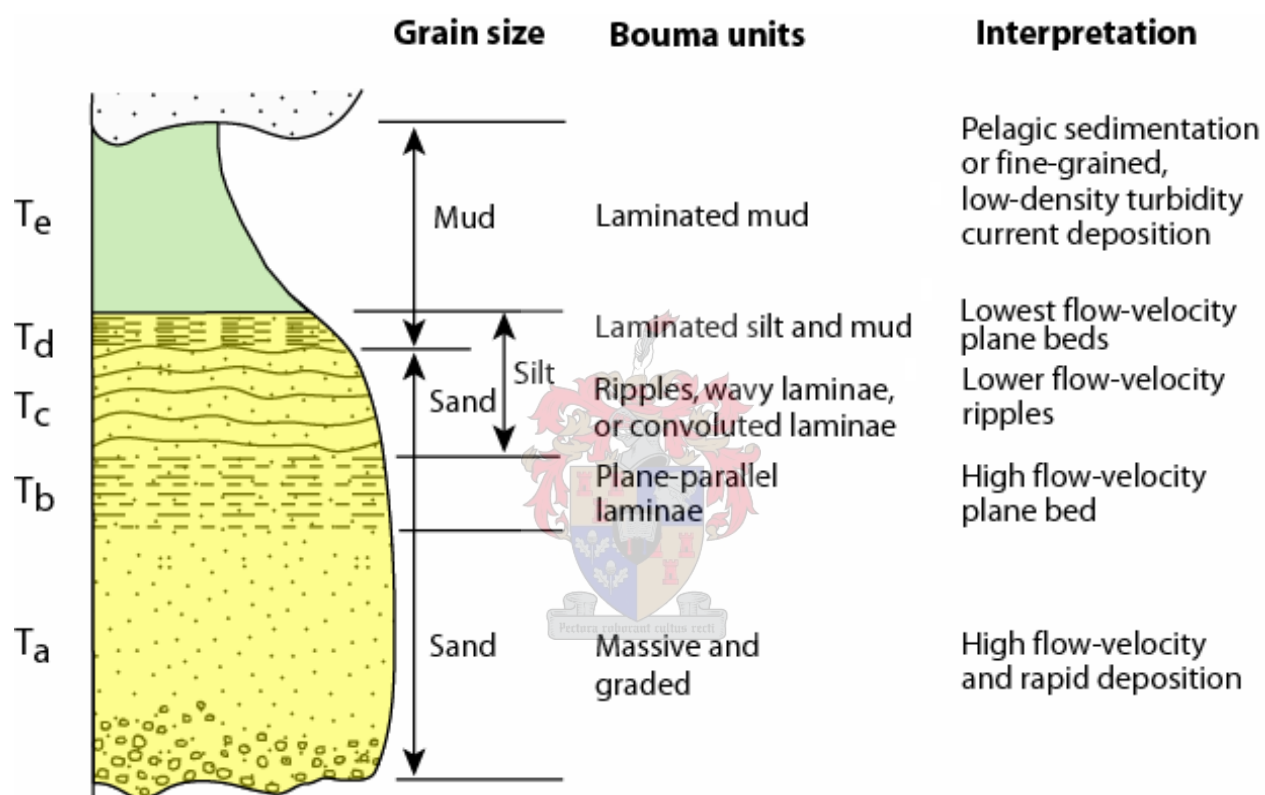


Figure 3.2 Ideal Bouma Sequence showing the sedimentary features of the different divisions of turbidity current deposits (from Shanmugam, 1997).

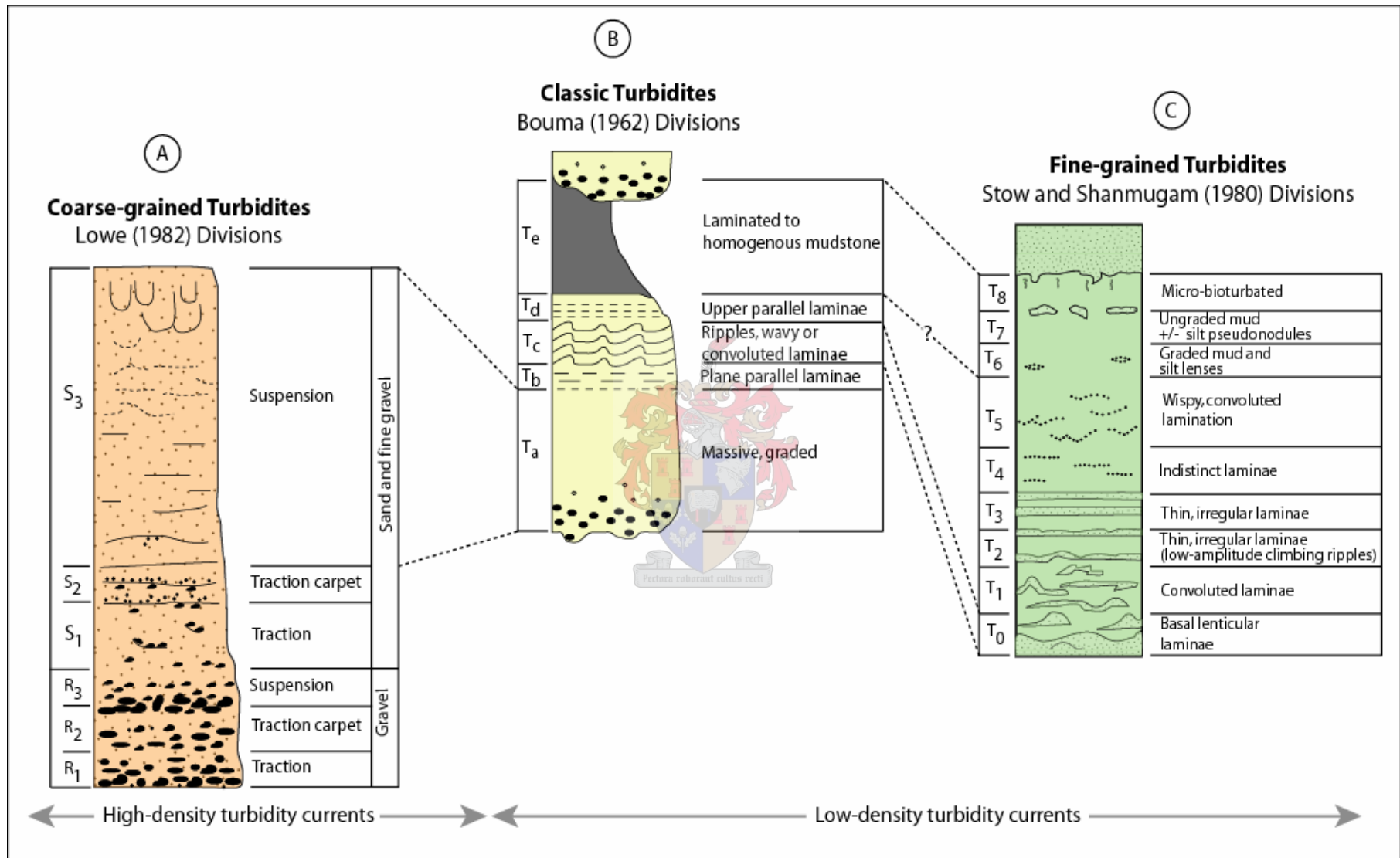


Figure 3.3 Different models of turbidites. (A) Coarse-grained turbidites (Lowe, 1982), (B) Classic turbidites (Bouma, 1962), and (C) Fine-grained turbidites (Stow and Shanmugam, 1980).

(1980) model, turbidites are subdivided into nine intervals termed T_0 to T_8 . The basal interval (T_0) presents silt laminations, load casts and mud-injection structures. This is successively overlain by a convoluted to laminated interval (T_1), low-amplitude climbing ripples (T_2), thin regular laminated interval (T_3), thin indistinct laminated interval (T_4), thin wispy or convoluted laminated interval (T_5), graded mud interval (T_6), ungraded mud interval (T_7) and a bioturbated interval (T_8).

The Lowe (1982) model was built on a gravel-to-sand succession (Fig. 3.3). The lowest interval consists of gravel and comprises three subdivisions R_1 , R_2 and R_3 . The upper interval or sand interval was divided into S_1 , S_2 and S_3 . The base of the sequence comprises coarse gravel with traction structures (R_1). This is overlain by an inversely graded gravel interval (R_2), followed by a normally graded gravel interval (R_3). A plane- to cross-laminated sandstone interval (S_1) rests on R_2 . This is followed by an inversely graded and basal shear-laminated sandstone interval (S_2) and structureless to normally graded sandstone interval with fluid escape structures (S_3).

The high complexity and variability of facies recorded for turbidites show that the Bouma Sequence model is inadequate to accurately interpret all turbidites. According to Shanmugam (2000), there is a fluid dynamics reason that prevents a turbidity current, carrying gravel to mud, from depositing all the above divisions with a coarse section (R_{1-3} , S_{1-3}) at the bottom, classic turbidites (T_{a-e}) in the middle, and fine-grained turbidites (T_{0-8}) at the top. He proposed that a composite

model of an ideal turbidite bed should comprise 16 divisions combining all intervals of the three models above. However, he added that although such ideal turbidite bed has not yet been recorded, it is not unrealistic.

In this investigation, the three models are taken into account since they complement each other.

3.4 Submarine fan models

According to Mutti (1992), a turbidite system consists of an erosive component commonly situated upslope through which sediments are supplied and a downslope depositional component where sediments accumulate. This downslope component can be a submarine fan. The latter is defined as stacked bodies of genetically related mass-flow and turbidity-current facies deposited in virtual stratigraphical continuity (Mutti and Normark, 1991; Stelling *et al.*, 2000).

Submarine fans result from a complex interplay between various allocyclic controls, such as changes in relative sea level, and autocyclic controls, among which are avulsion, thalweg migration and lobe switching (Richards *et al.*, 1998). The first group of controls is responsible for the genetic relationship of many deep-water sequences whereas the second are responsible for creation of the facies architecture of these sequences (Hickson and Lowe, 2002).

The first model for submarine fans was proposed by Normark (1970). He suggested a subdivision into upper fan, middle fan, and lower fan (Fig. 3.4). Normark (1978) and Walker (1978) revised the fan description of Mutti and Ricci

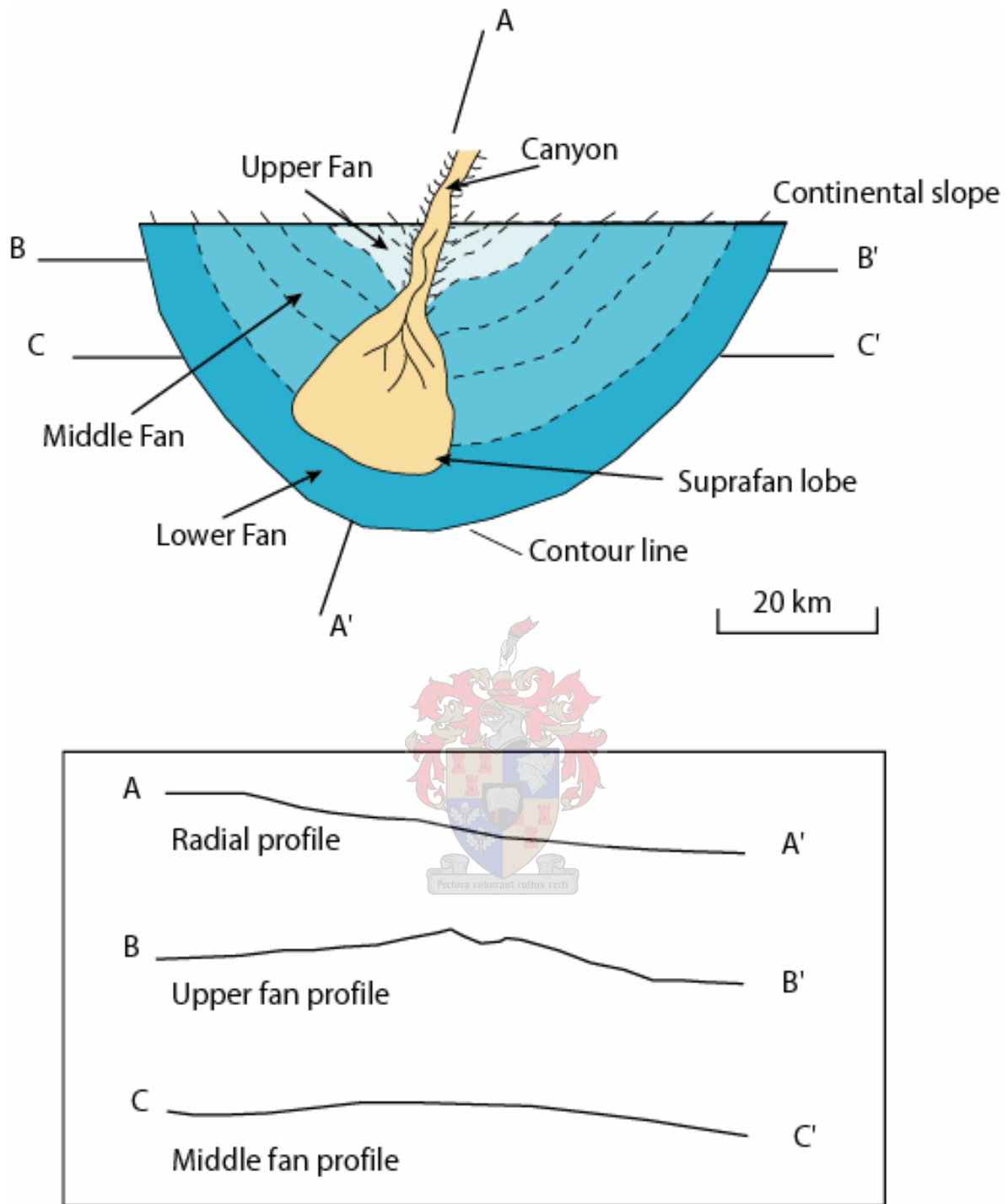


Figure 3.4 Model of modern sand-rich submarine fan system (from Normark, 1970).

Lucchi (1972) by grouping facies into groups, based on grain-size and sedimentary structures. This description was later improved by Shanmugam and Moiola (1985) who classified turbidite fan systems on the basis of facies characteristics and extended the subdivision of submarine fan systems into shelf and slope settings, inner, middle and outer fan settings, and a basin plain setting. This resulted in the turbidite fan models presented in Figure 3.5, generated for passive margin settings.

Generally, the upper fan corresponds to a leveed-channel valley serving as main conduit for sediments deposited in the middle fan. The latter is a distributary channel system that originates at the end of the leveed-channel valley. The lower fan consists of unchannelized sheet-like deposits produced by the unconfined character of flow at the end of channel systems.

Reading and Richards (1994) proposed a classification of submarine fans based on grain-size composition. Their different models can be grouped as mud-rich, mud/sand-rich, sand-rich and gravel-rich, fed either from a single source, multiple point sources or a line source. Single-source mud-rich and mixed sand/mud-rich systems will be discussed here because they are common in passive margin settings (Shanmugam and Moiola, 1988).

Mud-rich systems are submarine fans with less than 30% sand (Fig. 3.6). These commonly form large and thick successions of sediments, likely due to large source areas such as river and deltaic feeder systems with fine-grained suspended load. Deposition of sediments is driven by low-density turbidity currents. From the shelf to basin plain, mud-rich submarine fans consist of canyons associated with channels usually filled with slump deposits, meandering channel-levee systems,

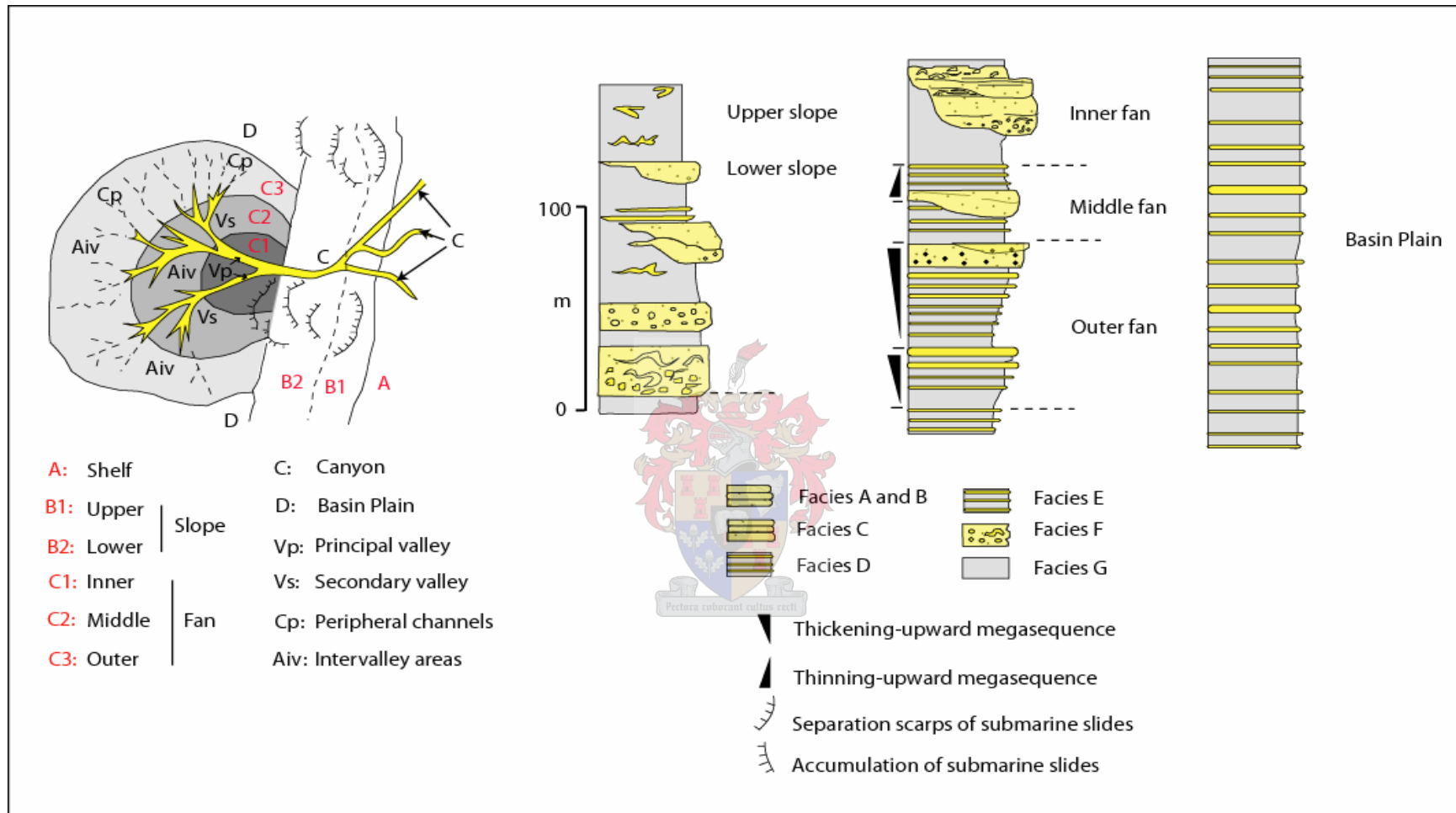


Figure 3.5 Illustration of the three distinct intervals along a submarine fan system and respective facies succession within each interval (from Mutti and Ricci Lucchi, 1972).

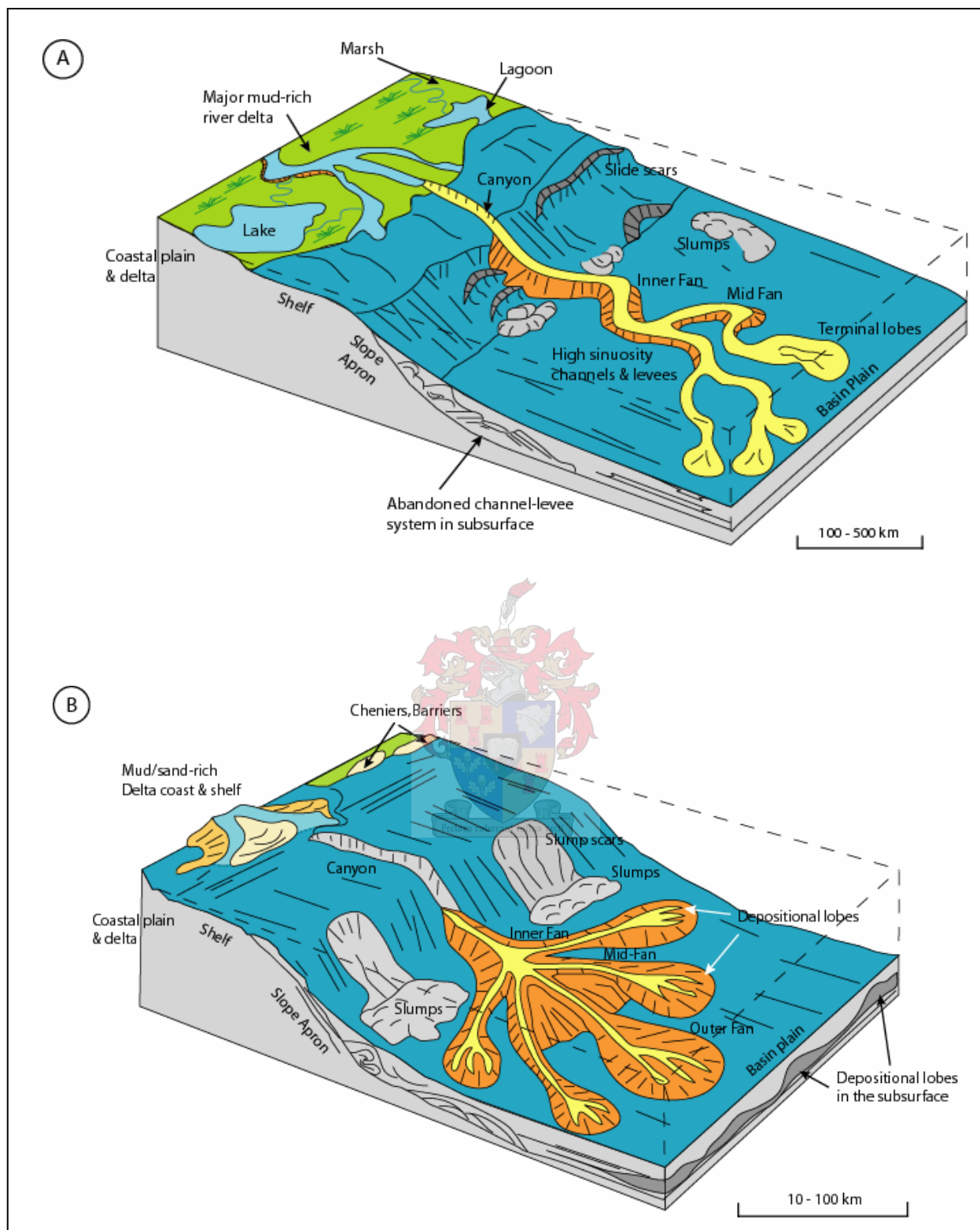


Figure 3.6 Depositional models for single-sourced submarine fans, (A) mud-rich system, and (B) mixed sand/mud-rich system (from Reading and Richards, 1994).

and lobes comprising thin-bedded sandstones, siltstones and mudstones. In contrast, mixed sand-mud-rich systems are submarine fans with 30% to 70% of sand (Fig. 3.6). These submarine fans are formed by direct sediment input from deltas or an active shelf feeding a canyon. The upper fan consists mainly of a canyon followed by single channel-levee systems through which sediments are transported. This channel splits into multiple channels between upper and middle fan, and ends with prograding lobes in the lower fan.



CHAPTER 4

FACIES AND FACIES ASSOCIATIONS

4.1 Introduction

According to Mutti and Ricci Lucchi (1975), a facies represents a bed or group of beds with similar characteristics such as grain characteristics, bedding characteristics, nature of overlying and underlying contacts and sedimentary structures. The use of the term facies in this investigation is in accordance with that definition. Facies result from depositional processes, which strictly reflect flow behaviour at the time of deposition (Gardner *et al.*, 2003). Facies analysis enables recognition of the bounding surfaces critical for vertical and lateral changes of the sedimentary succession of systems tracts and related lithology.

Core data from the central Bredasdorp Basin provided the foundation on which sedimentologic observation and interpretation are based. The existing core descriptions, provided by the geological well-completion reports, describe only the lithology of the cores. This investigation describes cores in terms of facies. Nineteen cores were described, taking into account grain size, primary and secondary sedimentary structures. Only 13 cores were photographed (see Appendix). Coregraphs and core descriptions of previous studies were referred to for depth indication and characteristics not obvious to the naked eye. Figure 4.1 shows a virtual sedimentary log representing the eight

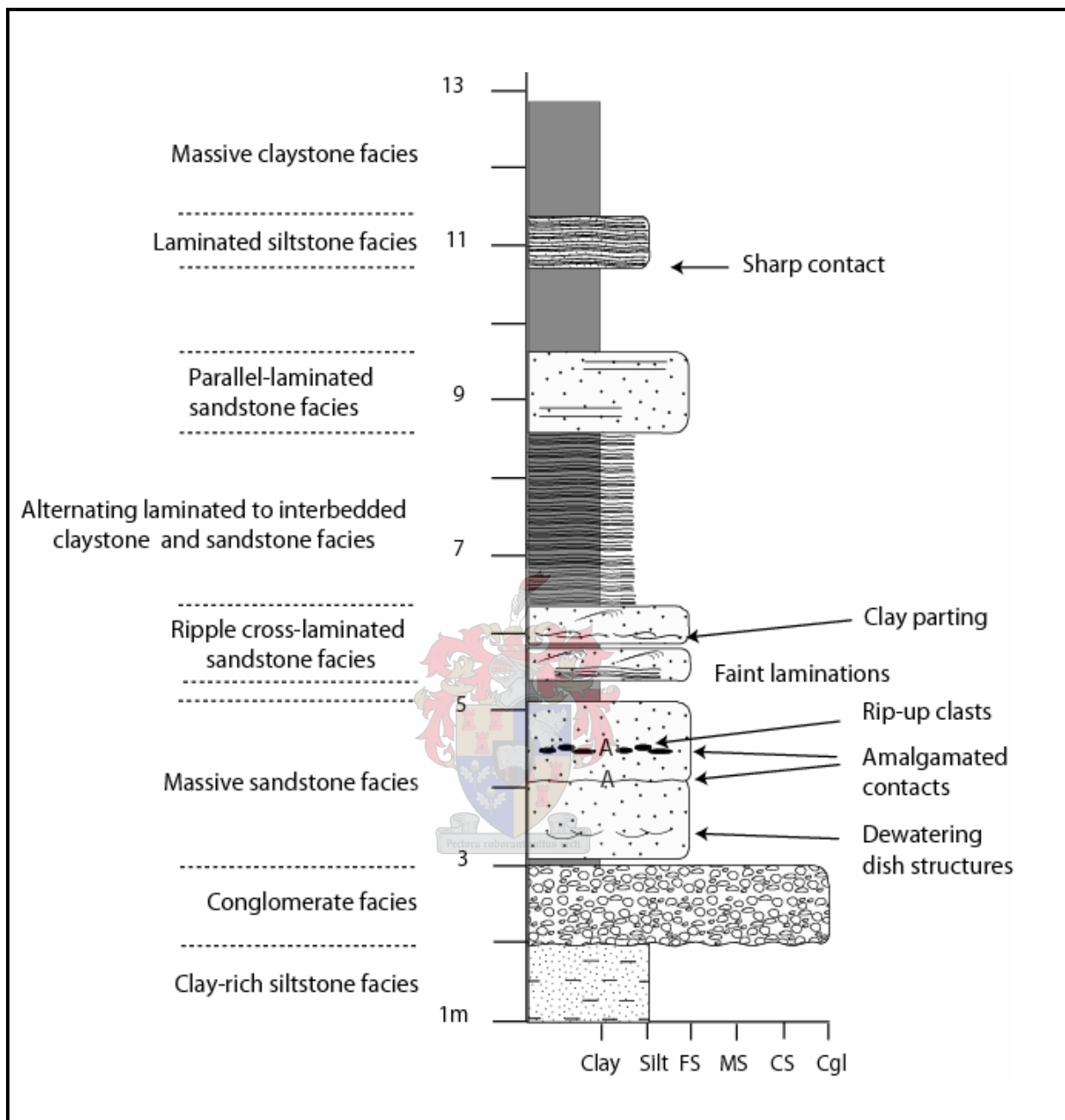


Figure 4.1 Virtual sedimentary log representing the sedimentary facies observed.

facies identified for the deep-water deposits of the central Bredasdorp Basin. Each facies illustration includes the gamma ray log of the cored interval. The scale of supporting pictures is given by the paper scale bar of 5cm.

4.2 Sedimentary facies

4.2.1 Facies A: Massive sandstone

Description

This facies is present in most cores. Massive sandstones consist of fine- to coarse-grained sands. Colour is generally grey, but dark grey and brownish colourations are also present. Individual beds range between 8 cm and 4 m of thickness or even more, whereas stacked amalgamated beds can reach a thickness of 7 m. Lower and upper contacts are sharp to erosive, but rarely gradational. Sharp contacts display local irregularities that are probably due to loading processes during deposition. Internal amalgamated surfaces are common. They are indicated by an accumulation of clay clasts, clay partings, and an abrupt change in grain size (Figs. 4.2a and 4.2b).

Occasionally, thin clay laminae forming faint parallel laminations are present. In places, they occur with iron-stained nodules that concentrate as layers (e.g. at 2945.26 m in core 6 of E-AD1, Fig. 4.2b). Soft-sediment deformation is observed also in places. This include fluid escape structures, i.e. pipes filled with clay material (e.g. between 2954 m and 2954.5 m in core 6 of E-AD1) and dish structures (Fig. 4.2a). Massive sandstones are thought to represent the T_a

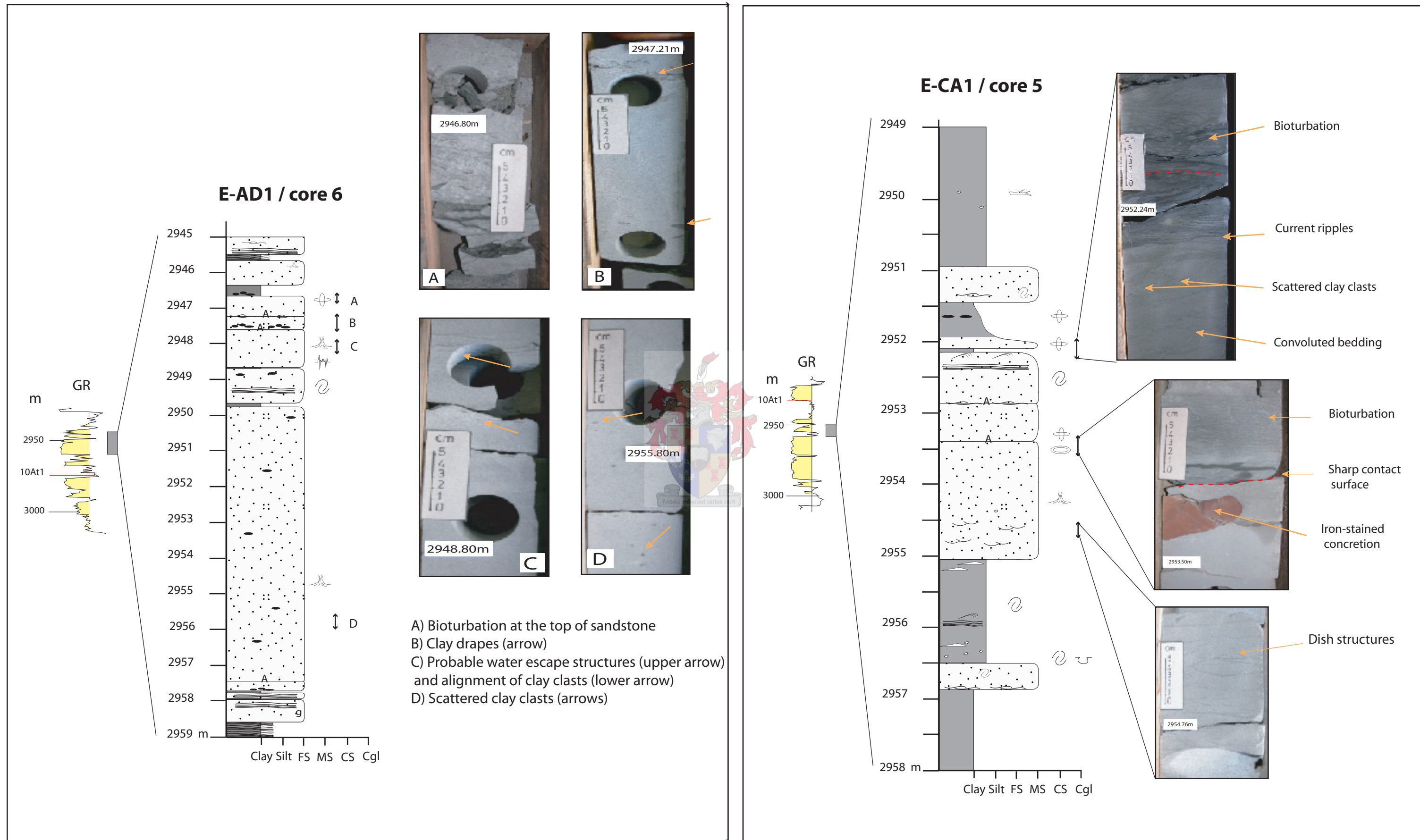


Figure 4.2a Illustration of massive sandstone facies. It displays various primary and secondary sedimentary structures such as bioturbation, fluid escape features, clay laminae and clay clasts.

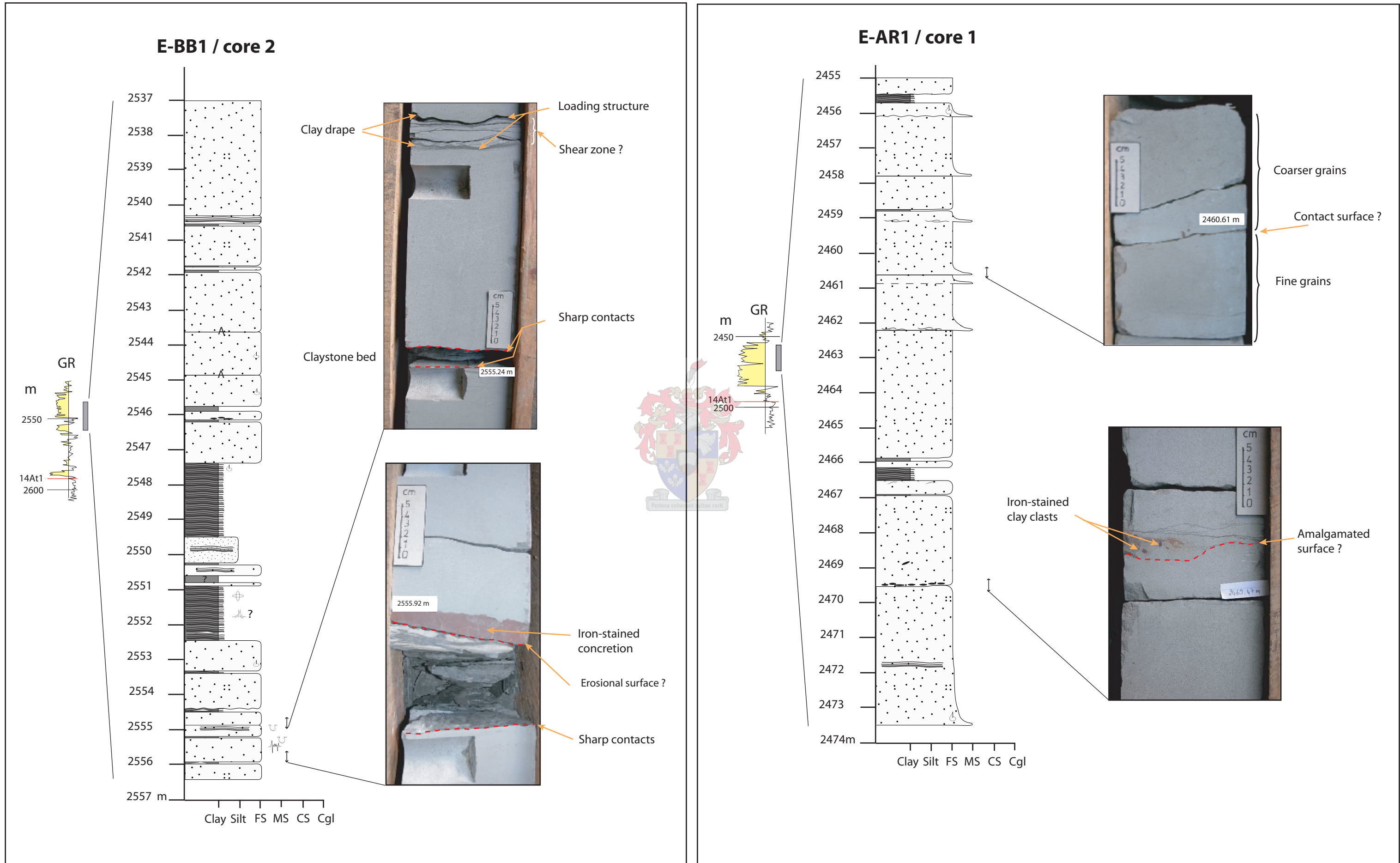


Figure 4.2b Illustration of massive sandstone facies. Loading structures occur associated with clay intervals. Clay clasts are seen above possible amalgamated surfaces.

interval of the Bouma sequence despite the presence of these secondary structures.

Bioturbation is rare but present in the upper part (e.g. at 2945.8 m in core 6 of E-AD1) and at the bottom of some beds (e.g. at 2952.5 m in core 5 of E-CA1) (Fig. 4.2b). Spherical to elongated concretions, with brownish colour, of variable size are present (Fig. 4.2a). These are interpreted as sideritic calcareous concretions.

Grading is rarely seen within the beds, except where coarse grains are present at the base of beds (Fig. 4.2b). A thick bed of coarse-grained to pebbly sandstones, about 80 cm thick, was intersected only in core 1 of E-AD1. The overlying succession of this bed is medium-grained to fine-grained, which reflects a clear fining-upward trend for the whole unit.

Clay clasts are frequently scattered in this facies, but commonly accumulate at the base of beds or along amalgamation surfaces within the beds. When accumulation is basal, the number of clasts progressively decreases upward. Some beds contain clay clasts near their upper contacts. In terms of shape, clay clasts are rounded and elongated. Elongated clay clasts are more frequent in the lower parts of beds and are usually parallel to bedding. Well-preserved shell fragments are occasionally present in this facies. They can be abundant in some beds.

Interpretation

Massive sandstones refer to sandstone without apparent primary traction structures. They are deposited by high-density turbidity currents (Bouma, 1962; Eschard *et al.*, 2003). Sixsmith (2000) suggests that the lack of structures may be due to (1) rapid deposition of the suspended load from a high-density turbidity current (2) the “*en-masse*” freezing of the flow, such as debris flows, and (3) rapid deposition from sustained currents. The latter agrees with Kneller and Branney (1995) who suggested rapid deposition of sediment in a steady process. They proposed that faint laminations result from a pulsed aggradational process. The “*en-mass*” freezing process results from a grain flow process as suggested by Lowe (1982) and Amy *et al.* (2005).

Sharp contacts indicate abrupt deposition of sand. Observed load structures are commonly syn- to post-depositional structures that occur on the interface of two beds with different physical properties. When sand is deposited onto a less dense mud, it tends to sink into the mud.

Clay clasts within sandstone beds give variable information of the host beds. Concentration of clay clasts at the base of sandstone beds, for example, indicates erosion of the clay substrate with subsequent incorporation of clasts and concentration thereof near the base of the flow. Alignment of clay clasts within beds indicates the presence of amalgamated surfaces. Clasts floating within beds suggest high-energy flows capable of eroding the substrate (Kneller and Branney, 1995). When large clay clasts are observed at the top of beds, this

an inverse grading process resulting from a tractional carpet (Lowe, 1982). However, the absence of tractional structures and grading at the base implies a rapid fall-out of suspension due to a rapid decrease of flow velocity. This is in contrast to gradual fall-out that generates grading at the base.

The presence of bioturbation may indicate escape structures of organisms brought in from a shallower environment.

A concretion is a compact mass of mineral cement that occurs in a host rock of different composition. Concretions develop when a considerable amount of cementing minerals, i.e. calcite together with siderite precipitate locally as a bed or around a nucleus (Seilacher, 2001). Siderite is an iron carbonate ore, which rarely exist in its pure state as FeCO_3 . Most of the sideritic concretions are of epigenetic origin (Seilacher, 2001). Their reddish colour is caused by the iron.

Massive sandstones observed through cores can be interpreted as either sheet sandstones or channel-fill facies. Sheet sandstones are inferred when sandstones are parallel-sided, whereas channel-fills correspond to sandstone packages displaying erosive bases or showing a channel geometry. The latter can only be seen in outcrop or reflection of seismic data.

4.2.2 Facies B: Ripple cross-laminated sandstone

Description

This facies consists of fine-grained sandstones with colour varying between light grey and yellowish. Upper and lower contacts are generally sharp. Bed thickness ranges between 2 cm and 20 cm, but can reach 2 m when amalgamated.

A few parallel to sub-parallel laminations are interbedded to facies F but remain very subordinate. In some beds, ripple cross-laminations occur above parallel to sub-parallel laminations suggesting the T_{bc} interval of the Bouma sequence (Fig. 4.3). The T_b interval corresponds to parallel and sub-horizontal lamination, whereas the T_c interval corresponds to ripple cross-lamination. Distorted laminations occur locally, in the upper part of beds, and are thought to result from fluid escape shortly after deposition. The fluid escape features observed are dish structures and dewatering pipes (Fig. 4.3).

Very commonly, ripple cross-laminated sandstones are interbedded with alternating laminated to interbedded sandstone/siltstone and claystone facies.

Interpretation

The ripple cross- and sub-parallel laminations are traction features resulting from bed-load transport during deposition. The traction features indicate that this facies was deposited by turbidity flows that may have segregated from high- to

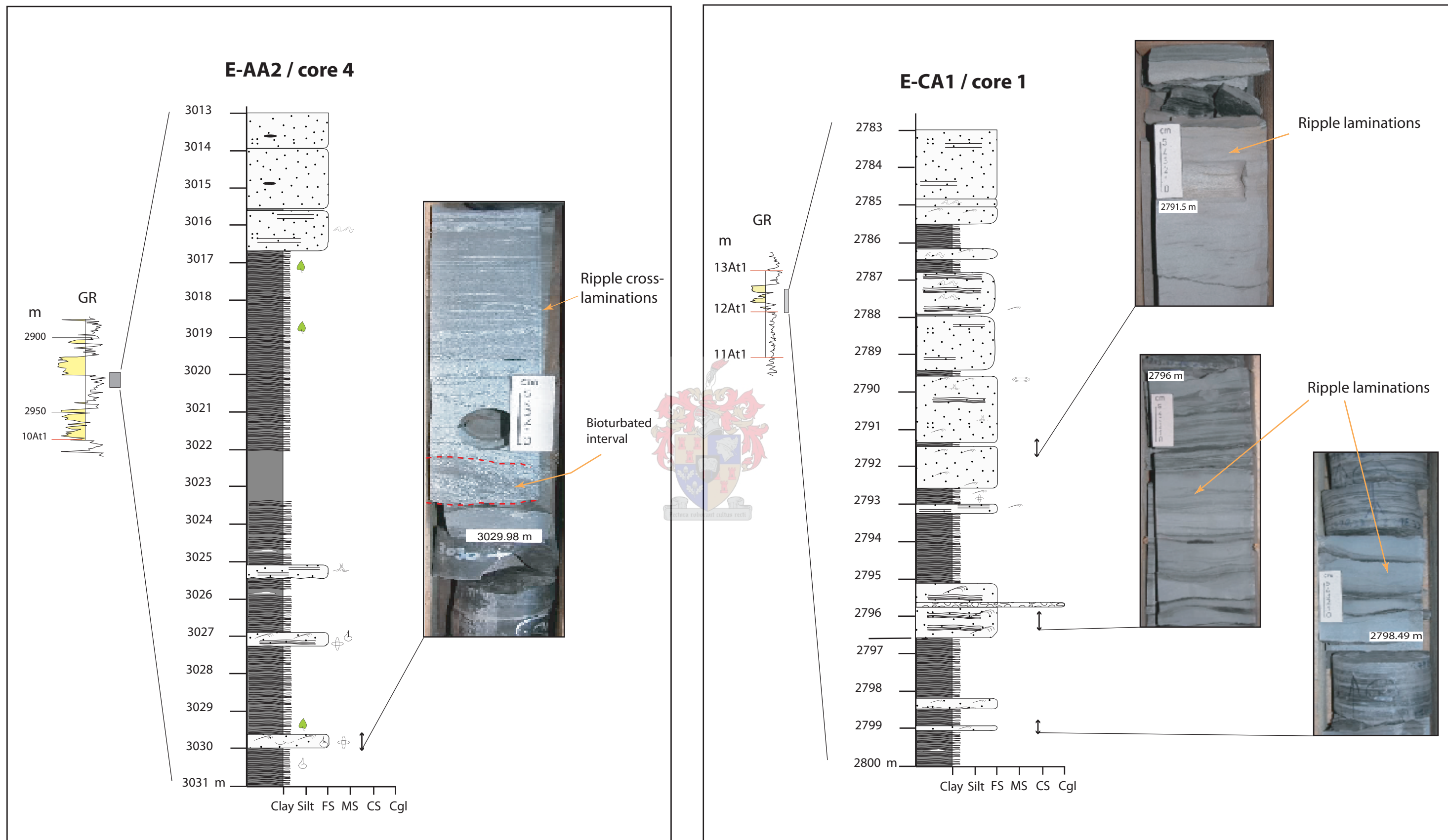


Figure 4.3 Illustration of ripple cross-laminated sandstone facies. Faint parallel laminations are associated with ripple laminations. Note that the facies shares sharp bounding surfaces with the alternating laminated to interbedded sandstone/siltstone and claystone facies.

medium density turbidity currents (Lowe, 1982; Pickering *et al.*, 1986). Lowe (1982) indicated that sub-parallel laminations are tractional features common in low-density currents. This is accepted by Paola *et al.* (1989) who think that parallel-lamination is produced in the lower portion of the “upper flow regime”, in contrast to ripple cross-laminations that are common in the high flow regime.

Cronin *et al.* (2000) and Sixsmith (2000) interpreted a facies comprising parallel laminations and ripple cross-laminations as overflow deposits. These deposits result from rapid deceleration of turbidity currents, from the channel to the outside of the channel-fill area. Similar facies was interpreted as sheet-like turbidite units by Saito and Ito (2002). According to them this facies results from unconfined turbidity currents in the middle and outer domain of a submarine fan.

The proximity of the ripple cross-laminated sandstones to channel-fills suggests off-axis or overbank deposits. Their interbedding with alternating laminated to interbedded sandstone/siltstone and claystone emphasises this interpretation. However, it remains a possibility that this facies represents sheet-like deposits if it is considered that flows are more extensive downslope of channels due to unconfinement and can form sheet-like beds (Habgood *et al.*, 2003).

4.2.3 Facies C: Parallel-laminated sandstone

Description

This facies is rare and is intersected only in core 4 of E-AA2, core 6 of E-AD1 and core 2 of E-BB1. Parallel-laminated sandstone facies consists of fine-grained

sandstones with light to medium grey, and rare dark grey colouration. The facies was mostly seen bounding massive sandstone (Facies A) with sharp lower and upper surfaces. Thickness of facies varies between 23 cm and 76 cm.

Common sedimentary structures are parallel laminations. Low-angle laminations are observed in places (Fig. 4.4). Rare bioturbation is present in places which rendering laminations indiscernible. Convolute laminations are remarkably common in the upper part of beds.

Interpretation

Several depositional processes can be inferred for this facies. As mention earlier, parallel-laminations are tractional features common in low-density currents (Lowe, 1982). They are interpreted as the T_b interval of the Bouma sequence. They are also attributed to near-bed turbulence or migration of low-relief bedforms, or a combination of both (Pettijohn, 1975).

Sharp bounding surfaces with other facies indicate abrupt changes in grain motion, i.e. due to changes in flow regime which again relates to grain size. Presence of low-angle laminations is attributed to large slump structures. These slumps are clearly emphasised with small slump structures in places (Fig. 4.4).

The presence of convolute laminations in the upper part of the facies is interpreted as fluid escape structures related to a readjustment of sediments due to compaction.

Bioturbated structures may be due to the presence of organisms brought in with

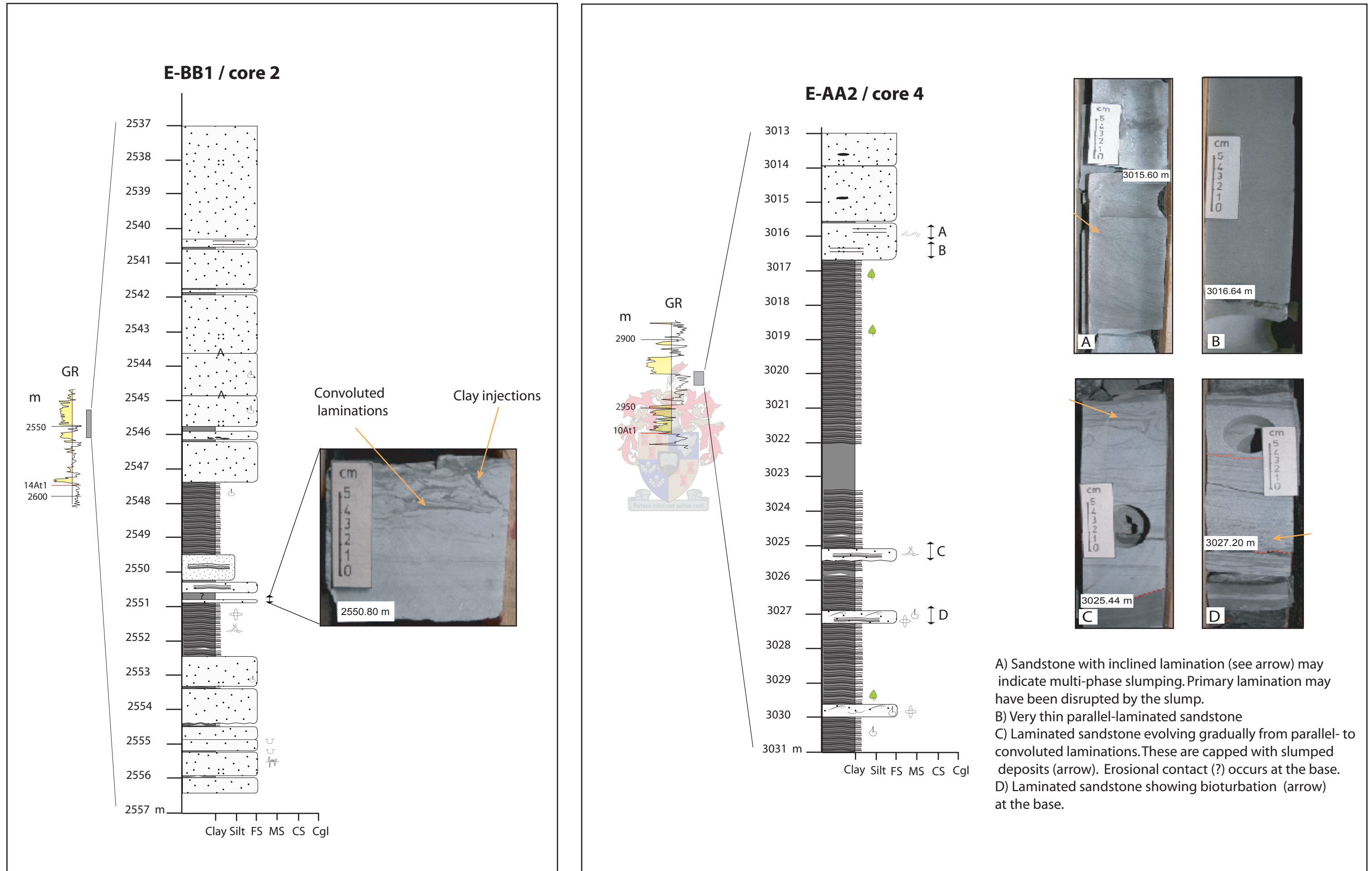


Figure 4.4 Parallel-laminated sandstones facies with secondary structures such as bioturbation, water escape features and distortions.

deposition.

4.2.4 Facies D: Conglomerate

Description

The conglomerate facies was only occasionally intersected in cores. All conglomerates are polymictic with various compositions and are open framework. Two variants were observed based on the matrix.

The first type of polymictic conglomerate facies consists of fine-grained sandstone as matrix, displaying a light grey, brownish to reddish colour (Fig. 4.5a). Pebbles are well rounded or elongated and sub-angular, are also weakly connected, and vary in size between 3 cm and 11 cm on the long diameter. The source rocks for these pebbles were massive sandstones, bioturbated sandstones, laminated sandstones and shales. Thickness of individual units varies between 15 cm and 3.5 m. The lower and upper surfaces of this facies are erosional. However, a gradational upper surface is also observed (Fig. 4.5a).

The polymictic conglomerate intersected at 2843.23 m in core 2 of E-BA1 shows an overall upward-fining trend. The lower part of the conglomerate unit is unstratified and reflects a disorder structure in contrast with the stratified upper part, where inclined beds with normal grading are present. Soft-sediment deformation is observed in the matrix. Replacement of shell remains by calcite has also been observed in places.

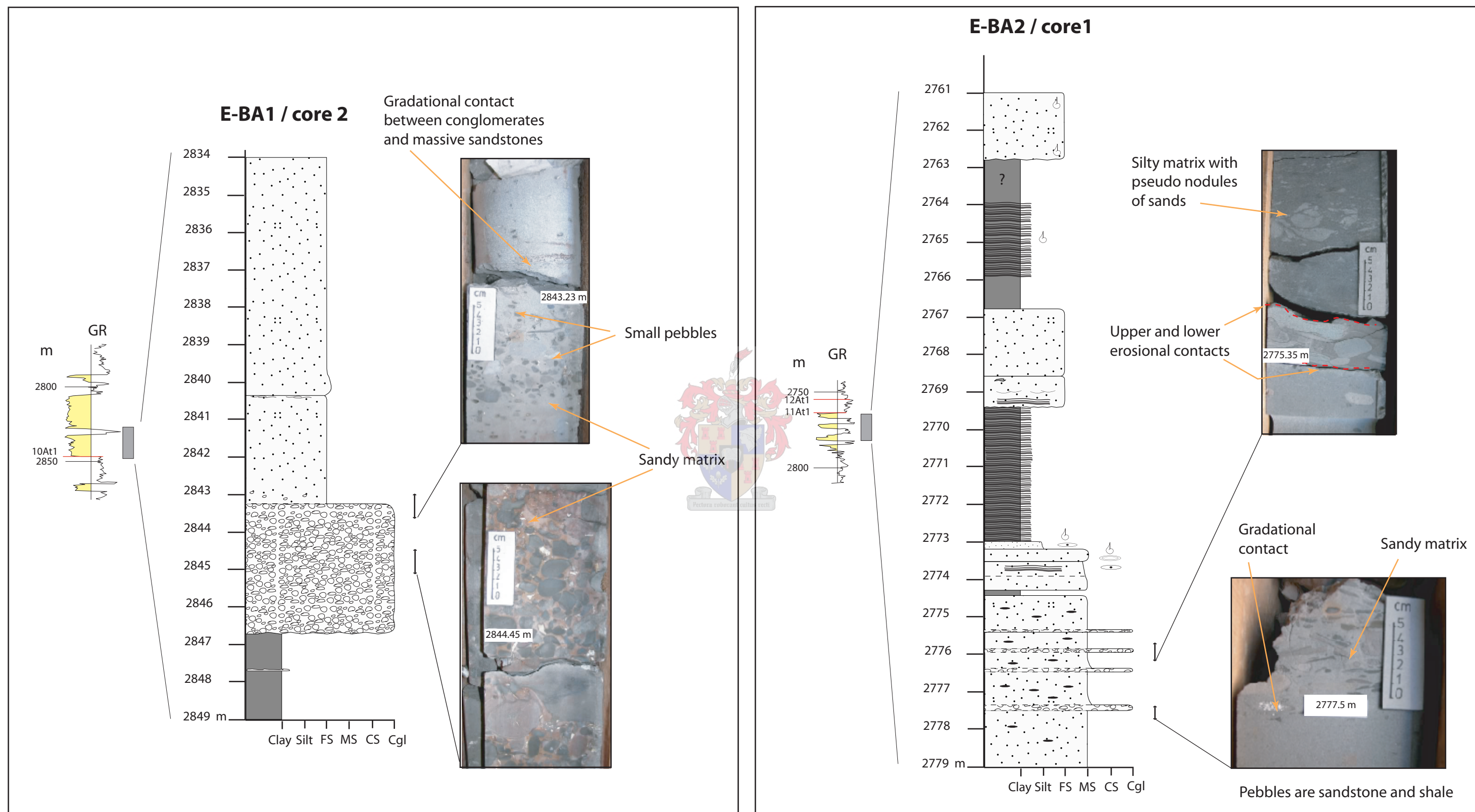


Figure 4.5a Illustration of polymictic conglomerate facies with sandy matrix. Conglomerate show organized and disorganized structures, from left to right. Note that the thicker conglomerate unit displays an upward-fining pattern.

The second type of polymictic conglomerate facies shows a roughly disorganised structure. Pebbles, consisting of sandstone, small shaly pebbles and probably large quartz grains are angular to sub-angular. These pebbles vary between about 5 mm and 5 cm in diameter and are encased within a silty matrix displaying a dark grey colour (core 1 of E-CA1) (Fig. 4.5b). Soft-sediment deformation is frequent in these conglomerates. Upper and lower bounding surfaces of these conglomerates are sharp (erosional).

Interpretation

The first type of conglomerate facies suggests generally high-energy conditions associated with channel-fills. The presence of large pebbles would suggest the proximity of the source for these conglomerates as suggested by Wickens and McLachlan (1990), but the roundness of these pebbles contradicts that and supports only the high-energy condition of a flow being capable to support movement of large pebbles. Organisation of the unit into unstratified and stratified beds is likely due to change from dispersive to organized flow from bottom to top, respectively. However, the presence of soft-sediment deformation may suggest prevalence of instability during deposition. Sharp and irregular lower contacts suggest erosion into underlying strata and may indicate channel lags. However, gradational boundaries with sandstones may reflect changes in flow conditions, such as periodical high-energy surges that could have brought in coarse sediments. Fine-grained sandstone matrix suggests that these conglomerates are bedload of highly energetic sandy flows that bypassed the

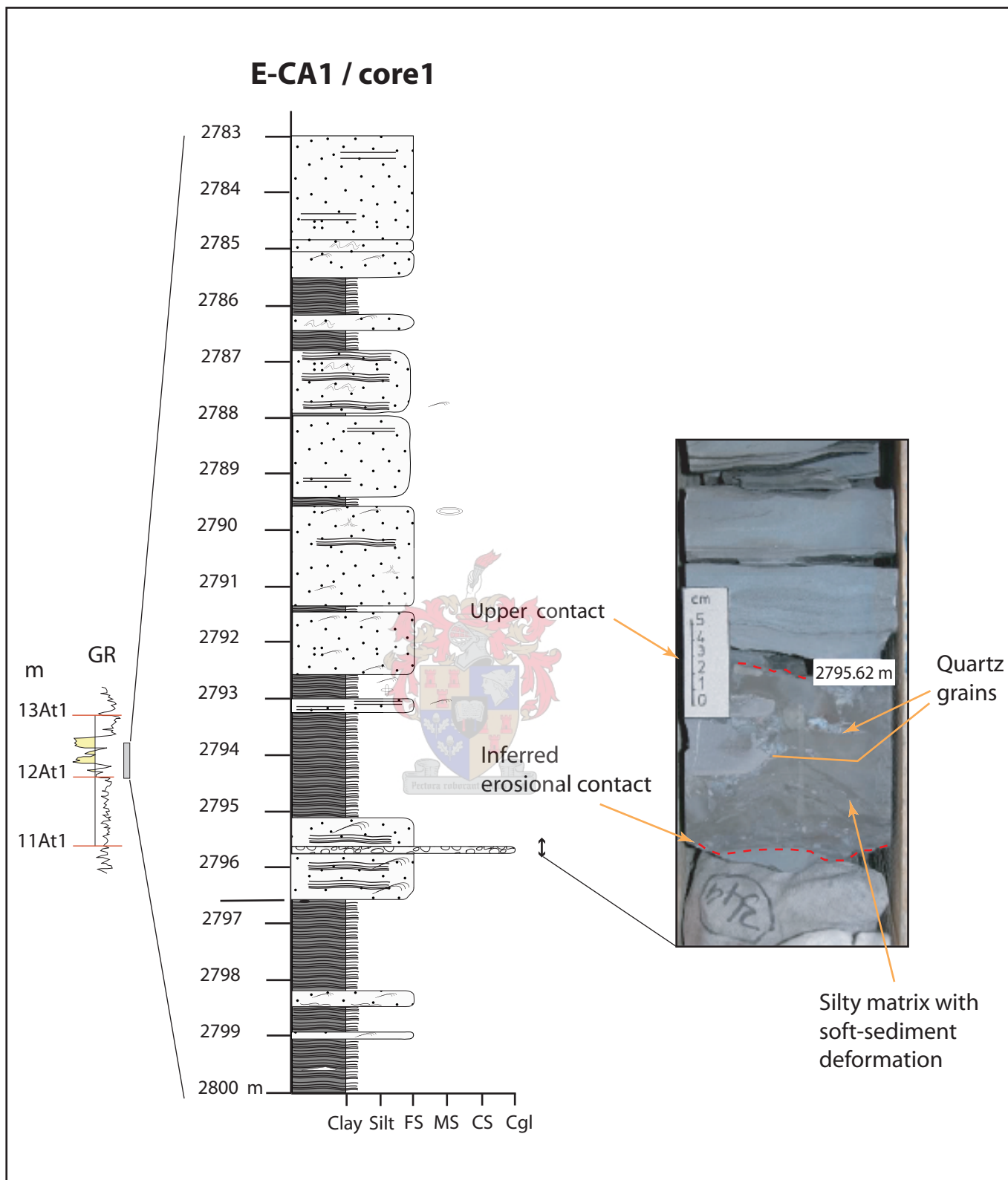


Figure 4.5b Illustration of polymictic conglomerate facies, with a silty matrix showing soft-sediment deformation. The facies shares sharp irregular contacts with the parallel- to ripple cross-laminated sandstone.

area to be deposited further basinward (Duerichen, 2000).

The second type polymictic conglomerates displays a deformed silty matrix with angular to sub-angular shaly pebbles, most likely indicating collapse deposits or slumping, similarly to those observed by Eschard *et al.* (2003) and Beaubouef (2004). In core1 of E-CA1, this facies is sharply bounded on top and bottom by parallel-laminated sandstone (Facies C) and displays about 12.5 cm in thickness. This may suggest local collapse in the proximity of or within a channel-fill. Saito and Ito (2002) describe similar feature as channel bank collapse deposits associated with turbidites. They postulated that slump deposits have been developed in response to readjustment of the topography in the channel-fill margins. The presence of soft-sediment deformation, even though not obvious, may suggest prevalence of uneven lower surface during deposition of sediments.

The presence of glauconite and body fossils such as shells, suggests deposition in a marine environment. The fact that shells occur within pebbles indicates that they were brought in from a shallow environment.

4.2.5 Facies E: Massive claystone

Description

This facies is generally massive and displays a black or dark grey colour, with thickness varying between 0.5 cm and 3.6 m. Both lower and upper contacts are commonly sharp but can be gradational. Bioturbation is occasionally observed, but seem not to occur at preferred zones in beds. In places, very thin silt laminae

of millimetre scale are observed parallel to the bedding (core 2 of E-BA1, Fig. 4.6). Sideritic concretions, light brown in colour, are common in some beds (e.g. at 2773.52 m in core 1 of E-BA2). These concretions are elliptical, rounded to sub-rounded but can also form layers within this facies. Pyrite and unbroken shell fossils are also abundant in places.

Interpretation

This facies, which corresponds to the mudstone facies of Sixsmith (2000), represents background sedimentation that occurs by suspension fall-out in a quiet and anoxic environment. This includes pelagic settling and hemipelagic sedimentation (Stow *et al.*, 2001). Pelagic settling is a vertical settling, typically very slow, but occurring as continuous or episodic pulse (Stow *et al.*, 2001). Hemipelagic sedimentation involves both vertical settling and slow lateral advection through the water column (Stow and Tabrez, 1998). Presence of thin sandy or silty laminae may result from low-density turbidity currents, which likely entered coarser grains together with fine grains in the environment.

This facies is believed to have been deposited when turbidite systems are no more active, i.e. when periods of starvation in sediment supply prevails (Sixsmith, 2000). Formation of sideritic concretions occurs as explained earlier. Pyrite mineralization, however, may result from the precipitation of iron-rich cement around vestiges of shells likely brought in by intermittent turbidity currents, or may occur as a result of diagenesis on the sea floor below the sediment-water interface during sediment starvation as suggested by Sixsmith (2000).

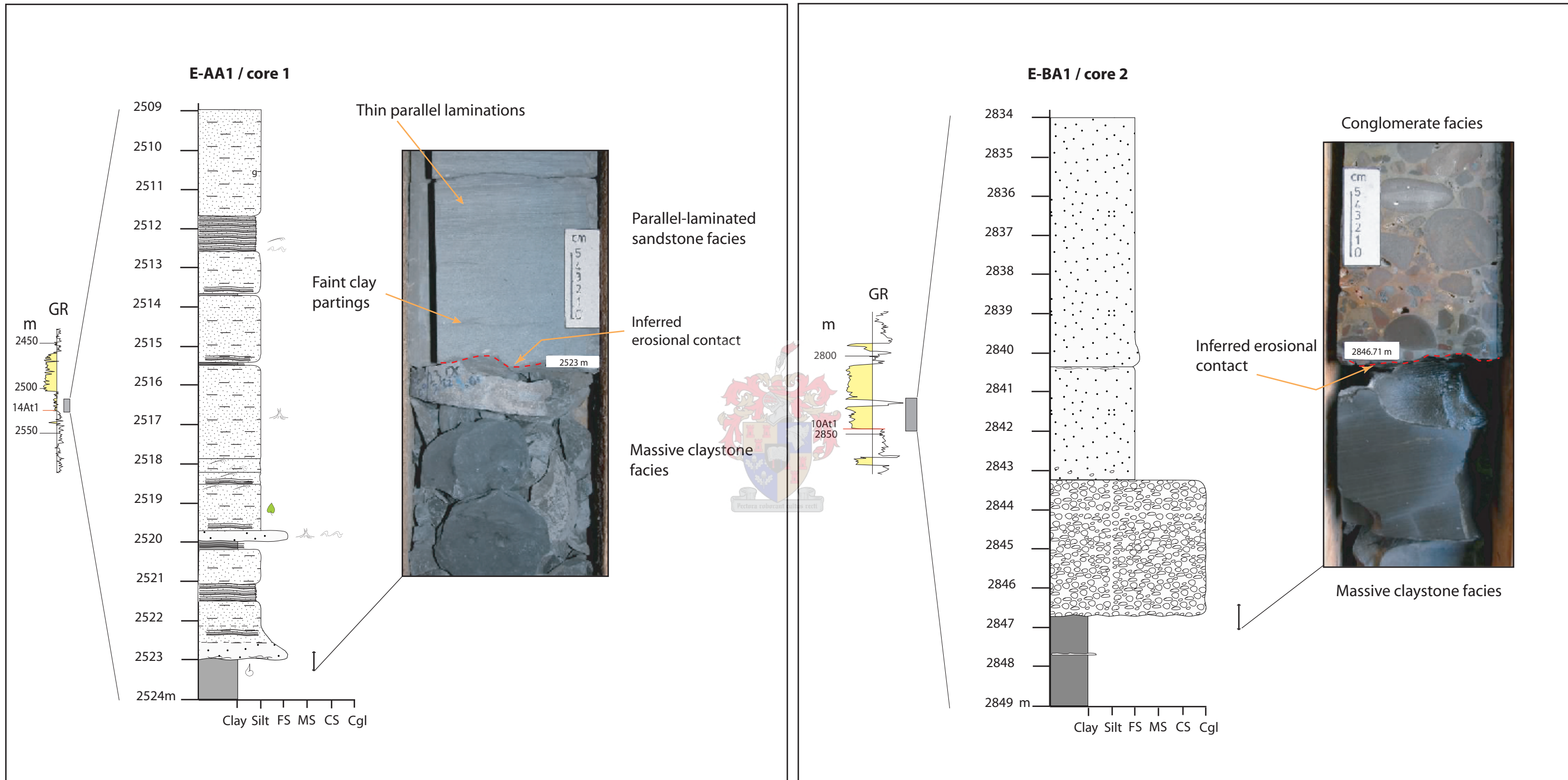


Figure 4.6 Illustration of massive claystone facies. Note the blocky appearance of this facies.

4.2.6 Facies F: Alternating laminated to interbedded sandstone/siltstone and claystone

Description

This facies is characterised by thinly interbedded sandstone, siltstone and claystone of centimetre scale (Fig. 4.7a-b). Sandstone and/or siltstone beds are frequently grey in colour, but yellowish to pale grey colour is observable in places. Individual sand interbeds can reach millimetre to tens of centimetres in thickness. The facies as such ranges between 5 cm and 2.3 m in thickness. The facies shares sharp lower and upper contacts with the surrounding facies, but presents also gradational contacts with laminated siltstone facies (e.g. core 1 of E-AA1).

Sand interbeds are horizontal but show uneven bounding surfaces. Some of these surfaces are erosive but can be confused with well-defined loading structures present at the base of some interbeds. Beds are both continuous and lenticular in shape. However continuous beds may be lenticular on a much larger scale. Some thin sand interbeds consist of faint parallel- and ripple cross-laminations (Facies B) (Fig. 4.7a) but others are massive sandstone beds (Facies A) (e.g. in core 1 of E-AR1, Fig. 4.7b).

Locally, sand injections occur vertically and horizontally to normal bedding (e.g. core 4 of E-AJ1). Carbonaceous concretions, brown to orange in colour, are observed locally as well as plant fragments and bioturbation.

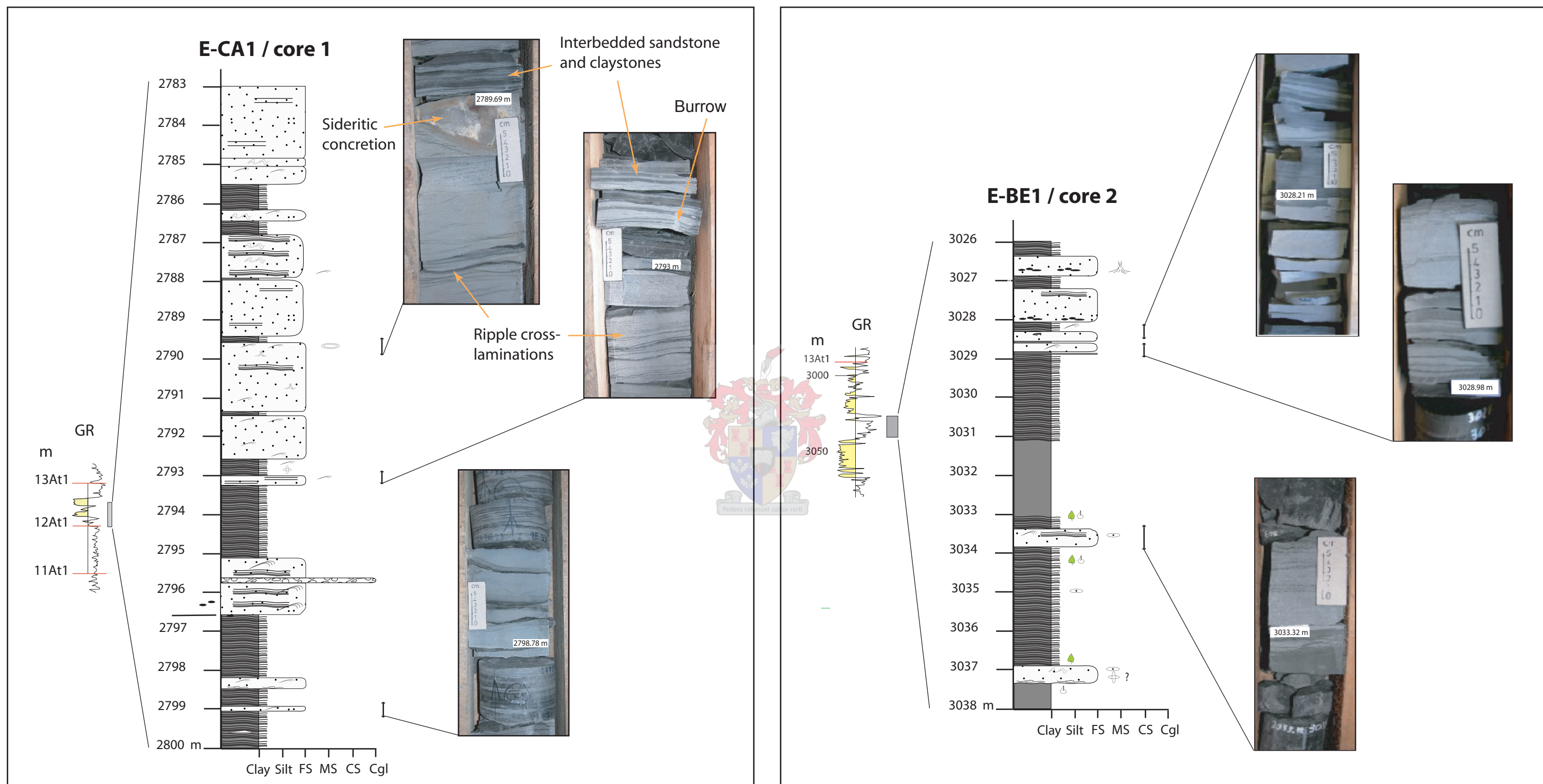


Figure 4.7a Illustration of alternating laminated to interbedded sandstone/siltstone and claystone facies. Beds appear slightly parallel to wavy and display a rhythmic alternation.

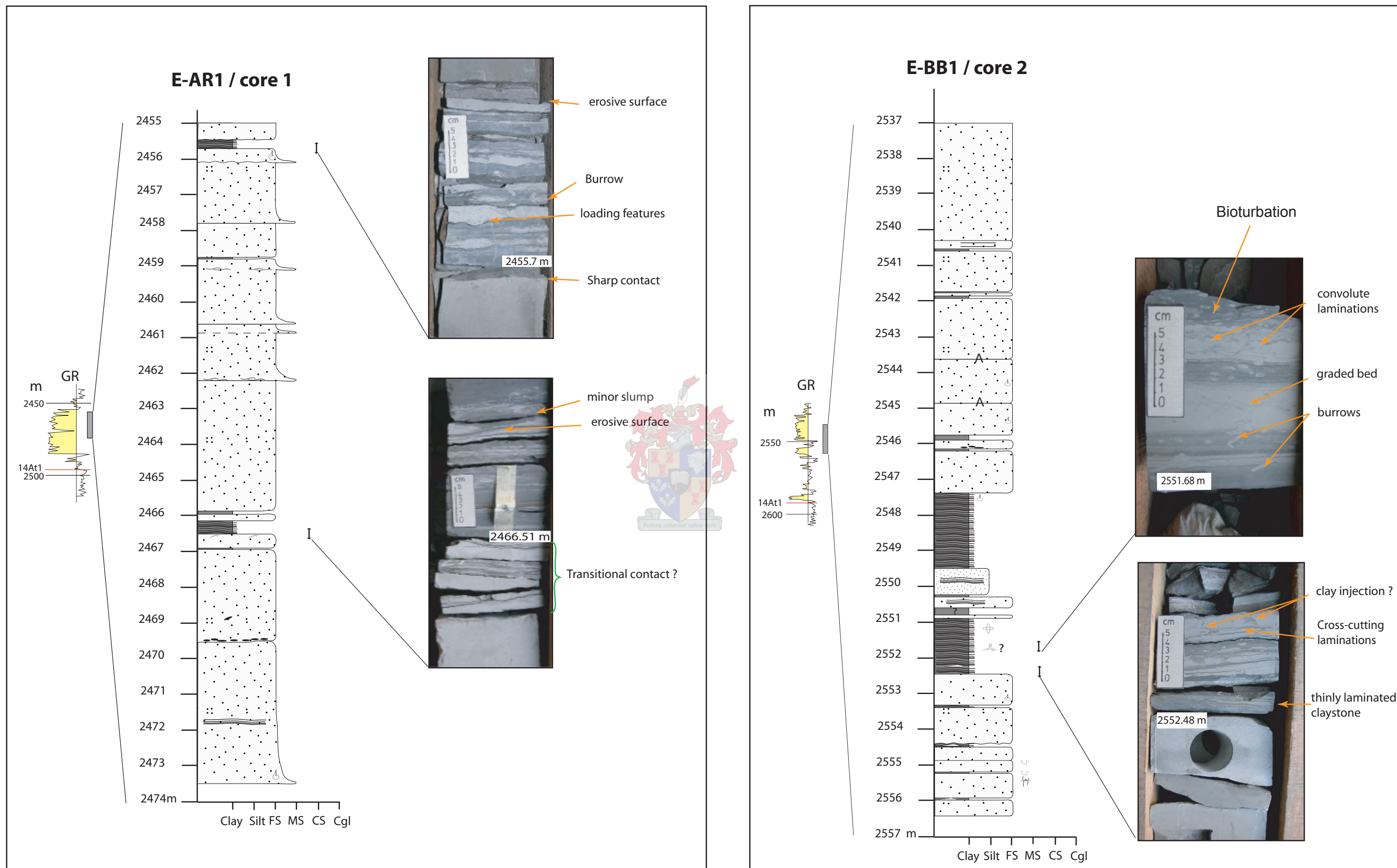
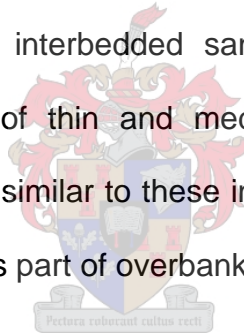


Figure 4.7b Illustration of alternating laminated to interbedded sandstone/siltstone and claystone facies. Rhythmic alternation of the beds is remarkable. Irregular contact surfaces as well as convolute laminations are frequent. Burrows are also present.

Interpretation

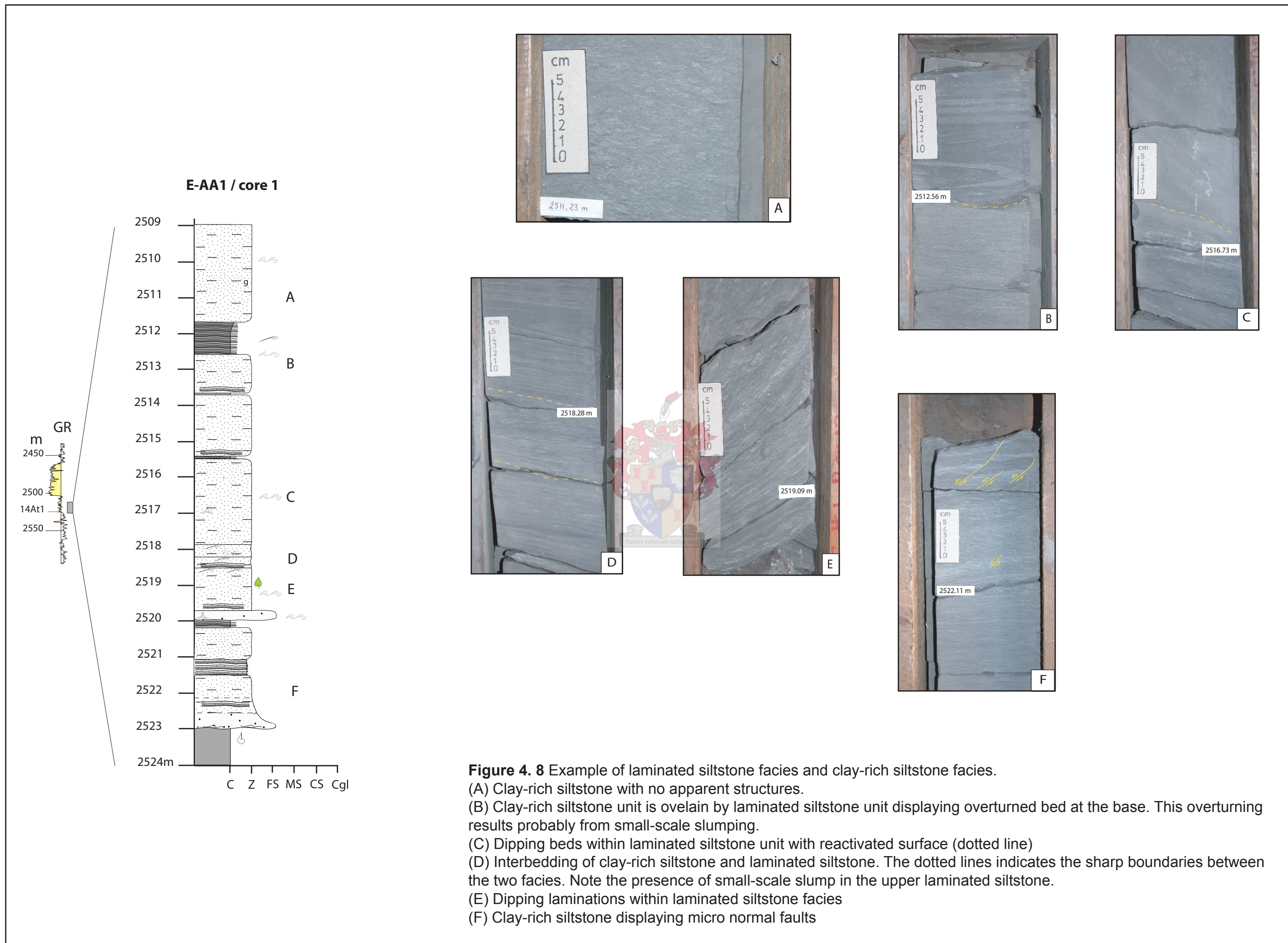
Shanmugam *et al.* (1994) and Sixsmith (2000) interpreted similar facies as being deposited from suspension settling of the finest grains in the water column. Alternation of thin beds may indicate rhythmic segregation from suspension. Clays were segregated from low-energy conditions whereas sand and silt were segregated from much higher energy conditions (Tye *et al.*, 1999). Parallel- and ripple cross-laminations result probably from tractional processes during low energy conditions. The sharp character of bounding surfaces of this facies indicates an abrupt change of type of sediments supplied in the suspension. Beaubouef (2004) interpreted interbedded sandstones and silty mudstones, showing rhythmic alternation of thin and medium beds, as interchannel or overbank deposits. Facies F is similar to these interbedded sandstones and silty mudstones and is interpreted as part of overbank deposits.



4.2.7 Facies G: Laminated siltstone

Description

This facies is largely composed of parallel-laminated siltstones (Fig. 4.8). Light grey laminae represent silt, whereas dark grey laminae represent clay. These laminae are very thin (< 1 mm), thin (1-3 mm), and thick (3-9 mm). Lower and upper contact surfaces of the facies are sharp and gradational. Gradational lower contacts are particularly seen with parallel-laminated sandstones (Facies C). Group of laminae range between 15 cm and 1.25 m in thickness.



Common sedimentary structures include parallel laminations, locally contorted, and occasional ripple cross-laminations. Parallel laminations display steep angles with normal bedding in places. Micro- normal faults, with displacement varying between 0.7 mm and 1 cm, are also present in places.

Interpretation

Sixsmith (2000) suggested that silt settles down from suspension after cessation of turbidity currents. This deposition occurs in channelized environments, inner and middle-lobe areas. He added that these deposits are commonly well preserved in distal parts, on the outer lobe and fan fringe areas, but also in fan proximal areas, in interchannel areas. This may justify the rarity of the facies in the cores since only sand-rich reservoir intervals were mostly cored.


The alternation of siltstone with thin claystone beds indicates a rhythmic deposition from very dilute turbidite currents at the tail-end of sand-rich high-density turbidity currents (Sixsmith, 2000). Laminated-siltstone facies is common between the sequence boundary and the base of massive sandstones because the slope gradient was likely not high enough to allow the later massive sandstones (Facies A) to erode deeply into previous deposits. Thin beds of massive sandstone (Facies A) and parallel-laminated sandstone (Facies C), with sharp or erosive bounding surfaces (Fig. 4.8), are interpreted as erosional remnants which are commonly lenticular in shape, similarly to the observation of Grecula *et al.* (2003) at the base of channel-fills. This facies could therefore

represent a by-pass facies constituting the basal infill of channels as suggested by Wickens (pers. Comm.).

Sediment instability caused slumping that resulted from collapse processes along incisions related to channelling. The same instability or uneven surface at the base of channels initiated probably internal failure of much more consolidated sediment along micro-surfaces causing micro-faults. The limited displacement of these faults and the discontinuity of faulted layers may probably suggest syn-sedimentary structures. Ripple-laminations suggest weak occurrence of tractional processes during deposition.

4.2.8 Facies H: Clay-rich siltstones

Description



This facies is similar in colour to the laminated siltstone facies (Facies G) with the exception that it shows practically no sedimentary structures or any stratification (Fig. 4.8). It occurs in core 1 of E-AA1 and core 1 of E-CA1. Apparently, floating silt and clay clasts seem to be convoluted. Abundant micro-faults are present. Lower and upper contacts of the facies are sharp. In places, dipping beds are present.

Sedimentary structures include rare ripple-laminations. These ripples are commonly seen near the upper boundary of units. Plant fragments are also present in the lower part of the facies, just above the underlying fine sandstone. Green minerals, likely glauconite, were seen in the upper part of this facies.

Interpretation

Based on the mosaic structures, and apparent floating clasts, this facies is interpreted as resulting from low-density turbidity currents (Stow and Johansson, 2000; Sixsmith, 2000). However, the alternation of clay-rich units with laminated units suggests alternation of different types of low-density turbidity currents within the water column. The presence of ripple-laminations, soft-sediment deformation and micro-faults suggests weak tractional processes and sediment instability as mentioned for Facies G.

The association of this facies with Facies G led to the interpretation that it was also deposited at the tail-end of sand-rich high-density turbidity currents.

4.3 Facies associations and depositional elements

The above sedimentary facies can be incorporated into facies associations that make up common deep-water architectural elements, such as channel-fills, overflow deposits, sheet-lobes, and basin plain deposits. This section describes briefly the facies characteristics of each architectural element in order to provide a background for interpretation of the central Bredasdorp deep-water deposits.

Channel-fills

Channel-fills are commonly identified by their concave basal surfaces in cross section in outcrop and seismic reflections. This reflects erosional bases, i.e. the negative relief produced by confined turbidity current flows.

Regardless of the complex internal stratigraphy that develops within channels throughout the time, the characteristic facies of channel-fills are amalgamated, thick, and massive sandstones (Facies A). To a lesser extent, parallel-laminated sandstone (Facies C) is present and combined with high-energy features such as a basal concentration of clay clasts, scour-and-fill structures. Conglomerates (Facies D), which represent the highest energy of all facies, are common in channel-fills as seen at the base of core 2 of E-BA1. An unusual facies association is intersected at the base of some channel-fills and consists of clay-rich siltstone (Facies H), laminated siltstone (Facies G), and to a lesser degree laminated claystone (Facies F) and parallel-laminated sandstone (Facies C). These facies suggest a marginal depositional environment, away from active channel processes but characterise early channel-fill deposits.

Well log expression of channel-fills commonly shows a blocky to serrated blocky pattern with a fining-upward trend. Figure 4.9 shows an outcrop example of a channel-fill complex in the Tanqua Karoo Basin.

Overflow / overbank deposits

Overflow deposits include levee and overbank deposits and develop as sheet beds outside channels apart from deposition that takes place inside the conduit (Miall, 1985). They consist typically of rhythmic thin- to thickly bedded units of ripple-laminated sandstone, or alternating laminated to interbedded sandstone/siltstone and claystone, which is close to the T_b and T_{0-3} intervals of the Bouma and Stow and Shanmugam Sequences. Ripple cross-laminated



Figure 4.9 Example of stacked channel-fill deposits in the proximal part of Fan 3 along the Ongeluks River, Tanqua Basin. View is towards the north. The channel-fills comprise massive sandstone units. Cliff section is 35 m. Note multiple erosional surfaces (photograph from Wickens).

sandstone (Facies B), parallel-laminated sandstone (Facies C), and laminated to interbedded claystone (Facies F) are interpreted as overflow deposits.

Two types of assemblages are observed for these deposits. The first assemblage consists of thin-bedded units displaying a rhythmic alternation of sandstone and claystone beds reaching rarely 1 cm in thickness, e.g. in Figs. 4.7a-b. The second assemblage consists of much thicker sandstone beds (3 cm to about 1 cm) predominantly ripple-laminated, e.g. in Fig. 4.3. Beds of the second assemblage are frequently tabular with flat lower surfaces.

Well log expressions of these deposits display high gamma ray values with serrated patterns probably due to the rhythmic alternation of beds. Stacking patterns on logs indicate frequently retrogradational or progradational trends for this facies association.

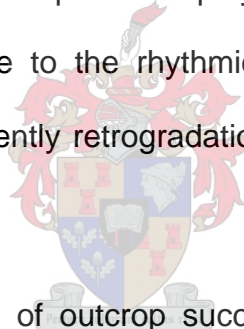


Figure 4.10 gives an example of outcrop succession interpreted to represent overflow (overbank) deposits in the Tanqua Karoo Basin.

Sheet-lobes

Sheet deposits refer to laterally extensive sandstone beds with planar upper and lower surfaces. These deposits can be amalgamated or simply form regionally extensive stacked layered sheets. Massive sandstones (Facies A) and parallel-laminated sandstones (Facies C) presenting sharp planar contacts are interpreted as sheet deposits where lacking highly erosional basal surfaces.

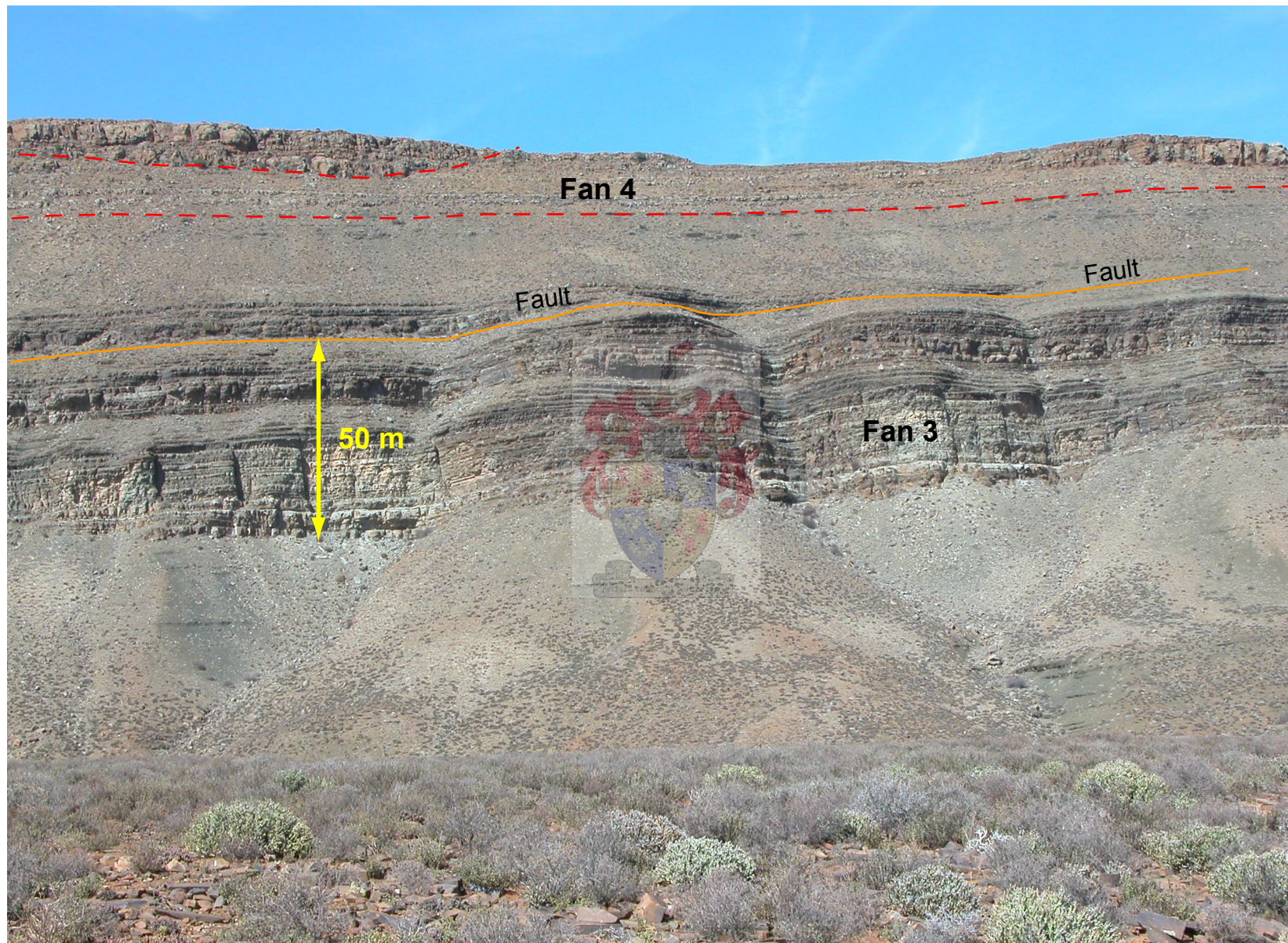


Figure 4.10 Example of overbank deposits. Thin, ripple-cross laminated sandstone beds of Fan 3 at Kleine Rietfontein, Tanqua subbasin. View is towards the south. Thickness is 50 m. Note extreme lateral continuity of beds, channel at the and the position of reverse fault (photograph from Wickens).

Well log expressions of this facies association can show blocky patterns where beds are amalgamated, but also show serrated blocky patterns when beds are stacked layered sheets. Figure 4.11 shows an example of succession interpreted to represent sheet deposits in the Tanqua Karoo Basin.

Basin plain deposits

Basin plain deposits comprise very fine-grained sediments that settle down during quiet times after turbidity flows. They are claystone, siltstone, and very thinly interbedded sandstone and siltstone. Massive claystone (Facies E) and alternating laminated to interbedded sandstone/siltstone and claystone (Facies F) are thought to represent continuous background deposition. The former represents true hemipelagic deposition from suspension, whereas the presence of thin laminations (Facies F) suggests dilute mud-rich turbidity currents on the distal basin floor.

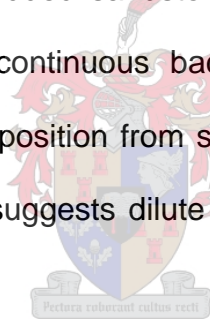


Figure 4.12 shows an example of basin plain deposits from the Tanqua Karoo Basin.



Figure 4.11 Example of sheet deposits. A) Fan A of the Laingsburg Fan Complex, Karoo Basin, Grootkloof, Laingsburg. B) Fan 3, Tanqua Fan Complex, Karoo Basin (photographs from Wickens).



Figure 4.12 Example of basin plain deposits representing interfan unit between Fans 3 and 4, Tanqua subbasin, and comprising finely laminated shale. Note overlying sandstone beds (photograph from Wickens).

CHAPTER 5

APPLICATION OF SEQUENCE STRATIGRAPHY

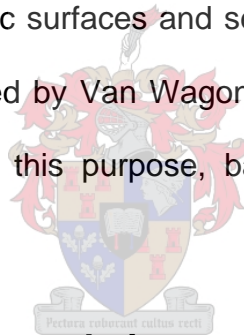
5.1 Introduction

Posamentier *et al.* (1988) and Van Wagoner (1995) defined sequence stratigraphy as the study of rock relationship within a time-stratigraphic framework of repetitive, genetically related strata bounded by surfaces of erosion or non-deposition, or their correlative conformities. Therefore sequence stratigraphy is considered as a genetic approach that provides a chronostratigraphic framework for correlation of sedimentary facies using key bedding surfaces and genetically related groups of rock strata with specific sedimentary characteristics. Sequence stratigraphy was used initially for shallow marine depositional environments, but its approach has recently been applied to deep-water deposits (Posamentier *et al.*, 1991 and Shanmugam *et al.*, 1994). The same approach is used to interpret the stratigraphic succession in the 9A to 14A Sequences of the central Bredasdorp Basin.

With the aim of applying sequence stratigraphy in the investigated sedimentary succession, well logs and cores form the data base for interpretation. The appropriate well logs are gamma ray, resistivity and sonic logs. Gamma ray logs segregate primary coarse-grained units (sandstones and conglomerates) from fines (siltstones and claystones). Sandstones present usually low gamma ray

values (15-45 API) in contrast to claystones that present high gamma ray values (100-120 API). A useful way to distinguish these rocks is to draw a vertical line at 60-80 API, depending on the log scale. The left hand side of the line is ascribed to sandstone and conglomerate, whereas the right hand side indicates fines (siltstone and claystone).

This chapter provides a brief background on sequence stratigraphic concepts that are used in this investigation. These concepts are outlined in Galloway (1989), Van Wagoner *et al.* (1990), Vail *et al.* (1991), Mitchum *et al.* (1993), Miall (1996), Posamentier and Allen (1999) and Sixsmith (2000). They are based on identification of key stratigraphic surfaces and sea-level cycles from lowstand to highstand. Methodology outlined by Van Wagoner *et al.* (1990) and by Kendall and Alnaji (2005) is used for this purpose, based on both gamma ray and resistivity logs.



5.2 Sea-level and accommodation

Sea-level and accommodation are critical to sequence stratigraphy models (Flint *et al.*, 1995), because they control the volume of sediment that can accumulate in a basin. Posamentier *et al.* (1988) and Van Wagoner *et al.* (1990) recognised that facies architecture is dependent on variations in the rate of sediment supply and rate of change in accommodation. Two terms are used to define sea-level variation i.e. Eustatic Sea-level (ESL) and Relative Sea-level (RSL). ESL is the absolute sea-level variation relative to a fixed point, commonly taken at the centre of the earth (Fig. 5.1). RSL is a combination of eustatic sea-level and

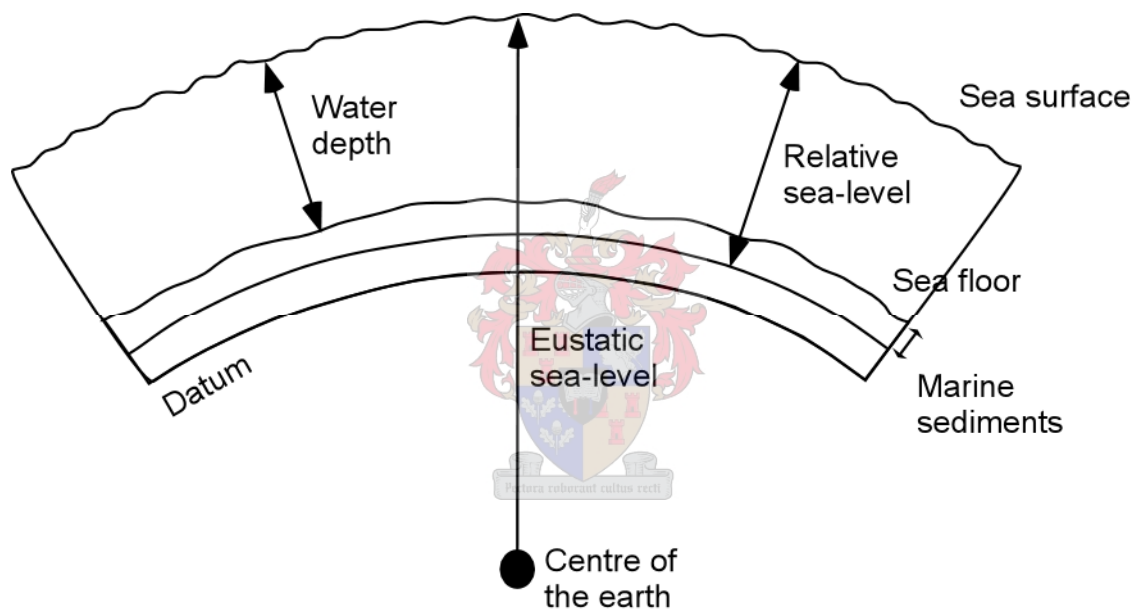


Figure 5.1 Difference between eustatic sea-level and relative sea-level. The datum is an imaginary, reference horizon taken just beneath the sea floor to monitor the magnitude of vertical tectonics relative to the centre of the earth (Catuneanu, 2002).

subsidence or uplift of the seabed (Fig. 5.1). Relative sea-level changes control accommodation space, which is the available space for deposition of sediments. A rise in relative sea-level will increase accommodation space, whereas a fall in relative sea-level will decrease accommodation space. Accommodation space is always high in the deep basin, and low in the shelf and slope. This leads sediments to bypass the shelf and slope to be deposited in the deep basin.

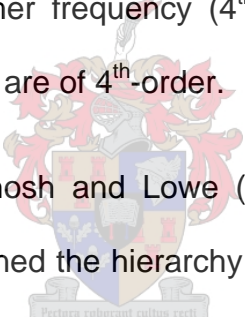
Autocyclic and allocyclic processes control deposition of sediments and play a major role in the distribution of depositional elements within a depositional system (Catuneanu *et al.*, 2005). Autocyclic processes occur at facies scale and are evaluated through sedimentology and facies analysis (see Chapter 4). Allocyclic processes, on the other hand, take place within the basin and control the regional architecture of the basin-fill. Relative sea-level changes, which are part of allocyclic processes, create stratigraphic key surfaces. The latter provide a platform to correlate depositional trends recorded at any given time in all environments established within a sedimentary basin (Catuneanu *et al.*, 2005).

5.3 Type of sequences and internal hierarchy within sequences

Mitchum *et al.* (1977) defined a depositional sequence as a sedimentary interval composed of a relatively conformable succession of genetically related strata bounded below and above by unconformities or their correlative conformities. Otherwise, a depositional sequence is a package of units deposited between a decrease and increase of accommodation space, related to sea-level fall and

rise, respectively. Most sequences identified in the Bredasdorp Basin are Type-1 sequences (Brown *et al.*, 1995), due to Type-1 sequence boundaries present below each sequence.

The fundamental sequences offshore South Africa are sequences of third-order frequency. Duration of these third-order sequences ranges between 1-3 Ma, whereas higher frequency fourth-order sequences represent approximately 0.1-0.5 Ma in duration (Brown *et al.*, 1995). Although duration was not estimated, the less widespread flooding surfaces (transgressive and maximum flooding surfaces) and unit boundaries (sequence boundaries) identified within third-order sequences may represent higher frequency (4th-order) surfaces, inferring that internal depositional sequences are of 4th-order.



Mutti and Normark (1987), Ghosh and Lowe (1993), Catuneanu (2002), and Hickson and Lowe (2002), outlined the hierarchy within turbidite sequences (Fig. 5.2). This hierarchy presents a turbidite complex as of first-order scale. Turbidite complexes are commonly composed of several turbidite systems or individual fans separated by basinal mudstone units. A turbidite system corresponds to second-order scale and consists of genetically related successions forming turbidite stages. Each stage (3rd-order scale) indicates a specific period of fan system growth bounded by erosion or correlating surfaces. Turbidite substages correspond to fourth-order scale and characterise the depositional facies or facies associations.

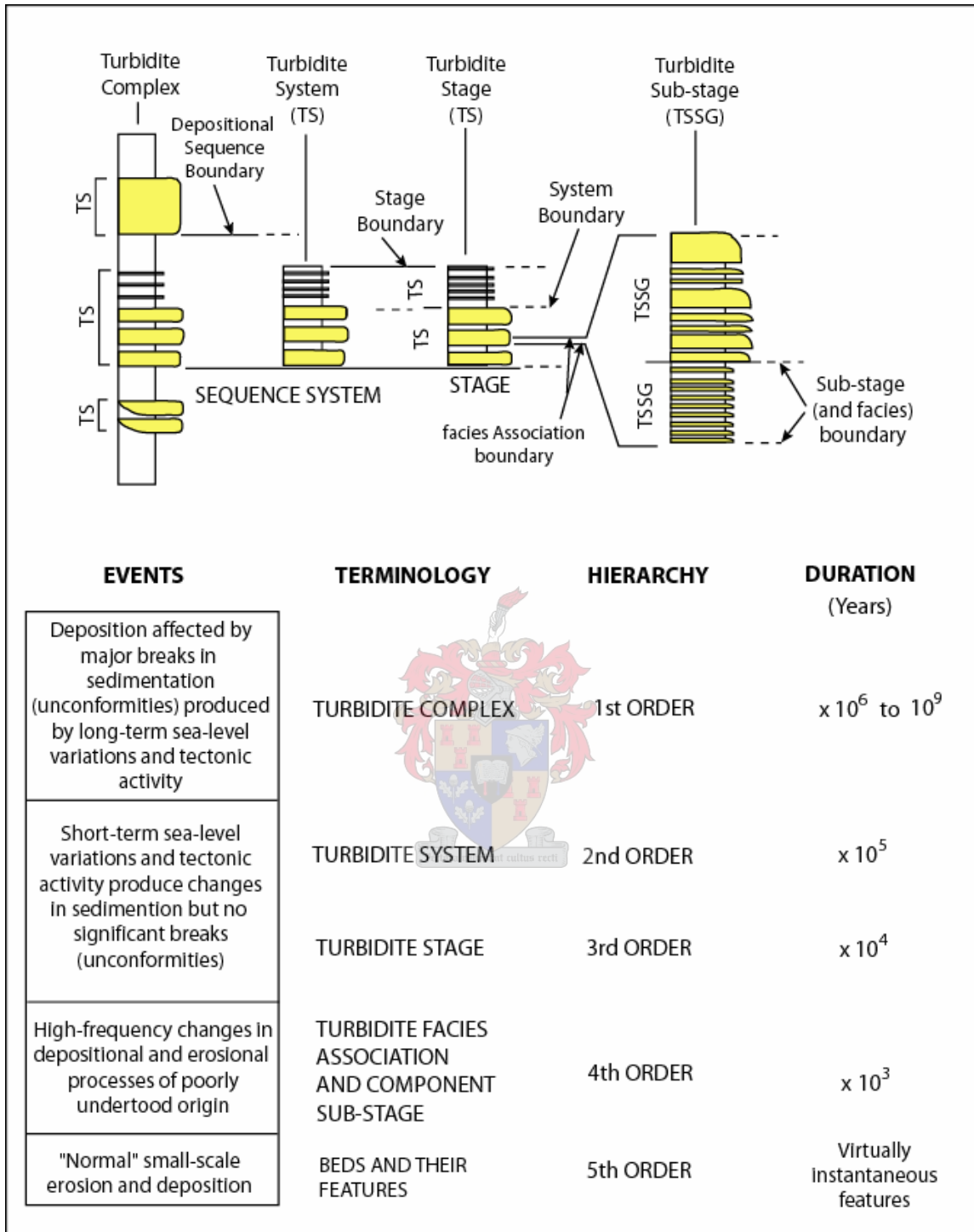


Figure 5.2 Hierarchical organization of turbidites by sub-dividing a turbidite fan sequence into a turbidite complex, system, stage and sub-stage based on physical scale of deposits (from Mutti and Normark, 1987).

5.4 Key surfaces

The major unconformities bounding the investigated third-order sequences in the Bredasdorp Basin were placed on the well logs, based on data provided by PetroSA. New positions were proposed for some of them after further analysis of gamma ray and sonic logs as indicated in Table 5.1. Stratigraphic surfaces identified during a high-resolution stratigraphic analysis include sequence boundary surfaces, transgressive surfaces (or initial fan flooding surfaces), and maximum flooding surfaces. Each surface defines a major change in deposition which is reflected on well logs as lithological breaks (Serra and Sulpice, 1975). Figure 5.3 illustrates the relationship between key surface and sea-level changes and the distribution of architectural elements along the depositional profile.

5.4.1 Sequence boundaries

The sequence boundary (SB) is an unconformity that characterises the base of a sequence, often marked by an abrupt increase in sand supply, frequently termed regression (Catuneanu, 2002). When a regression is normal, a SB forms a Type 2 unconformity, whereas a forced regression generates a Type 1 unconformity (Coe *et al.*, 2003). It has been demonstrated that sequence boundaries are not always erosive everywhere, despite that they are generated by a sea-level fall.

On well logs (Figs. 5.4 and 5.5), sequence boundaries are commonly recognized by an abrupt increase in gamma ray response below thick sandstones or sand-rich intervals and concurrently a decrease of resistivity values (Kendall and

	WELLS														
	E-AA1	E-AA2	E-AD1	E-AJ1	E-AO1	E-AO2	E-AR1	E-BA1	E-BA2	E-BA3	E-BB1	E-BE1	E-CA1	E-CB2	E-CR1
14At1	2525	2507	2570	2736	2635*	2628	2496	2355	2358	2358*	2592	2707	2478	2620	2719
13Amfs	2703*	2694	2754	2868*	2843*	2805	2720	2594	2580	2588.5	2761	2919.5	2704	2756	
13At1	2790	2789	2845*	2954	2910*	2911	2841	2694	2736.5*	2707	2877	2989	2771		
12At1	2806	2827	2865	2999	2940	2948*	2905	2735	2755	2740	2877	3030*	2800		
11At1	2806	2827*	2865	2999	2940	2948*	2905	2792	2770	2806.5	2877	3030*	2832*		
10At1	2939	2969	3014	3068	3015*	3008*	2955	2848*	2866*	2866	2975	3104*	2933		
9At1	3167	3061	3082	3261	3086*	3088	3057*	2906*	2913.5	2992	3047		3021		

Table 5.1 Depth, in meter below KB, of major unconformities in the investigated wells. Value with (*) are locations of proposed unconformities in this investigation, after further analysis of well logs.

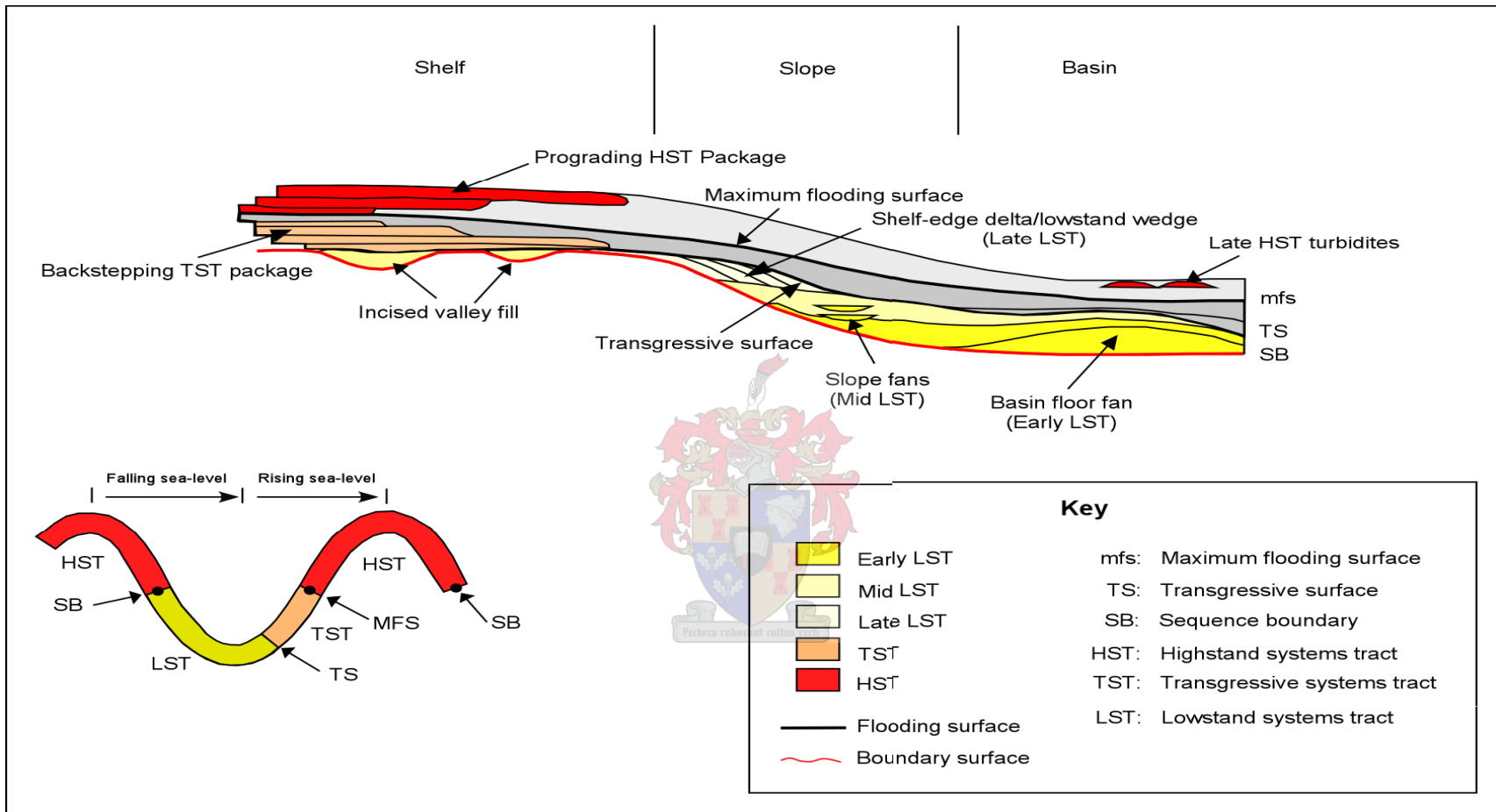


Figure 5.3 Idealised stratigraphy in a basin coupled with a relative sea-level curve. Position of systems tracts and key surfaces are given on the curve. The LST is recognised by erosional surfaces. Deposition of TST and HST is concentrated on the shelf and is represented in the deep basin by a condensed section (from Sixsmith, 2000).

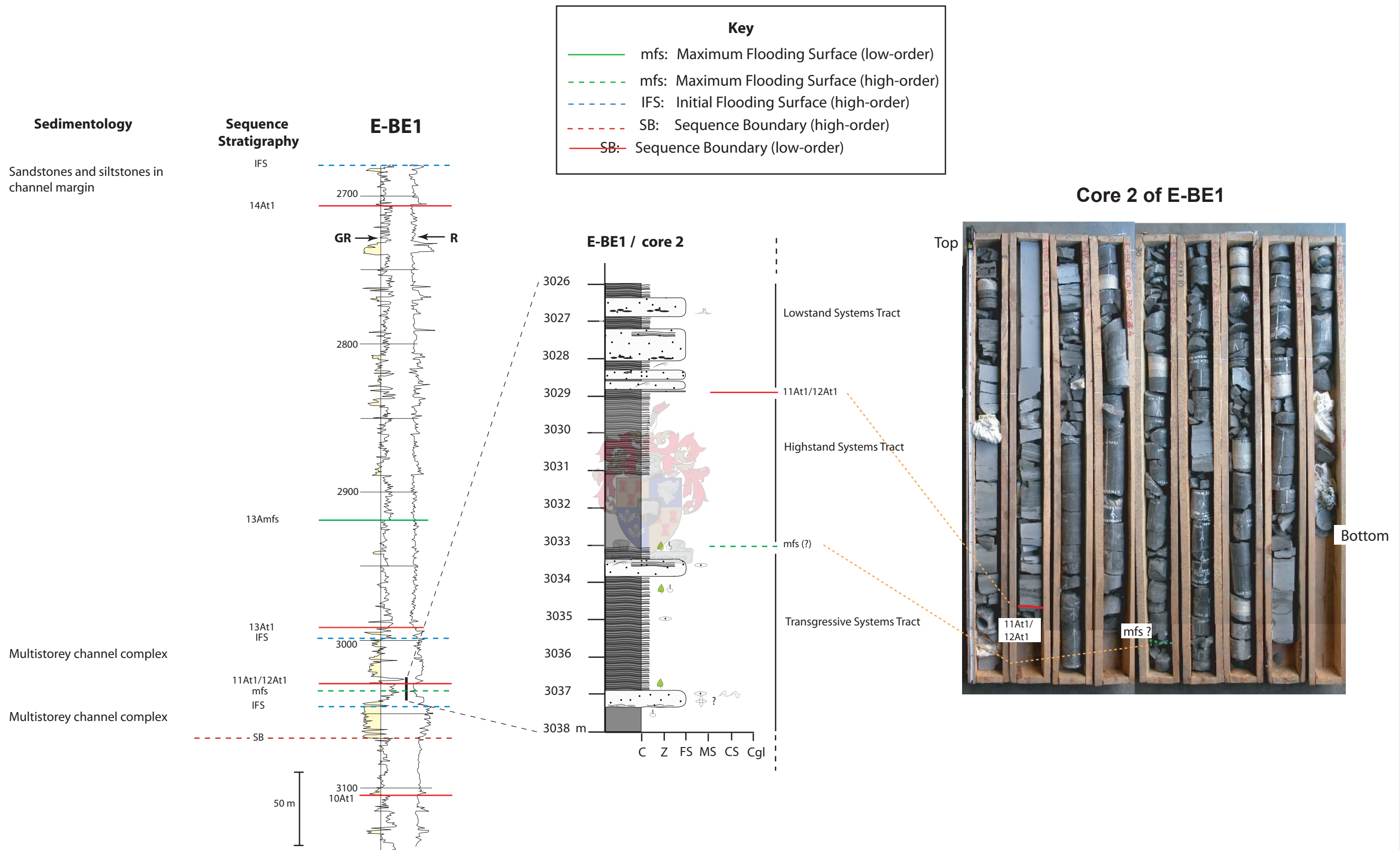
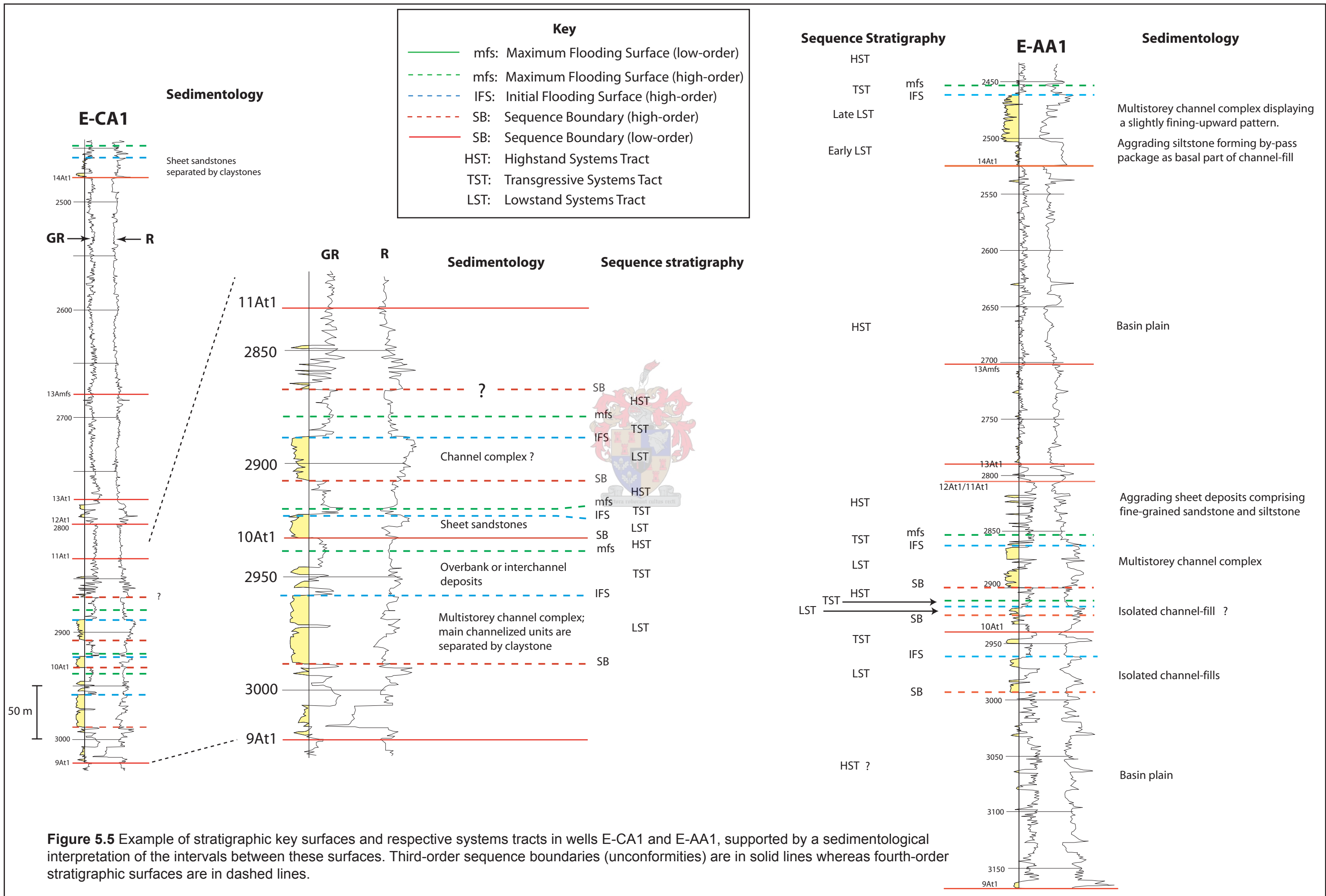
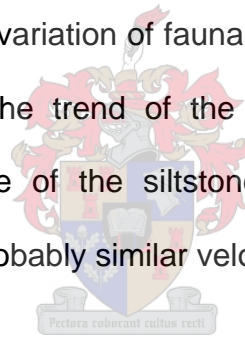


Figure 5.4 Application of sequence stratigraphy in well E-BE1, supported by core interpretation. Stratigraphic key surfaces, respective systems tracts and possible sedimentological interpretation of the intervals between these surfaces are given. Boundaries with solid lines are low-order (3rd-order) boundaries whereas dashed lines are high-order (4th-order) boundaries.



Alnaji, 2005). However, some sequence boundaries were picked below intervals of fine-grained sediments lying underneath major sandstone packages in this investigation (Fig. 5.6). The choice of this surface as a sequence boundary by PetroSA was probably supported by a palaeontology and a combination of well log expression across the lowstand package.

One of the log response characteristics picked for a sequence boundary surface below a siltstone unit underneath the major sand units in wells E-BA1, E-AA2, E-AA1, and E-AR1, is the drastic change of the sonic log but also the resistivity log across the base of a siltstone package. This change is not only related to a grain size contrast but also due to a variation of faunal occurrence across this surface. The sonic response follows the trend of the overlying sandstone units and changes only below the base of the siltstone. This may result from close lithological composition, and probably similar velocity of both units (Rider, 1986).



In cores, sequence boundaries commonly exhibit an erosive character (for example core 1 of borehole E-CA1 and core 1 of borehole E-AA1), but can also display a sharp surface without any sign of erosion.

5.4.2 Transgressive surfaces

Transgressive surfaces (TS), generally located at the top of sandstone-rich successions interpreted to represent lowstand systems tracts (Figs. 5.4 and 5.5). They mark the first major flooding surface after the sequence boundary, indicating a deepening of the environment during relative sea-level rise

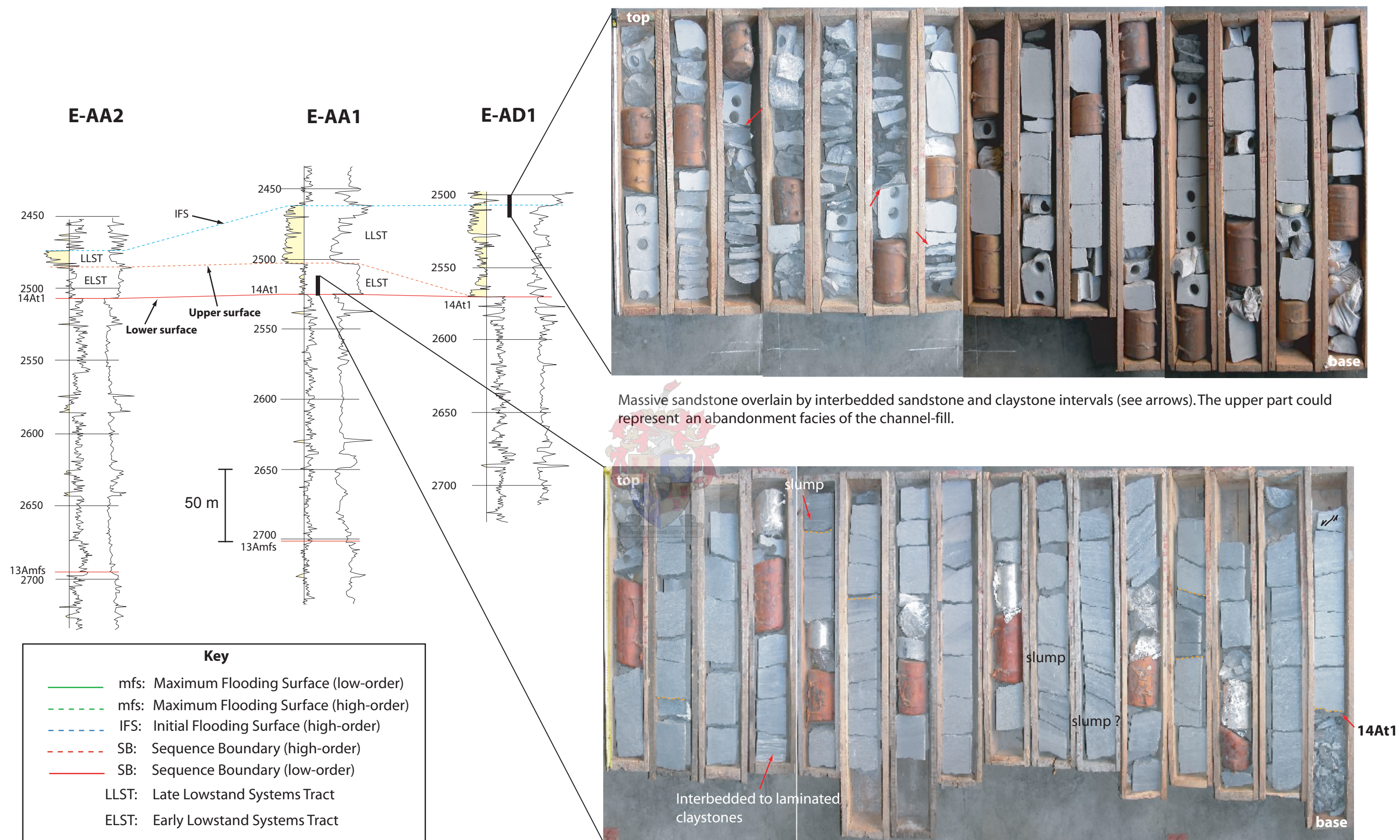


Figure 5.6 Example of two distinct surfaces, named here lower and upper surfaces within the lowstand deposits. The upper surface separates the lower deposits which are interpreted as a by-pass package underlying the channel-fill deposits. By-pass deposits consist of siltstone with minor sandstone beds. Channel-fill deposits consist of massive sandstones.

Siltstone succession above 14At1 unconformity is interpreted as a by-pass facies constituting the basal part of the channel-fill.

(Boyer *et al.*, 2005). As a result, finer sediments, mostly clays and silts, are introduced into the environment. Transgressive surfaces usually separate parasequences of the TST from the lowstand systems tract. It corresponds to the initial flooding surface (IFS) of Sixsmith (2000). There are cases where this surface merges with the sequence boundary into a single surface. Such situations occur commonly in the landward areas of passive margins.

The transgressive surface is recognised where the gamma ray values increase and resistivity values decrease above the lowstand systems tract (Boyer *et al.*, 2005). In core 2 of E-AO1, for example, transgressive surfaces clearly display sharp passages of sandstone into mudstone, more frequently consisting of siltstone and claystone layers.

Sixsmith (2000) proposed additional surfaces within the flooding interval overlying sandstone successions, which present evidence of increase of accommodation space. These surfaces are an initial fan flooding surface (IFFS) and a maximum fan flooding surface (MFFS).

The IFFS is the first surface that records the onset of fan termination. It is located between a sandstone-rich succession and an overlying retrogradational thinning- and fining-upward succession at the base of a mudstone interval. The MFFS is located between the retrogradational succession and the hemipelagic mudstone. The latter surface marks therefore the base of the hemipelagic mudstone interval.

5.4.3 Maximum flooding surfaces

A maximum flooding surface (mfs) marks the end of a transgression (Posamentier *et al.*, 1988; Van Wagoner *et al.*, 1988; Galloway, 1989) and marks the turn-around from retrogradational stacking in the transgressive systems tract to aggradational or progradational stacking in the early highstand systems tract. The mfs represents the last significant flooding surface found in the transgressive systems tract occurring during relative sea-level rise (Gibbons *et al.*, 1993), and marks the deepest water facies within a sequence. Condense section is characterised by slow deposition of pelagic-hemipelagic sediments and allows enrichment of autogenic minerals such as glauconite, pyrite, and siderite.

On the gamma ray log, the mfs corresponds to the maximum of radioactivity above the transgressive deposits (Fig. 5.4), coupled with the lowest values of resistivity (Boyer *et al.*, 2005). Core 2 of E-BE1 and core 2 of E-AO2 both intersected mfs, which are characterized by mudstone, enriched with shell fragments. Plant fragments (e.g. in core 2 of E-BE1) as well as pyrite (e.g. in core 2 of E-BE1) are also present.

5.5 Systems tracts

Systems tracts define a linkage of contemporaneous depositional systems, forming the subdivision of a depositional sequence (Brown and Fisher, 1977), and are related to cycles of relative sea-level changes (Boggs, 2001). Interpretation of systems tracts are based on stratal stacking patterns, position

within the sequence, and types of bounding surfaces. The Exxon model used to subdivide depositional sequences in this investigation is a tripartite scheme, with lowstand, transgressive and highstand systems tracts (Van Wagoner *et al.* 1988)

5.5.1 Lowstand systems tract

The lowstand systems tract (LST) is bounded at the base and top by a sequence boundary and a transgressive surface, respectively (Figs. 5.3, 5.4 and 5.5). The LST is the set of depositional systems that form during relative sea-level fall and commonly consists of sediment gravity flows deposited on the basin floor and slope environment. Two subdivisions were identified within the lowstand systems tract, based on the two surfaces recorded in a few wells. These are termed here early lowstand systems tract (ELST) and late lowstand systems tracts (LLST) (Fig. 5.6).



Sixsmith (2000) proposed a tripartite subdivision of the lowstand systems tract into early, middle and late LST. The early LST is characterised by gravity flow deposits with a basal erosional surface. The middle LST indicates slope deposition and associated slope fan systems. The late LST is characterised by shelf edge delta deposition and backfilling of incised valleys. In the deep basin, only mudstone is deposited during this phase.

In this study, the early LST deposits correspond to a siltstone interval directly overlying the sequence boundary in certain wells (e.g. Fig. 5.6). These siltstones are equivalent to sand-rich units on the basin floor. The late LST is characterised

by thick sandstones, indicating submarine fan or incised valleys (channel-fill and channel complexes). The middle LST was not identified. The late LST or simply LST are generally characterised by low gamma ray and progressive increase of resistivity. The gamma ray trends display fining-upward, blocky and serrated blocky patterns.

5.5.2 Transgressive systems tract

The transgressive systems tract (TST) is bounded by a TS or IFS at the base and by a mfs at the top. The TST develops during relative sea-level rise when the rate of rise exceeds the sedimentation rate (Figs. 5.3, 5.4 and 5.5). It commonly exhibits overall fining-upward profiles capped with shale at the top, indicating a marine transgression. The shales represent highstand deposits.

5.5.3 Highstand systems tract

The highstand systems tract (HST) is bounded by a maximum flooding surface at the base and a sequence boundary at the top (Figs. 5.3, 5.4 and 5.5). It corresponds to the late stage of relative sea-level rise from mfs to SB (Gibbons *et al.*, 1993). During this period, the rate of rise drops below the sedimentation rate and generates a normal regression of the shoreline. Commonly, these deposits constitute hemipelagic deposits (shales and silts) that form in an offshore environment.

CHAPTER 6

STRATIGRAPHY AND SEDIMENTOLOGY

6.1 Introduction

This section aims to propose an accurate description and interpretation of the sedimentology of each depositional sequence using facies association development and distribution within the concepts of deep-water sequence stratigraphy. Conventional wireline logs were used for constructing sections and maps in order to capture thickness variation and facies distribution within depositional sequences. The approach followed here for correlating key stratigraphic surfaces and stacking patterns within individual sequences compares with previous methods used by Bowen and Weimer (2003), Turner *et al.* (2001), and Tearpock and Bischke (2003).

6.2 Correlation criteria

From the eighteen wells in the area, of which the distance between the wells falls between ~ 1.70 km and ~ 14.14 km, four sections were constructed. Sections 1 and 2 extend roughly northwest-southeast (NW-SE) whereas Sections 3 and 4 extend roughly North-South (Fig. 6.1). The 13Amfs, which is considered as the only reliable datum for Bredasdorp Basin stratigraphy, was used as a flattened surface for correlation purposes. This is because it is intersected by all

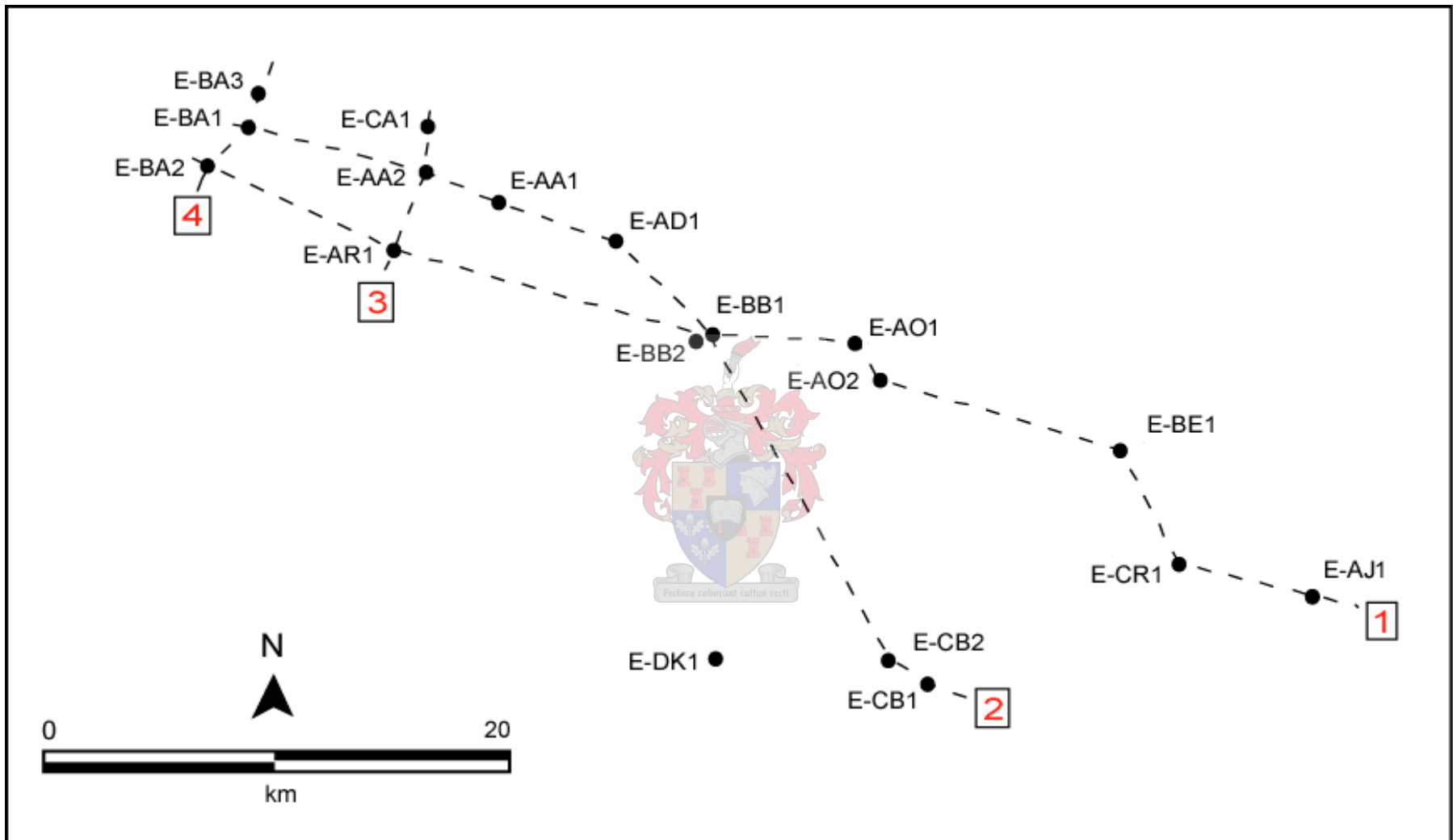


Figure 6.1 Well location and correlation sections over the study area. 1, 2, 3 and 4 indicate sections 1-4, respectively.

boreholes. The 13Amfs represents a marine condensed section resulting from deposition of mud and organics during a long period of basin starvation. Intersection of this surface by all boreholes as well as the compositional characteristic confirms the extensive development of this surface.

The purpose of these sections is to give a broad insight of possible vertical distribution of the depositional elements throughout the investigated interval. The log response models of facies association of Galloway and Hobday (1996) were used to build an interpretation of the depositional environment from the wireline-log data (Figs. 6.2 and 6.3). From these log response models, sand units with a blocky gamma ray shape may be interpreted as a channel-fill or channel complex or amalgamated sheet sandstones. Sand units displaying a bell shape indicate a fining-upward succession, indicating either a progressive change from sand to claystone or transition of sand beds to interbedded sand-clay unit. This bell shape may represent channel-fills and their abandonment facies. Sand units presenting a funnel shape, indicating an upward-thickening or coarsening succession, could be interpreted as a crevasse splay or prograding submarine fan lobes. Well log intervals displaying a serrated shape, indicating aggradation of thin clay and sand or silt layers, may represent basin plain setting or sheet lobe turbidites.

Well log characteristics and interpretation of the different facies or, more reasonably, facies associations, as described in the preceding chapters, form the basis for the interpretation of stratigraphic units identified within the sequences.

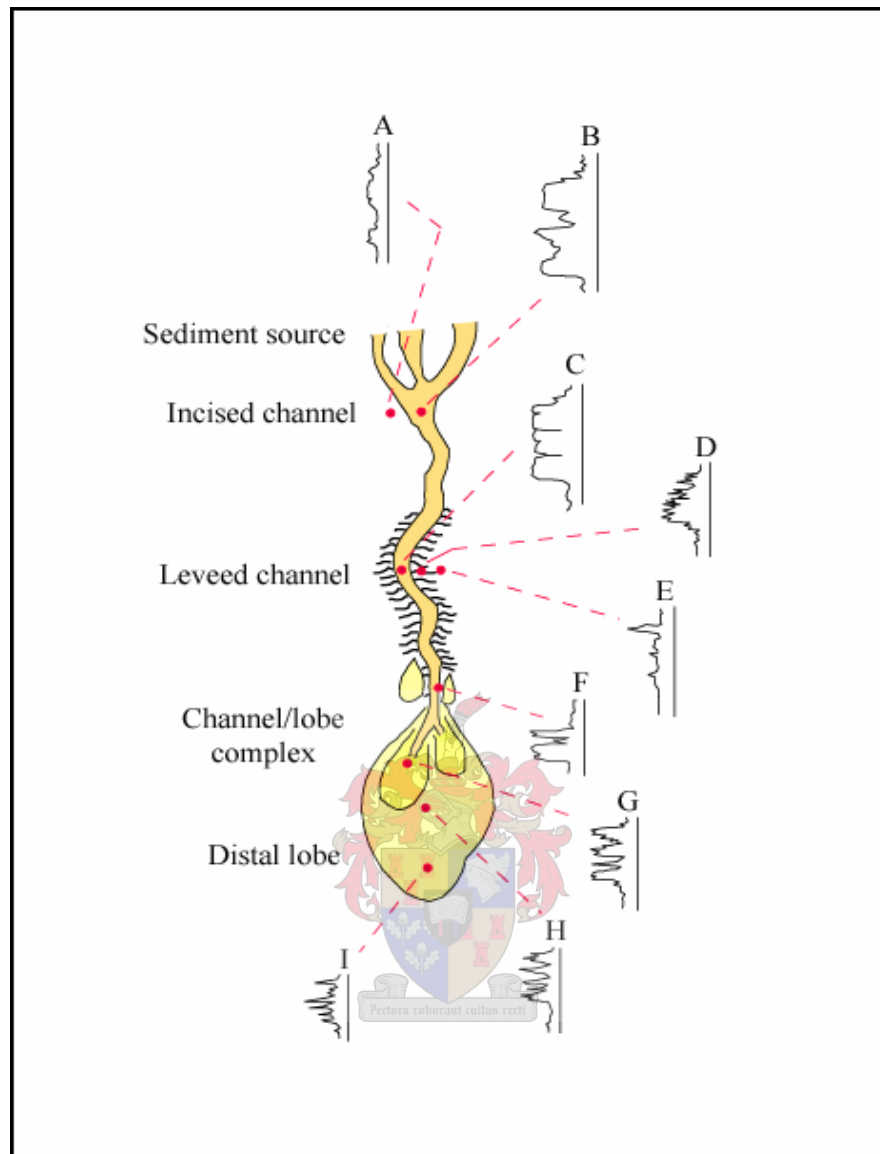


Figure 6.2 Depositional elements and generalized log responses of a channel/lobe complex. (A) Bounding upper slope slump and cohesive debris flow deposits. (B) Erosional channel-fill with sandy to muddy debris flow deposits. (C) Amalgamated channel-fills. (D) Interbedded levee deposits. (E) Overbank deposits, muddy interchannel mud flow, fine-grained turbidites. (F) Channel/lobe transition. (G) Stacked turbidites of the proximal lobe. (H) Interbedded turbidites of the middle lobe. (I) Basin plain deposits (after Galloway and Hobday, 1996).

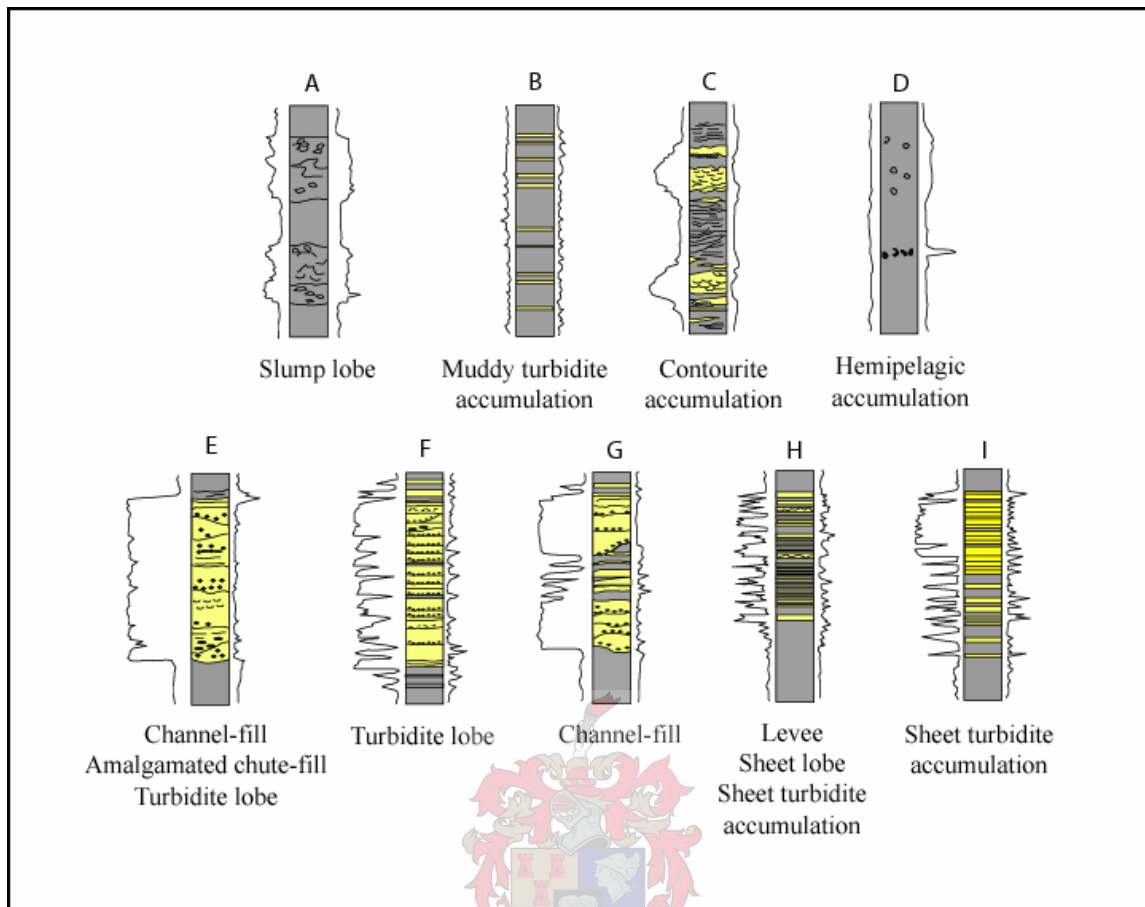


Figure 6.3 Typical vertical facies associations and log responses for deep-water deposits. Note that similar facies associations can occur in more than one environment. Each log segment may range from tens to a few hundred meters (after Galloway and Hobday, 1996).

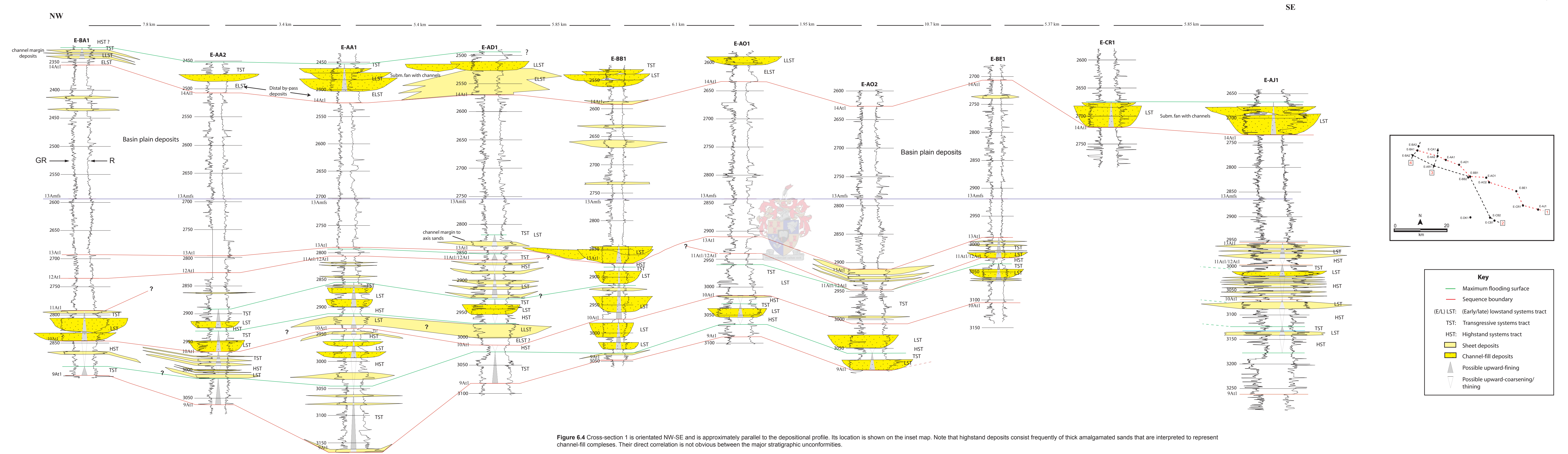
The surfaces that separate these facies associations reflect specific phases of sea-level fall and rise (Mitchum, 1977; Posamentier *et al.*, 1988).

Each 3rd-order depositional sequence was subdivided into several 4th-order depositional sequences, which comprise stacking of systems tracts, i.e. LST-TST-HST. Recognition and correlation of these 4th-order sequences require identification of 4th-order maximum flooding surfaces usually located within mudstone intervals overlying sand-rich successions. Autocyclic processes (or switching) within sequences render correlation of these surfaces difficult in places.

It appears, throughout the four sections (Figs. 6.4 – 6.7), that the sand-to-shale ratio is particularly high within the 9A and 12A Sequences. This sand-to-shale ratio was estimated to be between 12.3% and 65.5%, by using gamma ray curve. The ratio was calculated for each well by dividing the cumulative thickness of coarse clastic rock, sandstone and conglomerate, to that of the fine clastic rock, siltstone and claystone.

6.3 Stratigraphic evolution of sequences

Sequences are individually investigated based on gamma ray log responses in each well. The isochron map of 9A to 13A Sequences, shown in Figure 6.8, displays the time variation between the 9At1 and 14At1 seismic reflections. Its 280 ms contour line is used to show an outline of the depositional trend. Construction of thickness variation maps takes into account drilled thickness of



8.78 km

14.14 km

16.09 km

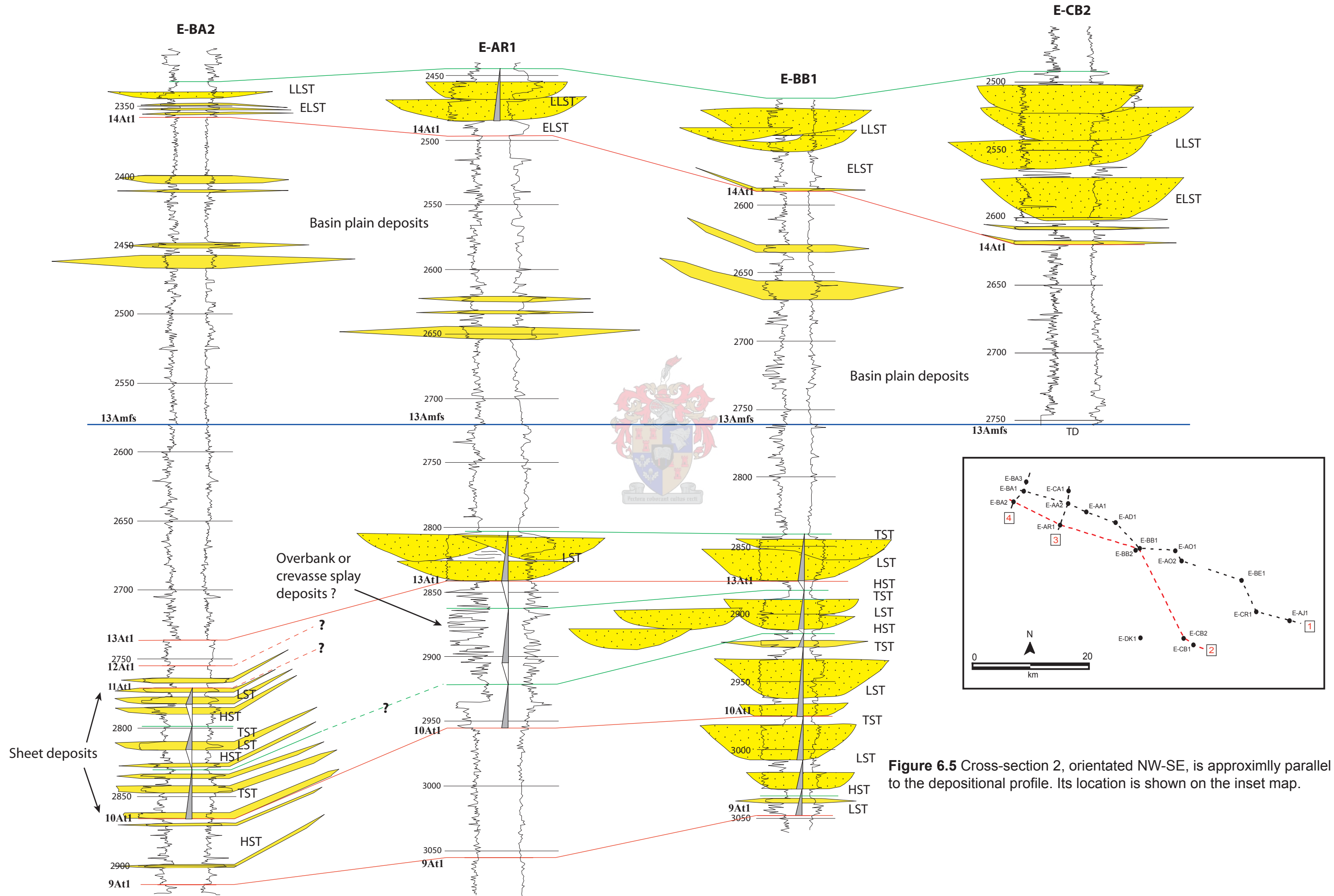


Figure 6.5 Cross-section 2, orientated NW-SE, is approximately parallel to the depositional profile. Its location is shown on the inset map.

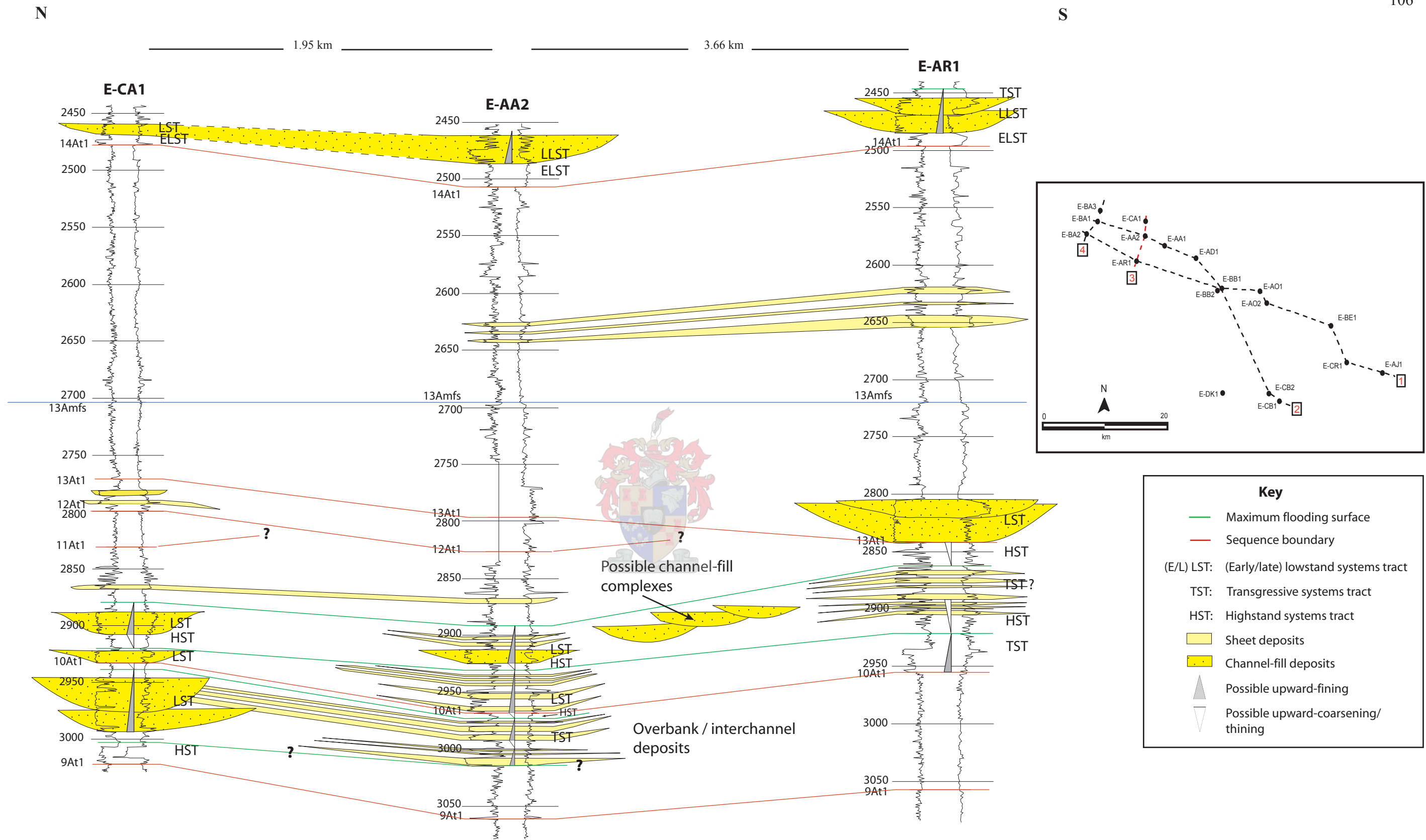


Figure 6.6 Cross-section 3, oriented North-South, is normal to the depositional profile. Its location is shown on the inset map on the inset map.

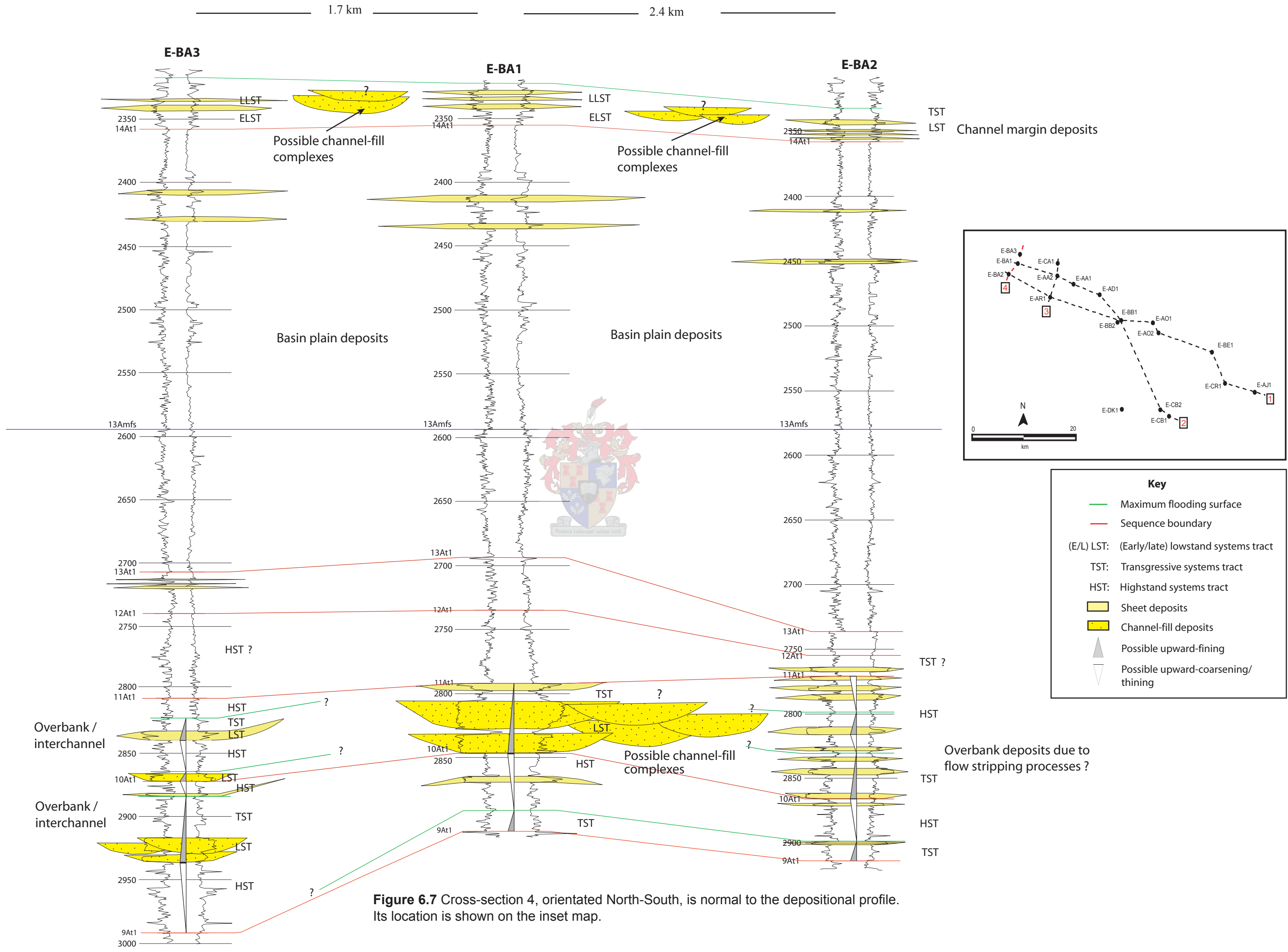


Figure 6.7 Cross-section 4, orientated North-South, is normal to the depositional profile. Its location is shown on the inset map.

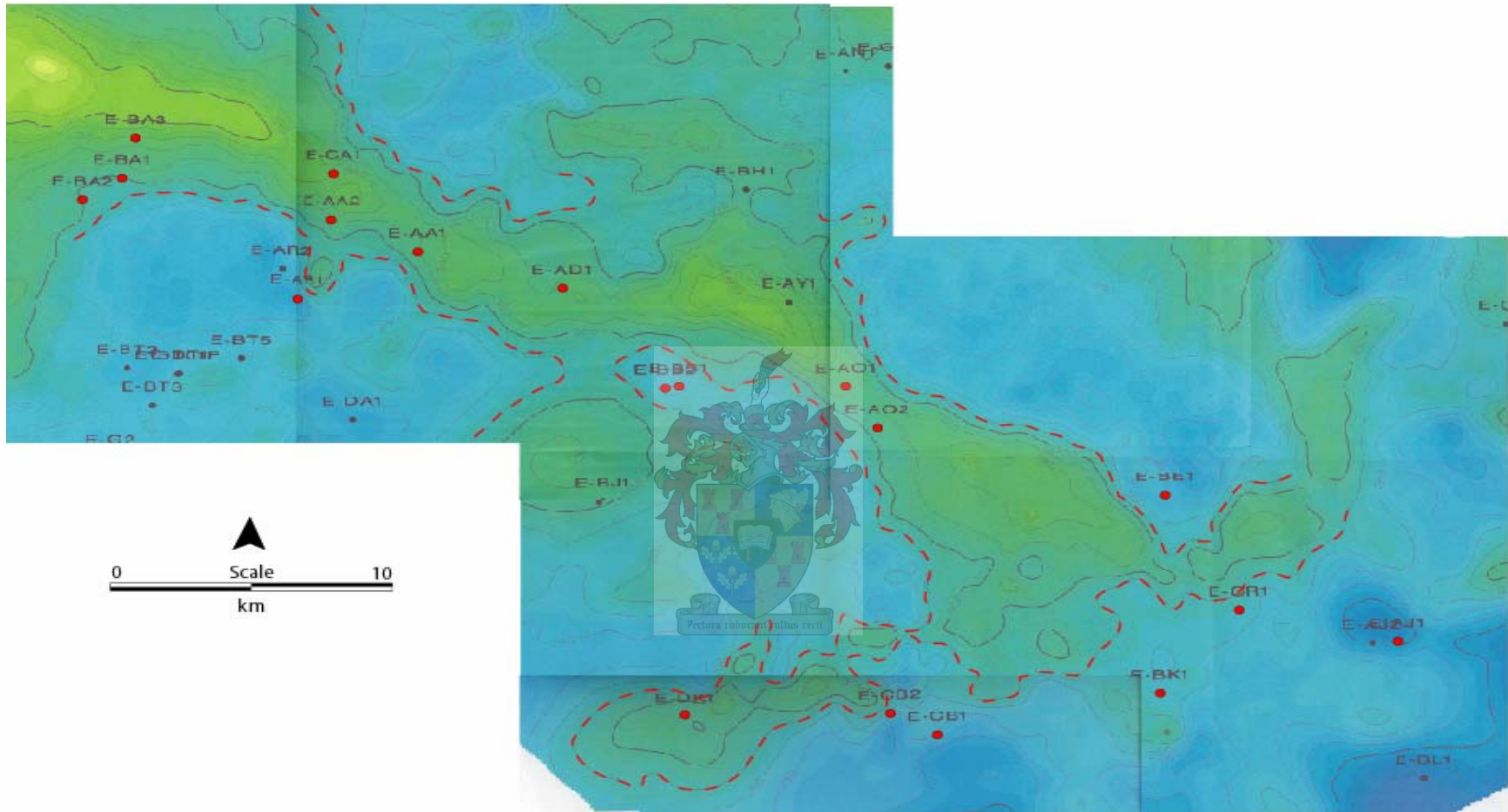


Figure 6.8 Isochron map of the 9A to 13A Sequence. Investigated wells and the 280 ms contour line, which is used for guidance of the general depositional trend, are outlined in red (Unpublished map from PetroSA, Turner, 2006).

sequences in each well. Net-sand maps show the cumulative thickness of sand layers crossed by the well. Facies maps display possible vertical stacking pattern of channel-fills, overbank deposits and basin plain deposits, considered to be the main facies.

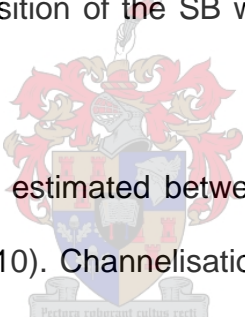
6.3.1 9A Sequence

The 9At1 unconformity, located at the base of the 9A sequence, was intersected in most wells, except for wells E-BE1, E-CB2 and E-CR1 where drilling was not deep enough. This surface is sharp and shows an erosive character only in E-AO2 and E-BB1, where it occurs at the base of channel-fills. It is overlain in the western side of the study area by bedded sand and clay intervals displaying successively a slight upward-fining trend, then an upward-coarsening trend. This bedded interval is in turn overlain by thick sandstone packages, displaying blocky to serrated blocky pattern, both interpreted as channel complexes. Two amalgamated blocky sand units are intersected in E-AO2 (Fig. 6.3) which suggest two depositional cycles bounded by a lower erosional surface. If so, the bedded interval intersected below the upper sand package in E-AO1, E-CA1 and E-BB1 may correspond to interbedded successions marginal to channel complexes. This lower channel complex was not intersected up-dip, hence its absence in boreholes.

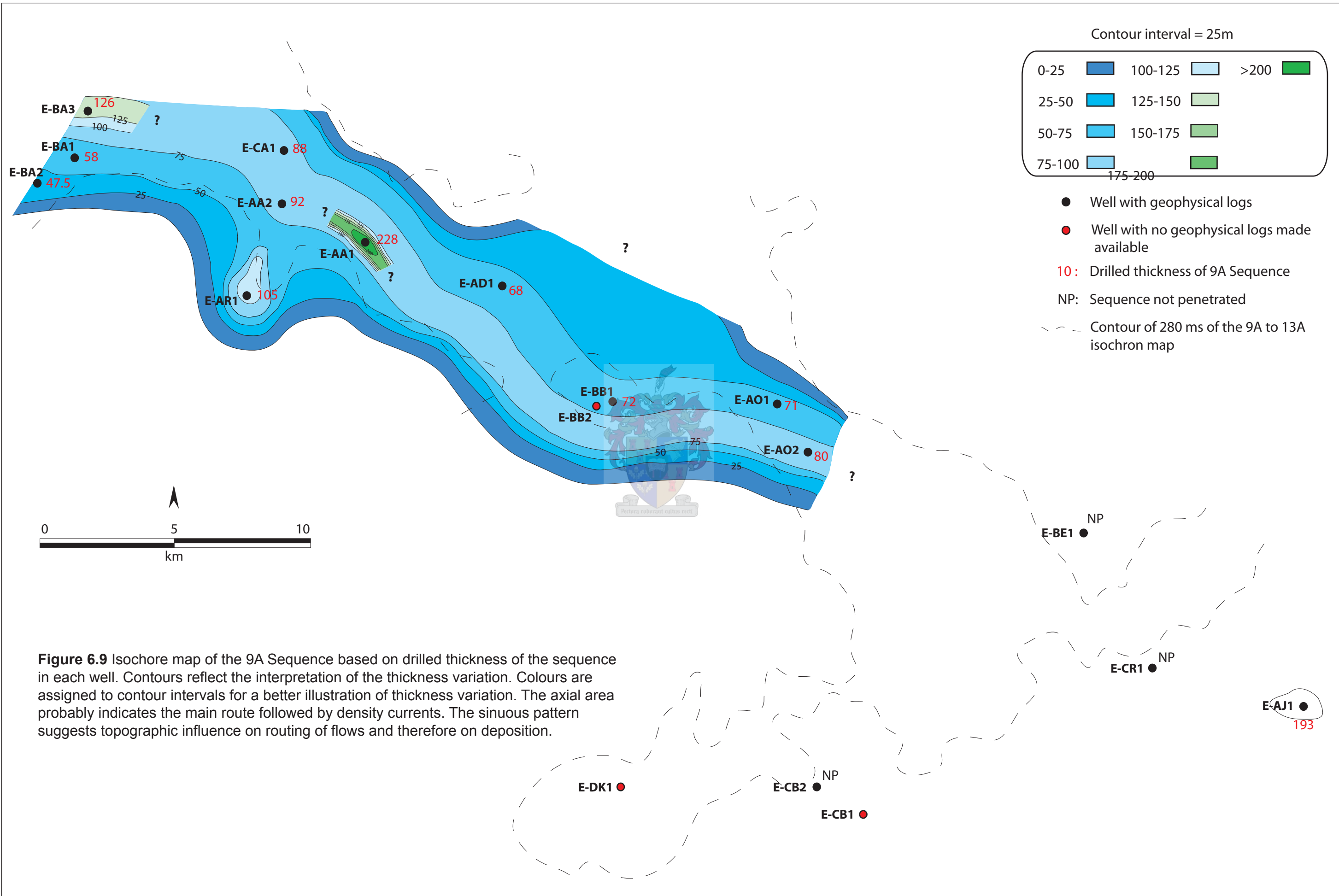
A common characteristic of the two depositional cycles is that lowstand deposits are overlain by progressively finer deposits suggesting a back-fill process that

develop as sea-level rises. At a certain point of sea-level rise, deposition is clay-dominated and characterises highstand deposits.

Thickness of the 9A Sequence shows great variation over the area (Fig. 6.9). Drilled thickness of the sequence was mapped and ranges between 47 m and 228 m. A difference of more than 136 m in thickness is observable within a distance of less than 10 km up-dip the depositional sequence. Remarkably, this thick area predominantly comprises thin-bedded sand and clay, except for a few thicker sand packages occurring in the upper part of the sequence. This anomalous thickness may relate a nearby fault where subsidence was active during fan deposition or the position of the SB was picked too low by PetroSA, i.e. at 3167 m in well E-AA1.



Net-sand of the sequence was estimated between 5 m and 78 m in thickness amongst the boreholes (Fig. 6.10). Channelisation with slight sinuosity is visible from E-BA3 up to E-AO1. The facies distribution map illustrated in Figure 6.11 groups facies as channel-fill sands, bedded sand and clay, and clay. The channel-fill shown in the figure follows the axial zone for the net-sand. It appears that channel complexes are frequently associated with overbank and/or levee deposits throughout the sequence, except down-dip where sand was deposited as sheet sands.



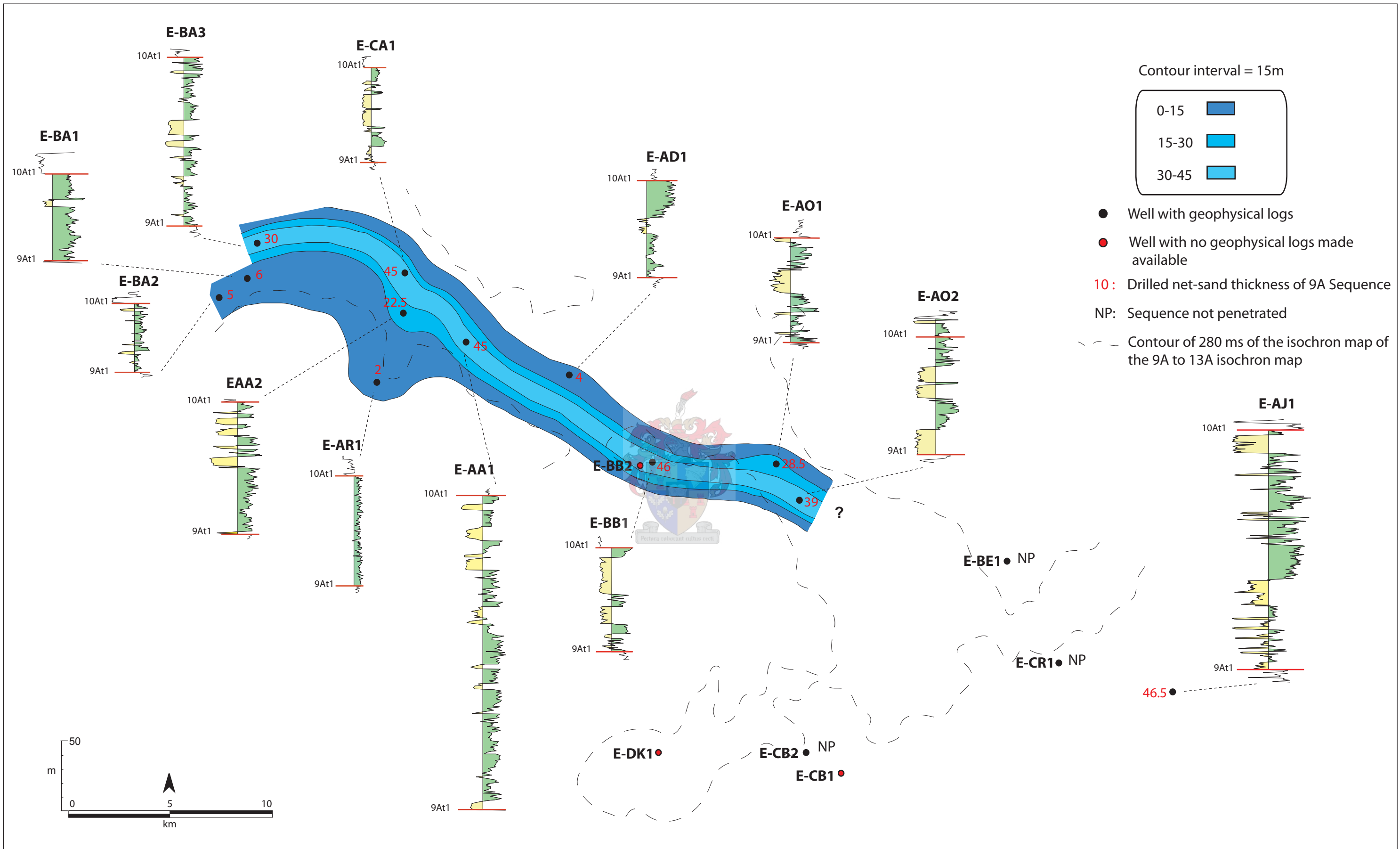


Figure 6.10 Net-sand interval map of the 9A Sequence. Contours reflect the interpretation of net-sand thickness. Colours are assigned to contour intervals for a better illustration of thickness variation. Corresponding GR logs of the interval is given. The net-sand displays a sinuous pattern fairly parallel to the axial part of the corresponding 9A isochore map.

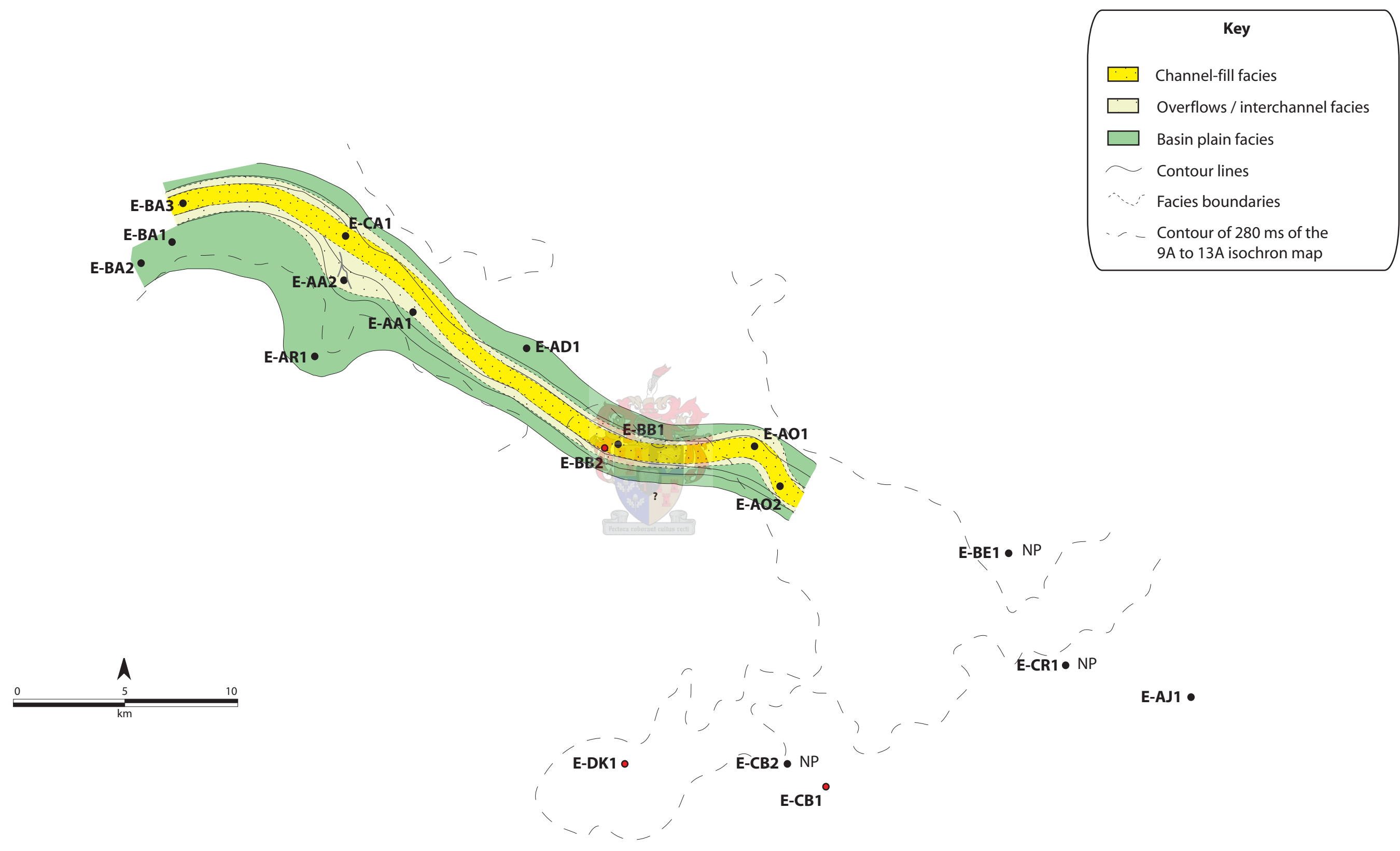


Figure 6. 11 Schematic illustration of facies in the 9A Sequence. Contours reflect a great deal of interpretation of facies distribution. The main channel-fill facies follows a fairly straight fairway. Secondary channel-fills seem to be present within overflow areas which could be interpreted as crevasse splays.

6.3.2 10A Sequence

The lower boundary of this sequence, also considered as the top of the 9A Sequence, was not intersected in E-CR1, and E-CB2. This surface is generally erosive, due to its frequent location at the base of amalgamated sandstone packages, except for wells E-AO1, E-AO2 and E-AJ1 where this surface is located at the base of a clay interval, reducing evidence for erosion.

Thickness of the 10A Sequence ranges from 56 m to 149 m (Fig. 6.12). Distribution of this thickness reveals a sinuous pattern, which is confirmed by the net-sand estimation (Figure 6.13). The facies distribution map (Fig. 6.14) supports the sinuous pattern but shows a good association of overbank or interchannel deposits with channel-fills. It seems as if crevasse splays were developed at channel bends in places. The channel-fill pattern may be more complex with regard to the complex superposition of sandstone packages within the sequence.

Three depositional cycles were identified. The three cycles host LST deposits that were well intersected in wells E-AA2, E-AA1 and E-AD1. The LST packages are separated by fine-grained sediments that display a retrogradational and then a progradational trend, interpreted as transgressive and highstand deposits, respectively. These LST packages consist of massive amalgamated sandstones (Facies A) and are interpreted as channel-fills. Their intercalation with ripple-laminated sandstones (Facies B) and thin-bedded clay and sand (Facies F) suggest channel-fill complexes. Conglomerates (Facies D) are observed at the

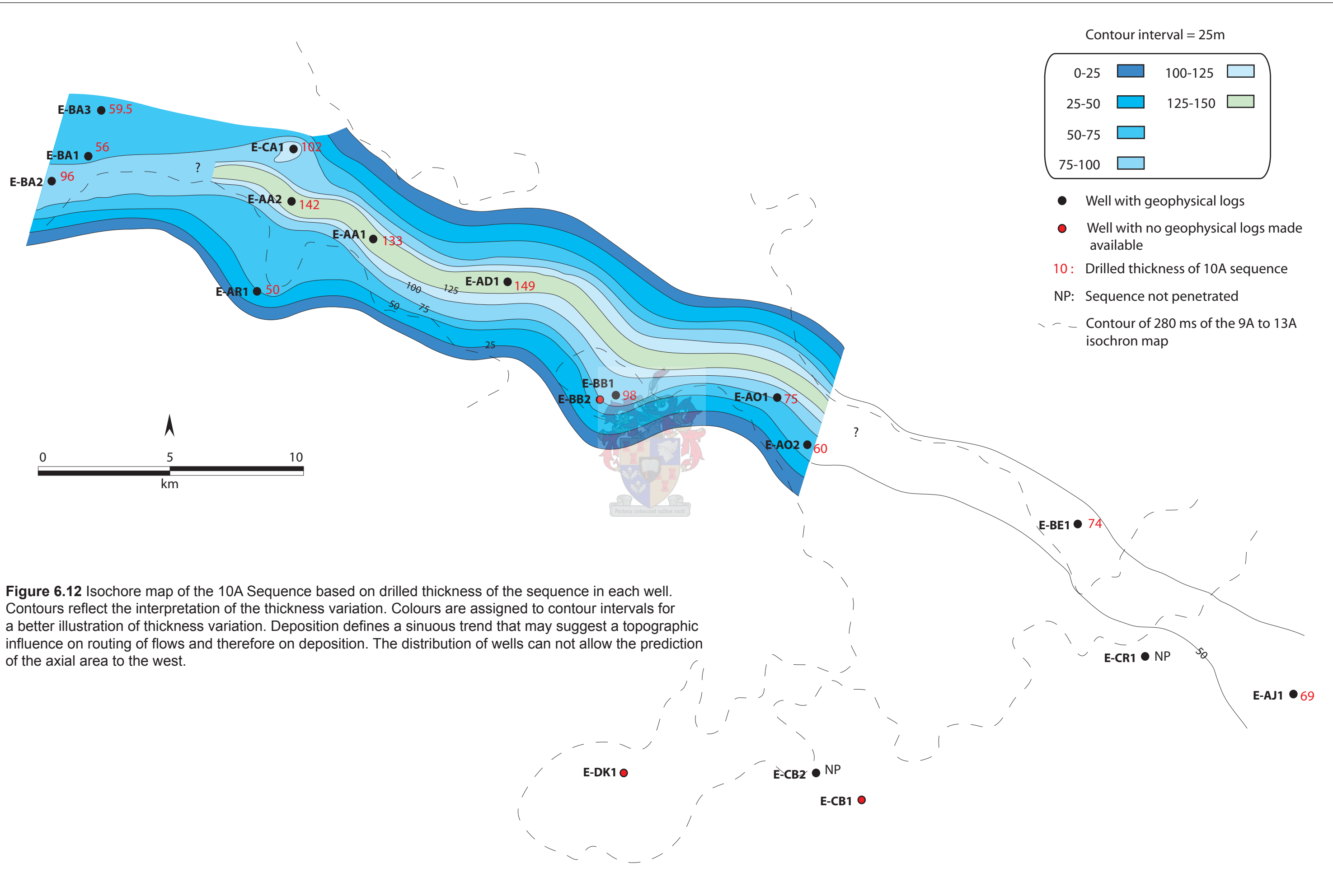


Figure 6.12 Isochore map of the 10A Sequence based on drilled thickness of the sequence in each well. Contours reflect the interpretation of the thickness variation. Colours are assigned to contour intervals for a better illustration of thickness variation. Deposition defines a sinuous trend that may suggest a topographic influence on routing of flows and therefore on deposition. The distribution of wells can not allow the prediction of the axial area to the west.

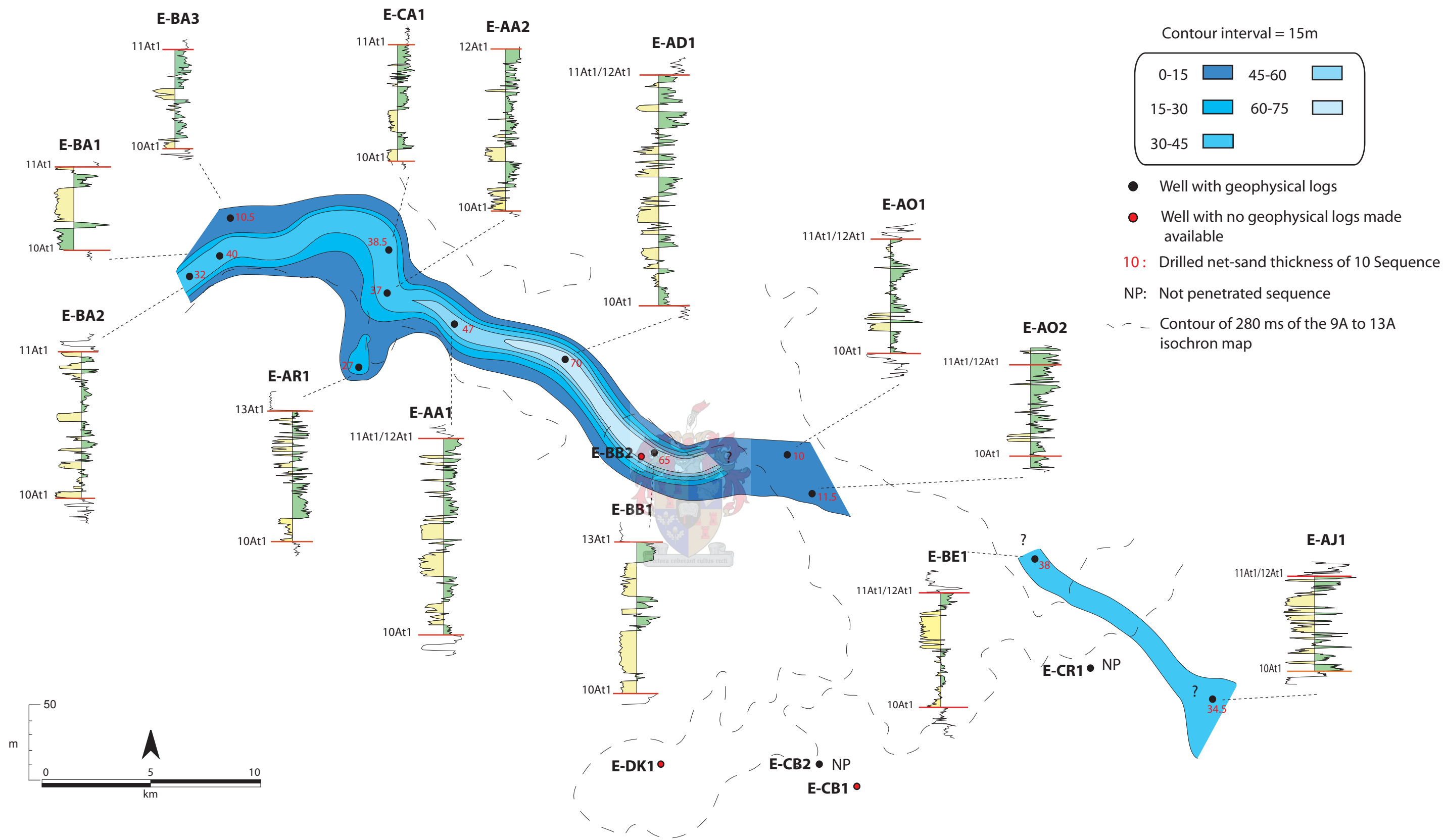


Figure 6. 13 Net-sand map of the 10A Sequence. Contours reflect the interpretation of net-sand. Colours are assigned to contour intervals for a better illustration of thickness variation. Corresponding GR logs of the interval is given. The sand trend displays a sinuous channel axis with minor off-axis deposition.

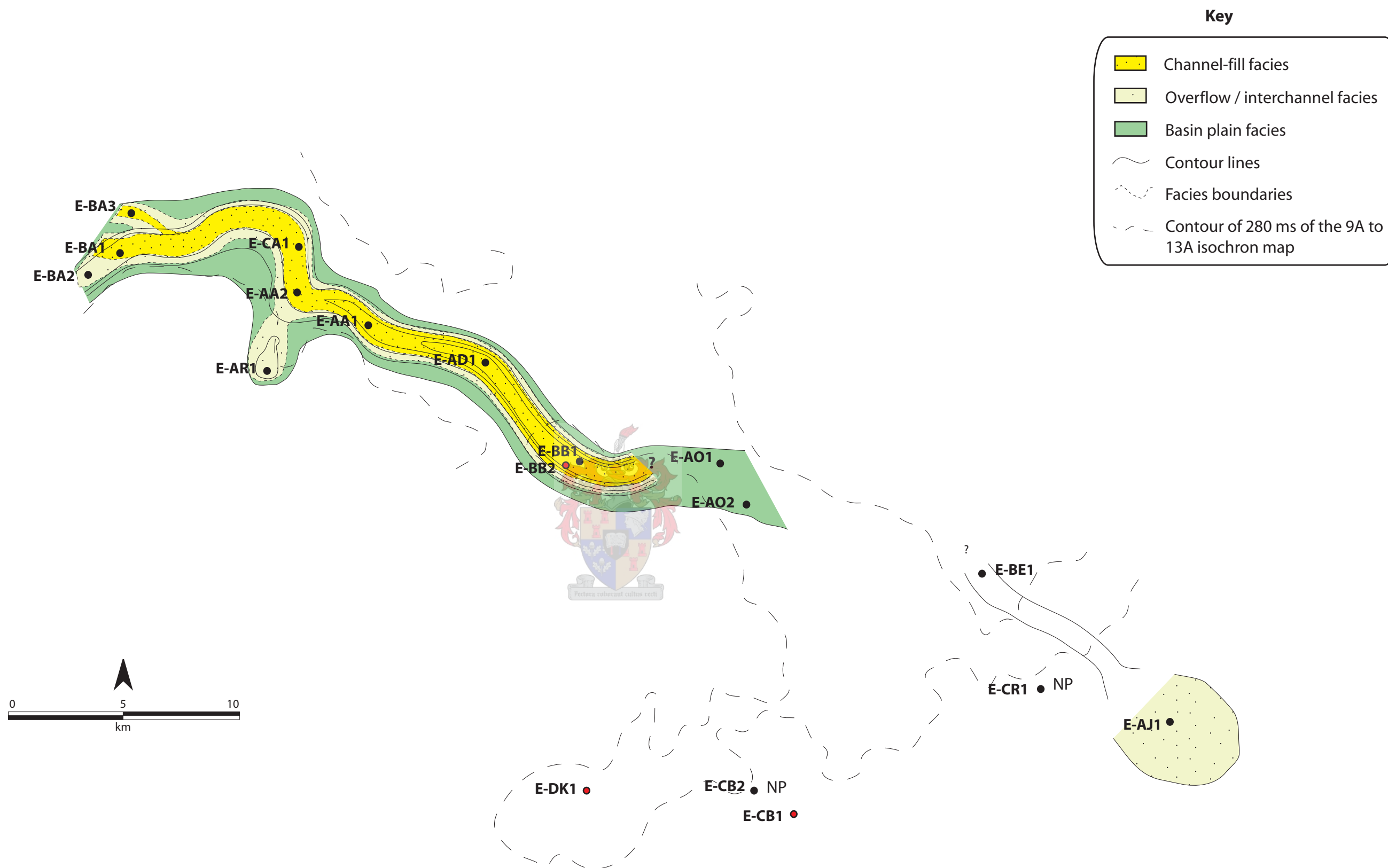


Figure 6. 14 Schematic illustration of facies in the 10A Sequence. Contours reflect a great deal of interpretation of facies distribution. The channel-fill trend may be more complex than illustrated. It displays a sinuous pattern that suggests compensation for topography during deposition. Secondary channel-fills intersecting the main channel in the north-western part may suggest a subordinate source for sediment gravity flows. Crevasse splays predominantly comprise sheet sands.

base of channel complexes in the proximal parts of the depositional profile.

The compensation process seems to exist between the channel-fills intersected between E-AA2 and E-AD1, if those channel-fills are correlated in Figure 6.2. Sand units intersected down-dip in E-AJ1 show an overall upward-thickening or a prograding pattern, which is capped with an upward-fining unit. The prograding sandstones were interpreted as lobe-sheet sandstones whereas the upward-fining unit was interpreted as a channel-fill (Fig. 6.2). Figure 6.15 gives an example of channel slope, stacked channels, sheet sandstones and their possible location on a submarine fan.

6.3.3 11A/12A Sequence

The 11At1 and 12At1 unconformities are clearly distinguishable only in the northwestern part of the study area, but appear to be merged in the rest of the basin. For this reason, 11A and 12A Sequences are considered as a single sequence in the investigation.

The basal unconformity, referred to as the 11At1/12At1 unconformity, does not show any evidence of erosion since it is overlain by a clay-rich interval, with intercalating thin sandstone beds in places. This indicates that the sequence developed probably during a period of relative sea-level rise. However, a high sand-shale ratio that is recorded in the distal part of the sequence suggests episodic deposition of sandy turbidity flows. This is supported by the sandstone intervals intersected above 2800 m in E-CA1 and above 2935 m in E-O2. In E-

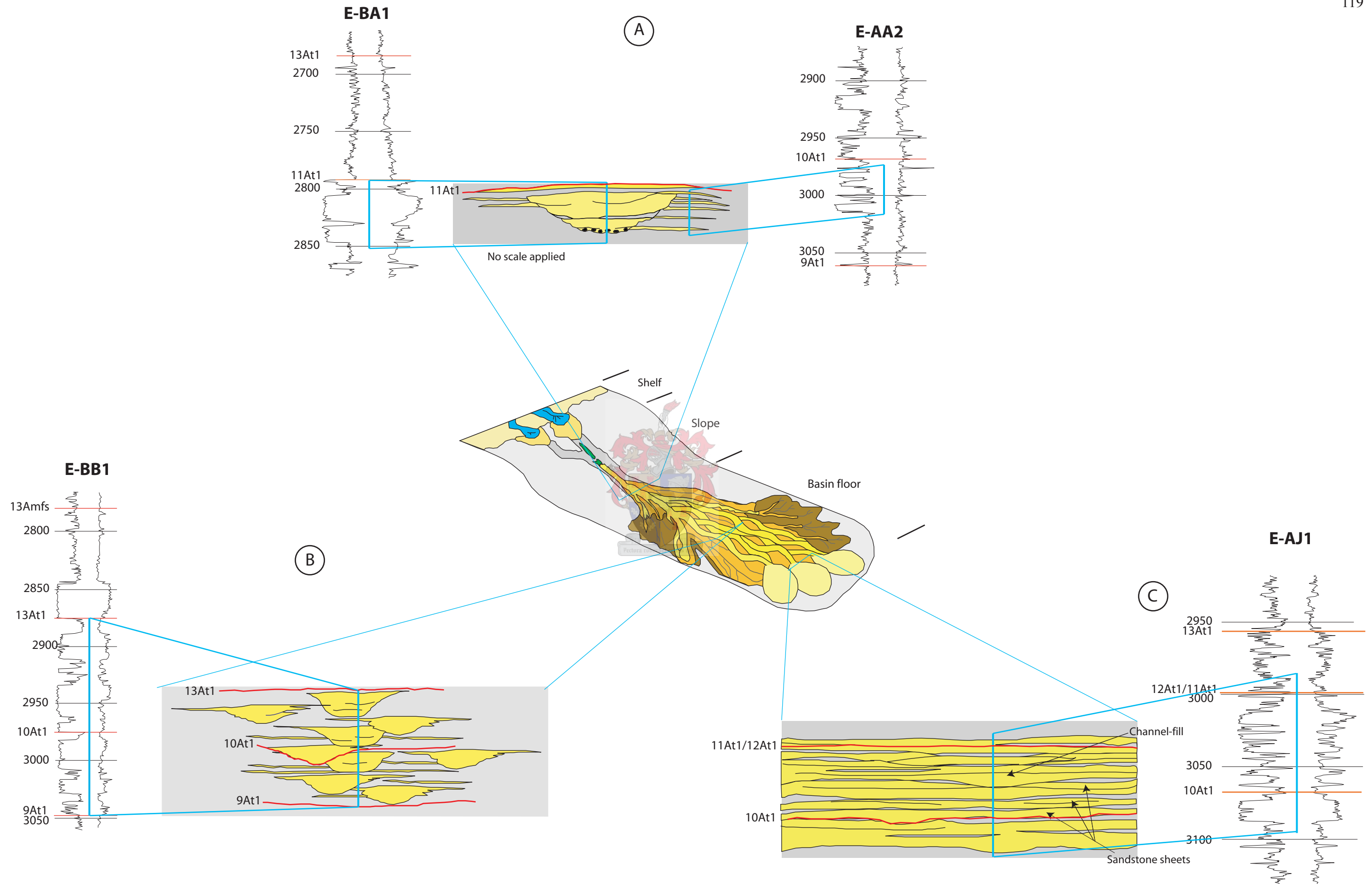
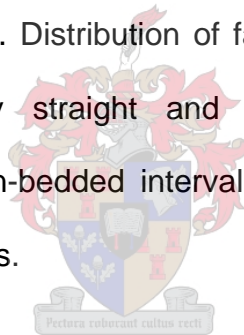


Figure 6.15 Schematic illustration of different elements within the 10A Sequence and their possible location on a submarine fan. A) Slope channel complexes erode deeply into underlying deposits and are associated with overbank deposits, which comprise sheet sands and possible small-scale channel-fills. B) Aggradational channel complexes are confined to a broad conduit and are associated with overbank deposits, sometimes well preserved between the channels. C) Distal sands of this sequence are predominantly sheet-like but comprise some channel-fills. Note that scale was not applied to any illustration.

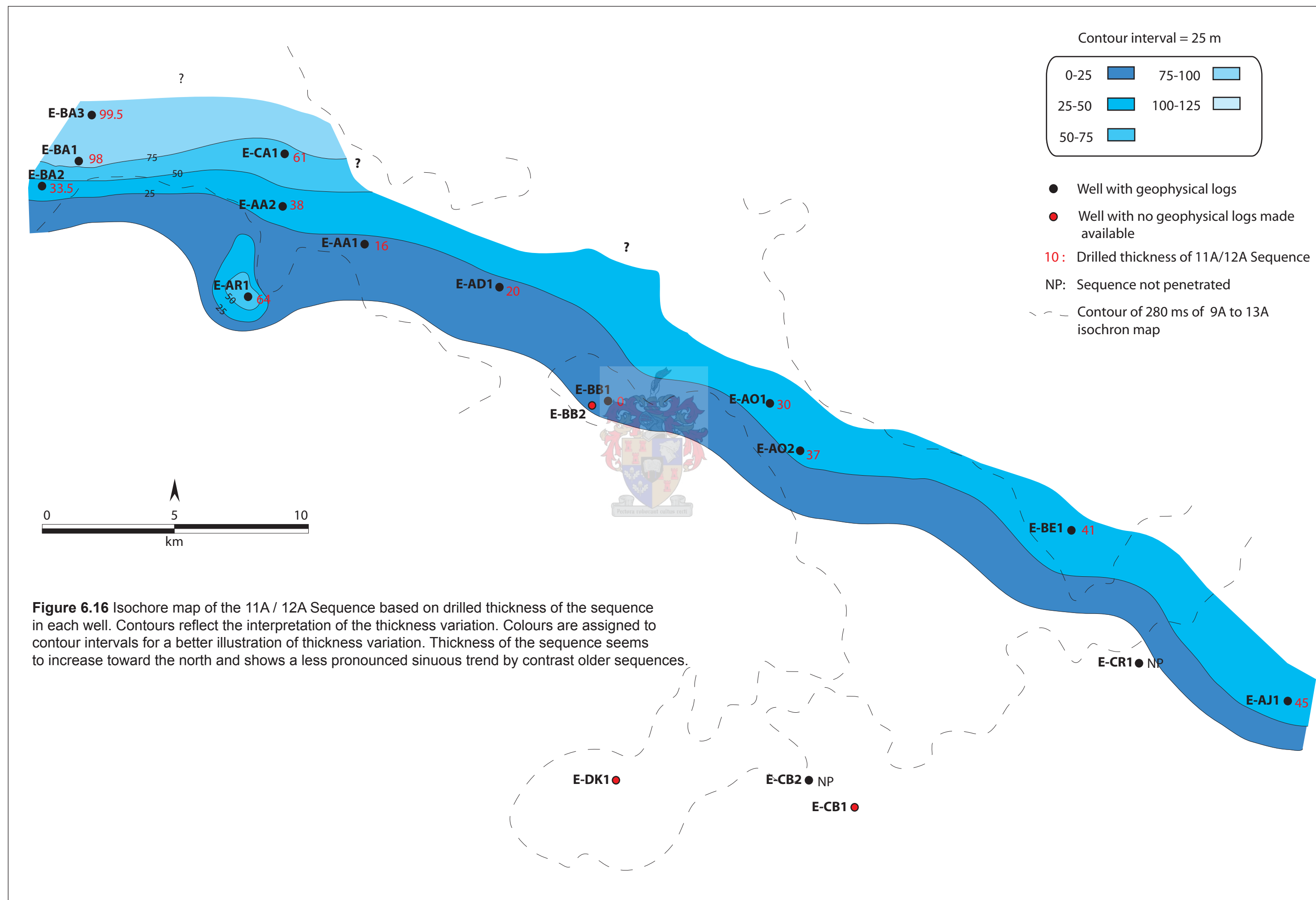
CA1, the sandstone beds are predominantly rippled-laminated (Facies B) and parallel-laminated (Facies C), whereas in E-AO2, sandstone beds are massive and amalgamated (Facies A) and, to a lesser extent, ripple cross-laminated (Facies B).

A thickness distribution map shows that the 11A/12A Sequence thickens progressively northward. Although its axial area is not well defined, it seems that the channel-conduit has shifted towards the north of that of the 10A Sequence (Fig. 6.16). Estimated net-sand map shows a poor development of sand in the sequence. It shows also that the axial area is near E-BA3 (Fig. 6.17) and is probably intersected by E-CA1. Distribution of facies in Figure 6.18 shows that channel-fills are small, fairly straight and associated with overbank or interchannel deposits. The thin-bedded interval intersected down-dip in E-AJ1 suggests sheet-lobe sandstones.



6.3.4 13A Sequence

The 13A Sequence consists predominantly of claystones with isolated sand units. Thick amalgamated sand units occur at the base of the sequence and consist exclusively of massive sandstone (Facies A). The erosive characteristic of the sequence is only obvious below these sand units, which are interpreted as channel-fill complexes. The latter represent punctual higher-order lowstand periods that interrupted the highstand period of the sequence. It appears as if the channel-fill incised deeply into the preceding deposits. The remaining sand units display a graded pattern and are interpreted as sheet sands, likely deposited by



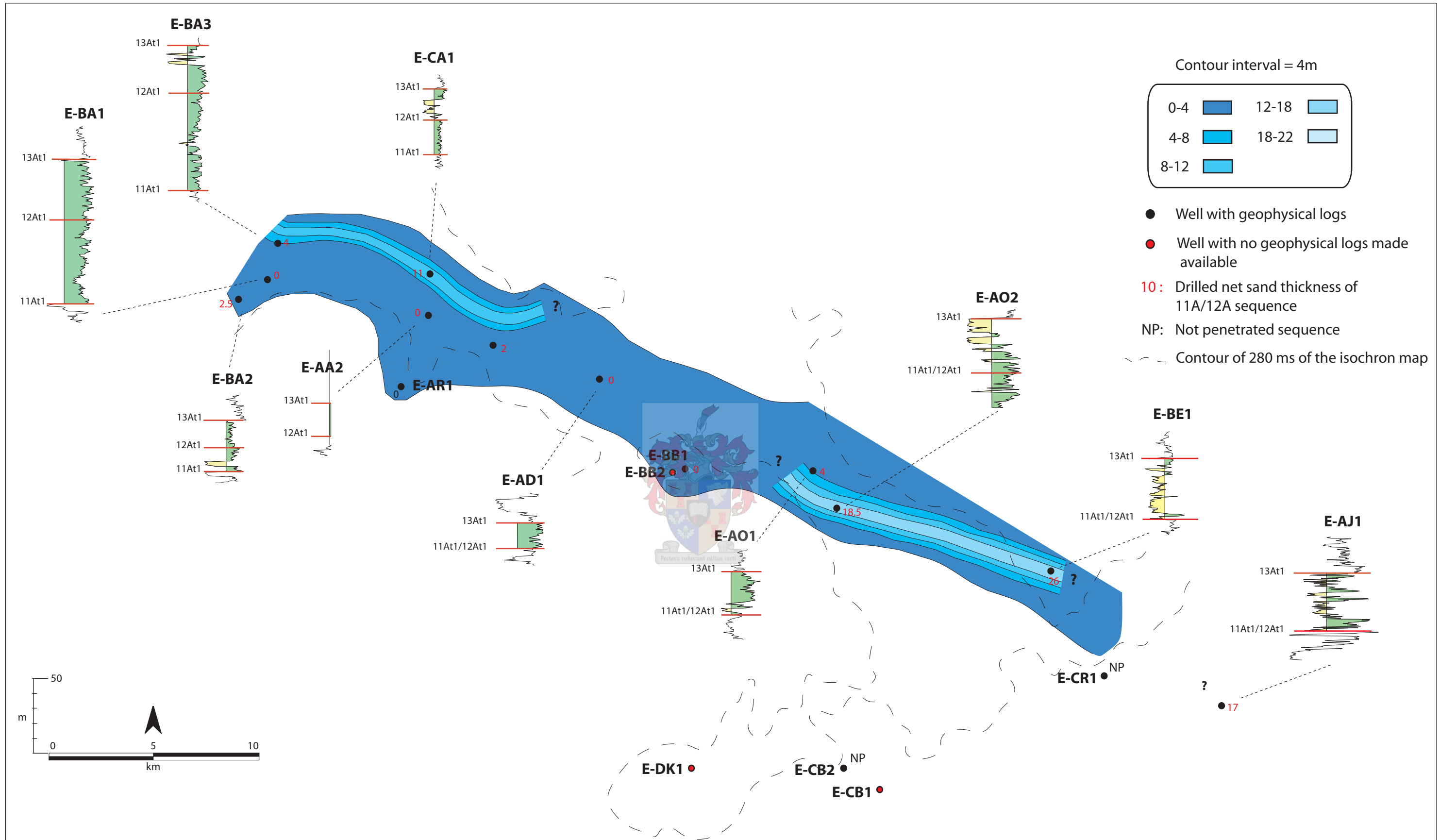
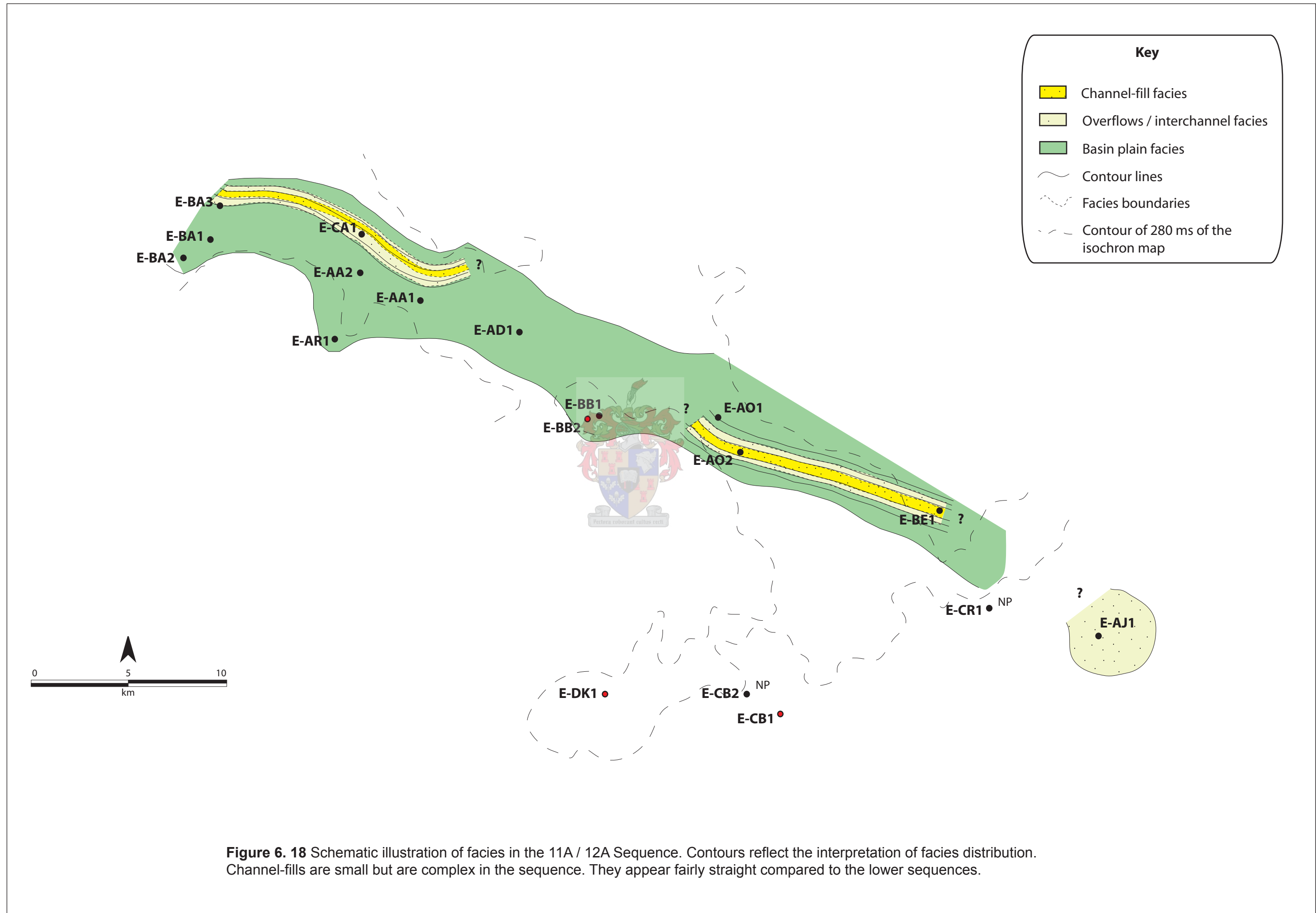


Figure 6. 17 Net-sand map of the 11A / 12A Sequence. Contours reflect the interpretation of drilled net-sand. Colours are assigned to contour intervals for a better illustration of thickness variation. Channel like patterns displays a fairly straight pattern.



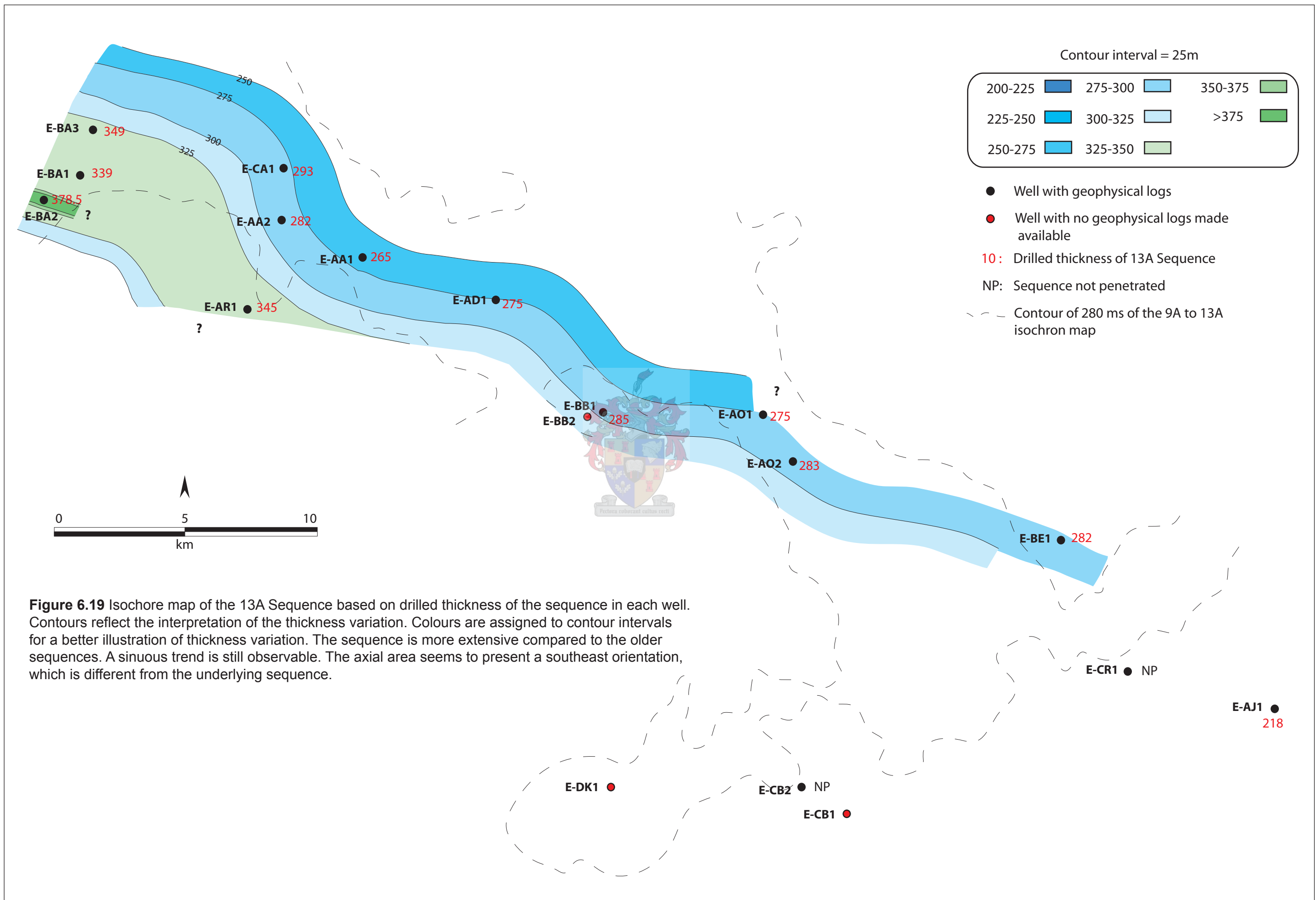
small local turbidity flows.

Thickness of the sequence ranges from 218 m to 349 m and shows that it is more extensive compared to the underlying sequences (Fig. 6.19). Due to a lack of data, it is difficult to estimate the boundaries of this sequence. The net-sand map (Fig. 6.20) shows a probable sinuosity of the channel-fill, which is seemingly not or rarely associated with overflow or interchannel deposits (Fig. 6.21).

6.3.5 The 14A Sequence (the lower sandstone unit)

The early deposits of the 14A Sequence consist predominantly of sandstones and subordinate mudstones grouped as the 14A sand unit, which rests frequently on massive claystones. The contact between this sand unit and the underlying massive claystones appears to be erosive in most places. These sand units can correspond to submarine fan lobes, channel-complexes and channel abandonment facies in different areas (Wickens, pers. comm., Burden and Davies, 1997a & b)

The gamma ray log expression reflects the architectural difference within the sand unit and suggests three distinct sub-units, which are well correlatable throughout the study area (Figs. 6.4 - 6.7). The lower unit, which rests directly on the 14At1 unconformity, consists of parallel, convoluted siltstone (Facies G and H), which seems to alternate with sandstone and claystone in places (Facies F). The overlying unit comprises amalgamated massive sandstone (Facies A), which in turn is overlain by ripple-laminated sandstone (Facies B) and parallel-laminated sandstone (Facies C). The lower unit is interpreted as by-pass depo-



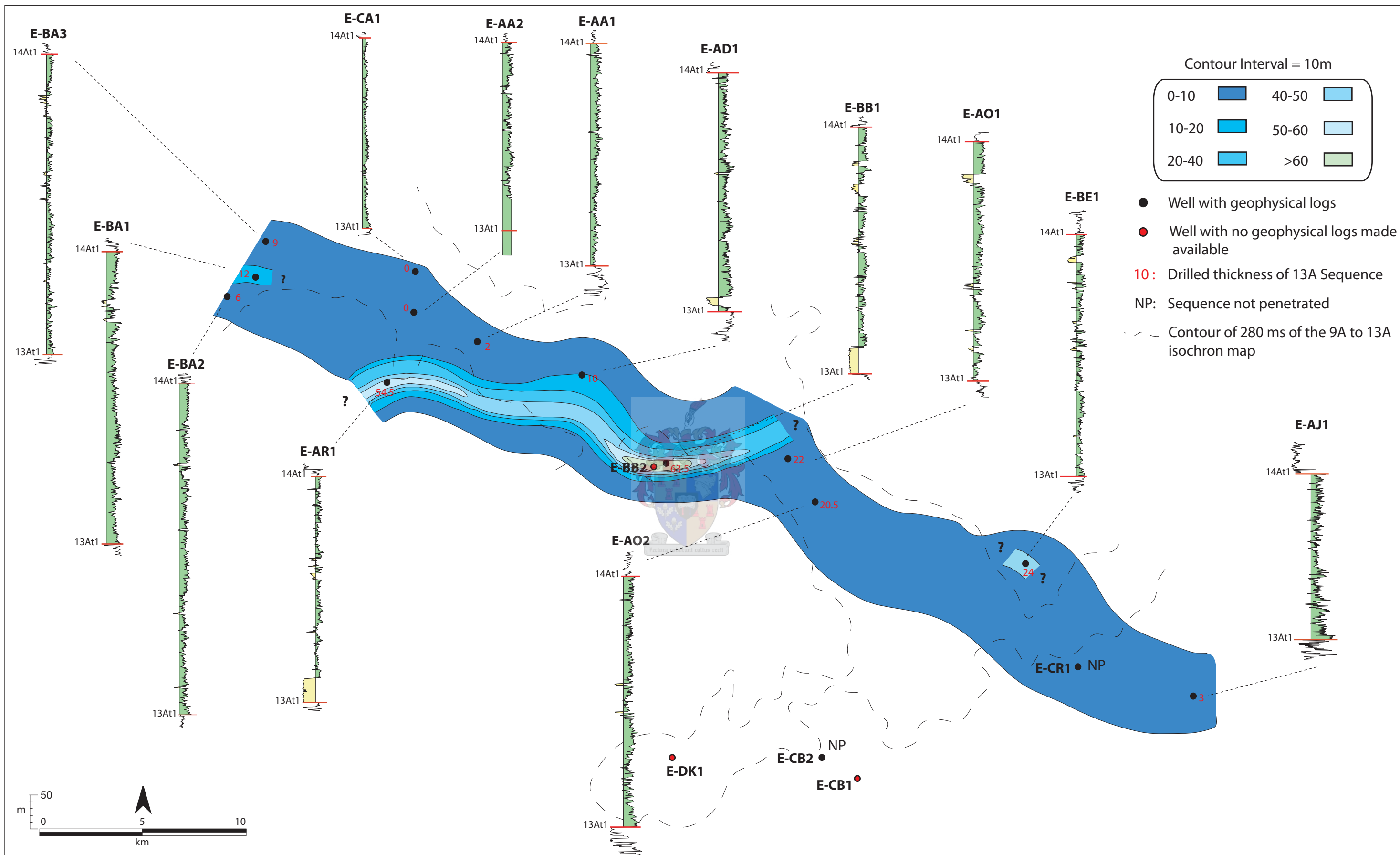
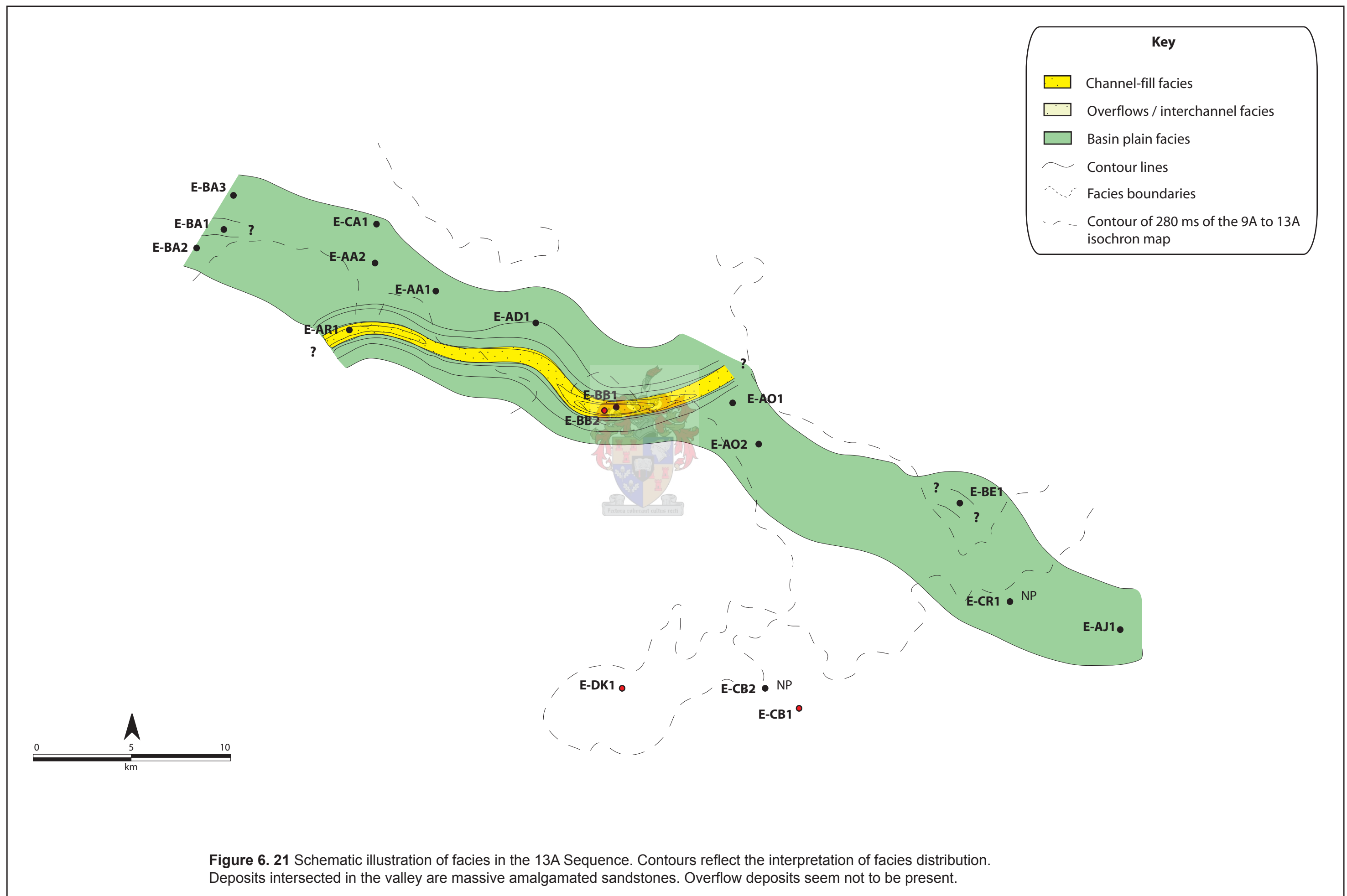


Figure 6.20 Net-sand map of the 13A Sequence. Contours reflect the interpretation of net-sand thickness. Colours are assigned to contour intervals for a better illustration of thickness variation. Corresponding GR logs of the interval is given. In places, net-sand displays a sinuous pattern trending in a west-east direction.



sits of ancient flows that transported sediments into the deeper areas of the basin (Wickens, pers. comm.). The lack of coarse material such as pebbles, and the presence of ripple-cross laminations may suggest that wells, such as E-AA1, intersected the unit in its marginal part. Thin sands alternating with claystones were intersected above the lower unit in E-BA1, E-AA2 and E-AO1. These sands may correspond to channel margin or overbank deposits. Thickness of the lower unit ranges from 10 to 35 m and may suggest that the flows, that by-passed the area during this time, were highly unconfined. This could perhaps be justified by the great extension of these deposits in the area.

Estimated net-sand map shows two possible main channel conduits and several subordinate channels (Fig. 6.22).

6.4 Depositional architecture

Segregation within sediment gravity flows along the depositional profile is controlled by basin floor morphology. The latter produces a distinct facies association, in which stacking of facies produces distinct architectures (Gardner *et al.* 2003). Four architectural depositional elements, namely channel-fill, overbank or interchannel, crevasse splay and sheet-lobe were recognized. These are channel-fill, overbanks / levee, lobe and crevasse splay deposits.

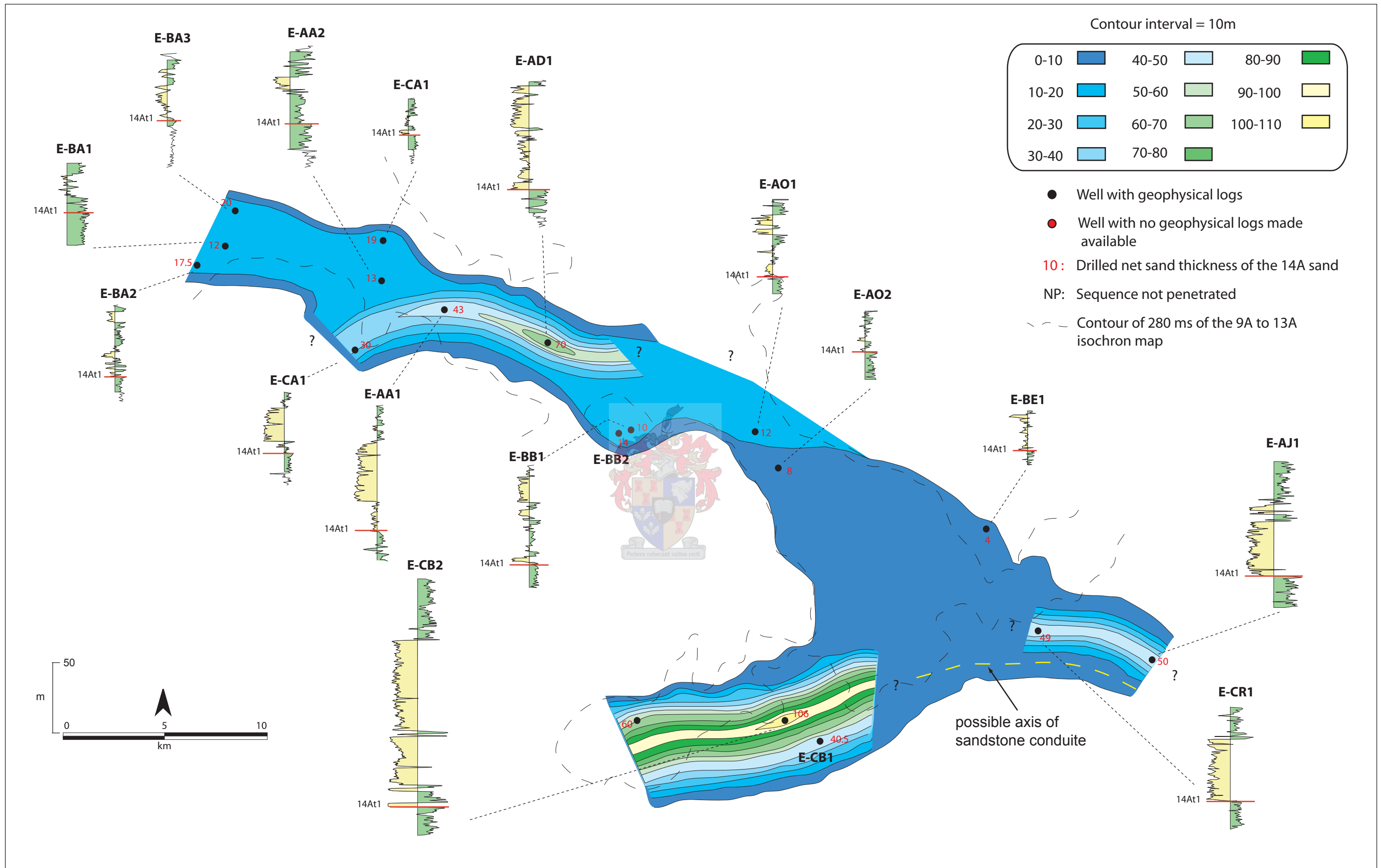


Figure 6. 22 Net-sand interval map of the 14A sand. Contours reflect the interpretation of the net-sand drilled thickness. Colours are assigned to contour intervals for a better illustration of thickness variation. Corresponding GR logs of the interval is given. Distribution of sand suggests two distinct conduits, with less sinuosity compared to the underlying sequences. Pattern of net-sand in the conduit suggests that E-CR1 and E-AJ1 intersect the marginal part of the conduit. The axial part of this conduit may trend as shown by the dotted yellow line.

Channel-fills

Based on well-log patterns integrated with core description data, several types of channel-fills were recognized within the studied stratigraphic interval. Note that channel-fill deposits predominantly consist of massive, amalgamated sandstones (Facies A), often associated with basal conglomerates (Facies D) and to a lesser degree, parallel-laminated sandstones (Facies C). Basal erosive contact is a characteristic of channel-fills.

Johnson *et al.* (2001) defined five types of channel-fills based on outcrop studies in the Tanqua depocentre (Fig. 6.23). These channel-fills are: (i) erosional, multiple-event channel with a complex fill, (ii) erosional, multiple-event channel with a simple fill, (iii) depositional and minor erosional channel, (iv) erosional channel with heterolithic and thin-bedded fill, and (v) channel complex.

Most channels identified in this study are called channel complexes because the resolution of the log cannot give a single channel event. The common log pattern representing these channel complexes are blocky, but serrated fining-upward patterns are also present. The channel-fills intersected above 2900m in E-AA1 and between 2900 m and 2960 m in E-AD1 (Fig. 6.13), at 3050 m in E-AO1 and between 3020 m and 3088 m in E-AO2 (Fig. 6.10), between 2845 and 3048 m in E-BB1 (Figs. 6.10, 6.13 and 6.20), are interpreted as channel complexes (type v). Those intersected above 2850 m in E-BA1 (Fig. 6. 10), above 2841 m in E-AR1 (Fig. 6. 20) are ascribed to type i. Type iii or iv channel-fills would be those

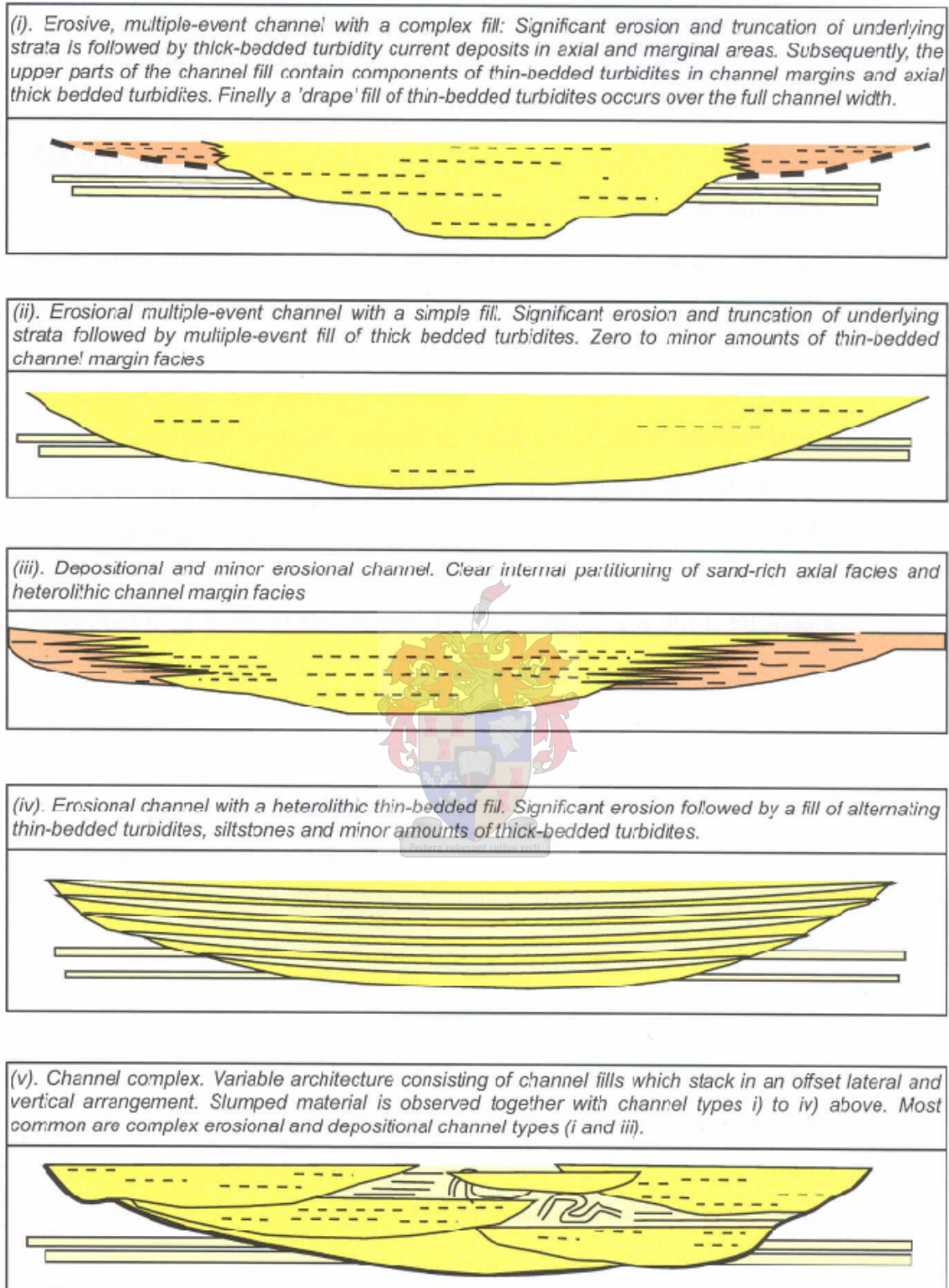


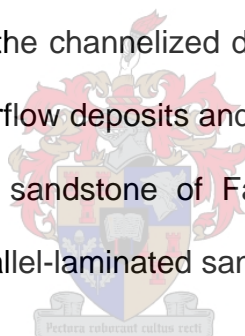
Figure 6.23 Schematic diagrams of the five types of channel-fills observed in the Tanqua depocentre (from Johnson *et al.*, 2001).

intersected at 2480 m in E-AA2, at 2340 m in E-BA1 and at 2340 m in E-BA3 (Fig. 6.22). Channel-fills with a single-fill were not identified.

Almost all channel complexes pass upward into thin-bedded, fine-grained deposits, except for the 13A channel and the channel complex above 2600 m in E-CR2, for example, that pass abruptly into claystone interval. The first transition indicates a progressive depletion of sand in the flow, in contrast to the abrupt flow termination or abandonment of the depositional event.

Overflow deposits

The thin-bedded units fringing the channelized depositional elements mentioned above, were interpreted as overflow deposits and consist of alternating laminated to interbedded claystone and sandstone of Facies F, ripple cross-laminated sandstone of Facies B and parallel-laminated sandstone of Facies C.



Based on well log patterns, overflow deposits appear to be frequently eroded by channel-fills, e.g. between 3020 m and 3088 m in E-AO2 (Fig. 6.10) and between 2920 m and 2970 m in E-AD1 (Fig. 6.13).

Sheet-Lobe deposits

Stacked sandstone beds commonly displaying a prograding stacking pattern are interpreted as sheet-lobe sandstones. The latter were deposited at a channel mouth or any place in the basin where flows become unconfined (Gardner *et al.*, 2003; Eschard *et al.*, 2003), resulting in the extensive character of the beds.

Sheet-lobe sandstones consist predominantly of massive sandstone. They are characterized by upward-thickening trends after progradation and thinning / fining-upward trends after and abandonment of the system (MacDonald, 1986). In this investigation, sheet sandstones were interpreted to be present down-dip of the depositional profile, in E-AJ1, but they were also interpreted to occur on top of some channel-fills, for example at 2795 m in E-BA1 and within crevasse splays in E-AR1.

Basin plain deposits

Basin plain deposits can be found in all regions of submarine fans. They consist predominantly of massive claystone (Facies E), which can also alternate with thin sandstone and siltstone beds (Facies F).

Basin plain deposits are frequently intersected away from channel-fill complexes as they are considered as being the product of continuous background deposition. Slow fall-out of clay particles from suspension result in a blocky pattern, whereas intermittent influx of sandy turbidite flows into the environment may cause an alternation between claystone and fine-grained sediments resulting in a serrated pattern of the deposits.

6.5 Influence of basin floor topography on deposition

When superimposed, isochore maps of the investigated sequences reveal evidence of basin floor topographic control. The decrease in sinuosity of channel conduits upward in the 9A to 10A Sequences seems to be related to a decrease

in topographic influence on gravity flows. The existing evidence for basin floor topographic control is the NW-SE trend of most axial parts of the sequences. This trend suggests that topographic highs were slightly parallel to this trend. It also suggests that these highs were sufficient to divert flows into topographical lows but subtle enough to allow deposition from flows over highs, hence the presence of overflow deposits along channel-fills and channelized “valleys”.

Although the palaeotopography of the underlying sequences is not known, it is assumed that these topographical highs are located where the 9A Sequence thins out onto the margins. From the 9A to 11A/12A Sequences, deposition seems to have followed the existing topographical lows of the underlying sequences. This is shown by the constant shift of the axial parts of sequences northward but parallel to the underlying axis. Note that the axial part of the 10A sequence intersects that of the 9A Sequence (Figs. 6.10 and 6.13). This was caused either by high confinement of flows that caused erosion across existing channels, or by late displacement of an underlying NW-SE trending fault located near E-AA2. Such late movement may have caused a reorganisation of topography across the existing channel-fills, which accommodated subsequent flows.

The trend of the 13A Sequence differs from the other sequences. It is not only more extensively developed but it also shows an axial part with a different direction. The prevailing wide-spread sedimentation of fines (mudstone) in the Early Aptian, after the 13At1 unconformity (McMillan *et al.*, 1997), justifies this large extension. However, the net-sand map indicates that major erosion

occurred in the southern part of the sequence, where probable topographic lows persisted.

Grecula (2000) postulated that sea-bed topography that parallels the main direction of sediment transport favours long travel distance of the gravity flows. This produces an elongated shape of turbidite deposits. As topographical highs and lows controlled the direction of gravity flows, they most likely exert lateral constraint on sediment transport. The two models of flow confinement proposed by Grecula (2000) may explain the different lateral extension of flows observed from the 9A to 14A Sequences (Fig. 6.24). According to this model, subtle topography along channel belts allows huge volumes of extensive fine-grained deposits outside the channel conduit. When significant erosion occurs at the base of flows, this induces a high confinement, with localised flow-stripping at channel bends. The complex architecture of channelized units within sequences suggests that both types of flow confinement can occur along the same flow path.

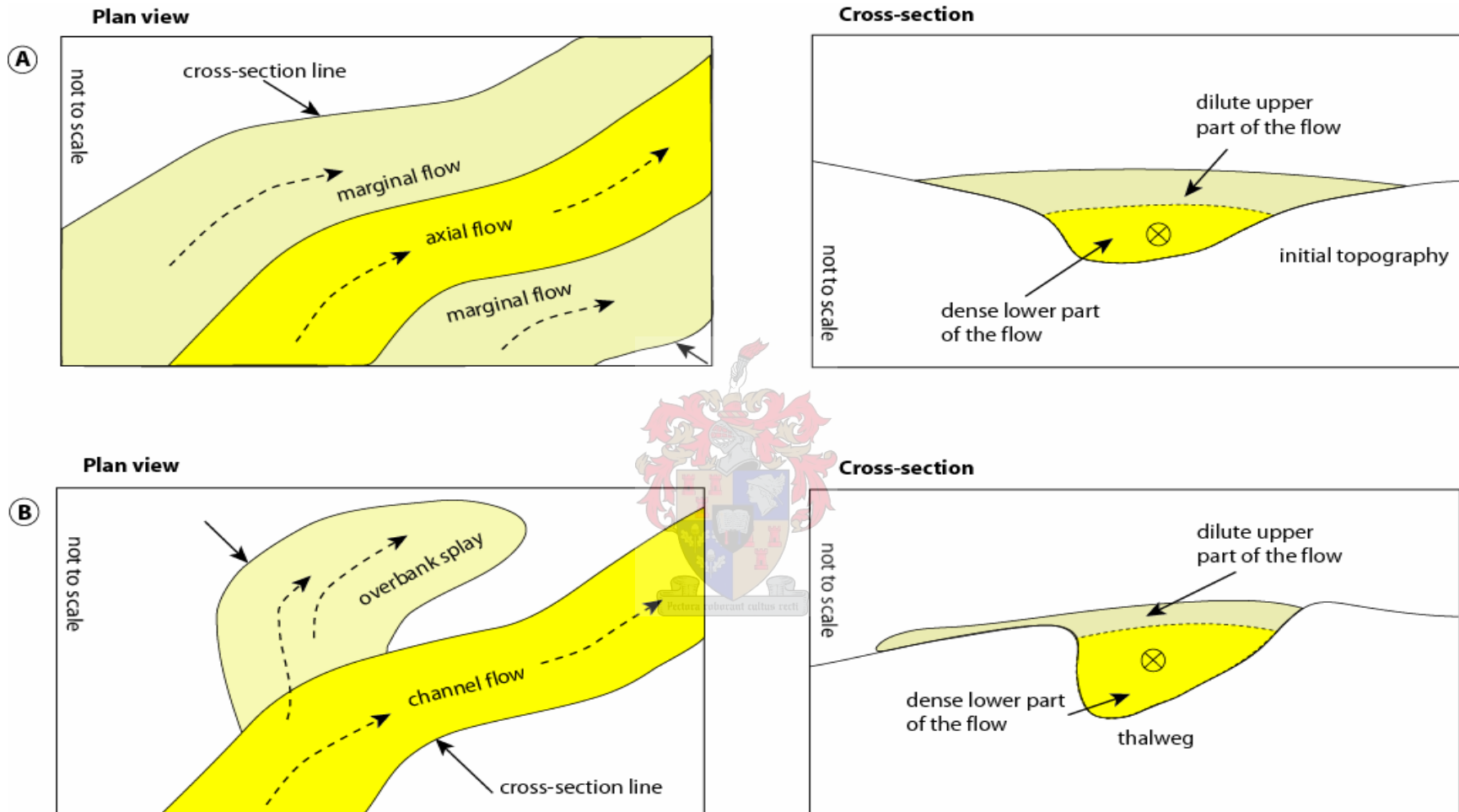


Figure 6.24 Schematic diagrams of two contrasting types of turbidity flow confinement. A) Subtle-topography control and B) Erosion control (from Grecula, 2000).

CHAPTER 7

DEPOSITIONAL MODEL

The depositional model proposed here integrates the results and perceptions expressed in the preceding chapters. The data used to develop a model are based mainly on the vertical and lateral facies development and their distribution within each sequence. Sketches proposed for the model are based on the submarine fan model of Beaubouef *et al.* (1999).

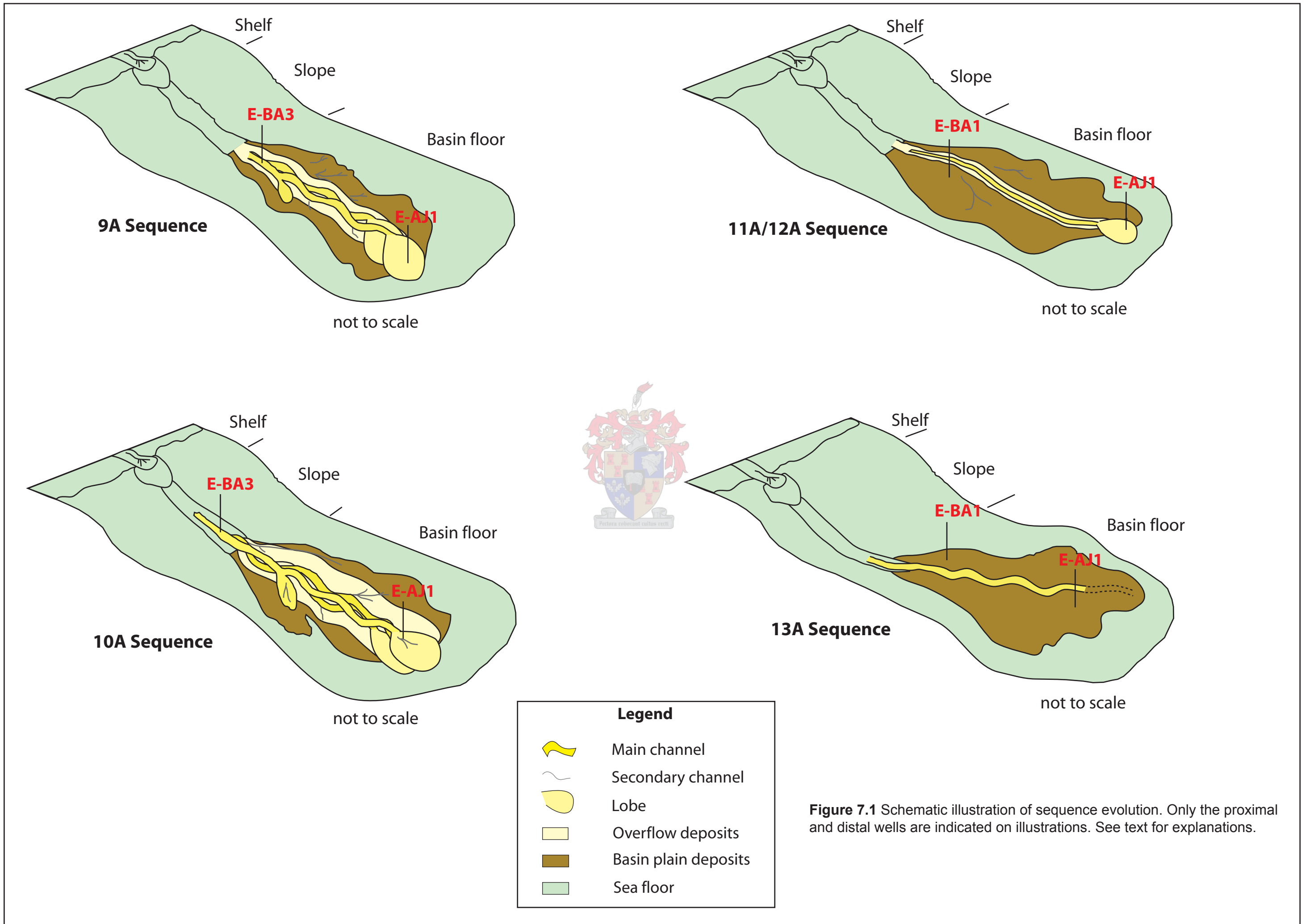
7.1 Depositional model for the sequences

The **9A Sequence** seems to consist of three depositional 4th-order sequences hosting lowstand channel complexes (Fig. 6.4). The vertical stacking of these channels indicates that deposition was controlled by compensating for local topographical differences created by the channel-fills. Maximum incision during the early lowstand period developed preferably along existing topographical lows. The lower LST package corresponds to the first filling phase of the valley-conduit. This filling occurred during relative sea-level rise as flow energy decreased. As the channelized conduit fills, gradual abandonment in sediment supply result in the overlying upward fining / thinning succession above the LST package. A subsequent sea-level lowering induced another LST incision, which was filled similarly to the lower one. Amalgamated channel-fills display blocky to serrated blocky patterns when intersected near the axis, but they reflect also

pronounced serrated patterns when intersected near the margin. The predominant facies observed are massive amalgamated sandstone (Facies A). Overflow deposits associated with these channels are made up of ripple cross-laminated sandstone (Facies B), parallel-laminated sandstone (Facies C), massive claystone (Facies E), and laminated to thin-bedded claystone and sandstone (Facies F). These overflow deposits are developed along the southern flank of the channel complex.

The investigated section of the 9A Sequence is thought to occur in a middle fan to fan lobe setting (Fig. 7.1).

The **10A Sequence** is interpreted to comprise three 4th-order depositional sequences that host lowstand channel complexes. The lower bounding surfaces of these sequences are erosional and are overlain frequently by thick sandstone units. Sequential evolution of channel complexes is similar to that given for the 9A Sequence. Common facies encountered are massive amalgamated sandstone (Facies A), ripple-laminated sandstone (Facies B), parallel-laminated sandstone (Facies C), conglomerate (Facies D), massive claystone (Facies E), alternating laminated to thin-bedded claystone and sandstone (Facies F). The association of these facies form channel-fills, overflow deposits, crevasse splays, and sheet sandstones. Thin-bedded sheet sand deposits in wells adjacent to those hosting channel sands may represent prograding crevasse splays or correlatable overbank deposits. Similar prograding sequences develop down-dip of channels but these are interpreted as sheet lobes (Fig. 7.1).



Thicker sandstone beds intersected within these lobes may be interpreted as channel-fills. An exceptionally, thick conglomerate unit consisting of large angular to sub-rounded pebbles and shell fragments, occurs below a thick amalgamated sand unit in E-BA1. These coarse-grained materials are the first sediments that were deposited in the valley-conduit when the flow began to lose energy.

The investigated section of the 10A Sequence is thought to have developed in a base-of-slope to upper middle fan domain.

The **11A/12A Sequence** predominantly consists of claystone. Except for the channel-fill intersected in E-BE1, it is difficult to assign the other sandstone units to channel-fills or sheet sandstones and hence their positions on a submarine fan. However, if the sandstone units intersected in E-AO2 are associated with overflow or sheet sand deposits, a middle fan to outer fan setting may be proposed because the sandstone units in E-AJ1 are interpreted as sheet.

The **13A Sequence** predominantly consists of claystone deposits, except for the thick amalgamated sand package intersected at the base. This shows that the sequence developed during a highstand period, which was subsequently interrupted by a higher-order lowstand period during which high-density flows incised preceding highstand deposits as well as older sequences (e.g. in boreholes E-BB1 and E-AR1). These lowstand deposits consist only of massive amalgamated sandstone (Facies A). The sharp top surface of these sandstones suggests an abrupt change of sedimentation, perhaps up-dip avulsion of channels, which may justify the absence of gradual abandonment or overflow

deposits that are commonly associated with adjacent channel complexes. It is difficult to assign the deposition of this sequence to a specific domain on a submarine fan. However, it is proposed to have taken place in a middle fan setting.

The **14A Sequence** overlies a sharp basal surface that represents a highly erosional sequence boundary in places, e.g. in boreholes E-AA1, E-AA2 and E-AD1. The top contact of its lower sandstone unit is, however, variable. It is either sharp or occurs on top of fining upward sand units. The three sub-units identified within this sandstone unit, i.e. a lower “amalgamated” siltstone unit, a middle massive amalgamated sand unit, and an upper bedded sand and clay unit (e.g. in boreholes E-AA1, E-AD1 and E-AR1), suggest three phases of channelized deposition.

During the early stage of channel formation, high-density gravity flows erode pre-existing deposits to form an erosional depression. During this phase, diluted sediments were deposited as turbidite tail-end deposits, here interpreted as a bypass facies. This unit probably evolved down-dip and likely also laterally into bedded sandy units as a result of flow transformation. The channel depression is subsequently filled by rapid fall-out of sediment due to a back-stepping process within the conduit. This develops the thick sand units in places displaying tractional structures. As the flow energy depleted a continued back-stepping depositional process favours the development of bedded units on top of massive sands. This depletive phase is abrupt in places and produces sharp upper surfaces.

The 14A sand is thought to have been deposited in an inner fan to middle fan area.

7.2 Prediction of reservoir distribution and development

Based on the stacking pattern of depositional units on well logs, two main types of reservoirs stand out within the investigated interval because of their facies assemblage. These are channel-fill reservoirs and interchannel (overbank/levee) reservoirs. Characteristics of these reservoirs are given bellow.

7.2.1 Characteristics of channel-fill reservoirs

Channel-fill reservoirs contain the highest proportion of coarse-grained and interconnected reservoirs. This interconnection results from sand-to-sand amalgamation that occurs commonly along the axial parts of individual channel complexes, which favours good communication between channel-fills. Vertical permeability (K) is frequently high in this axis (Beaubouef, 2004) because of the absence of claystone beds that could act as barriers to fluid flow. Stacking patterns on well logs within channel complexes show significant changes of grain size, bed thickness, and amalgamation from axes to margins that suggests existence of barriers in places, for example between 2900 and 2967 m in E-AD1 and between 3025 and 3088 m in E-AO2.

7.2.2 Characteristics of interchannel reservoirs

Interchannel (overbank) reservoirs are the most significant reservoirs associated with channel-fill reservoirs in almost all sequences. Sandstone beds are thin but can be thick where amalgamated. These sandstones are interbedded with claystones and are aerially more extensive than channel-fill reservoirs. Outcrop investigations in the southwestern Karoo (Sixsmith, 2000; Johnson *et al.*, 2001) show high lateral continuity of these reservoirs. These outcrops also show significant thickness variation of interchannel reservoirs, laterally from the channel-fill axis. Thick beds develop in the proximal areas adjacent to channels whereas thin beds develop in the distal areas away from channels. Overall, interchannel reservoirs suggest high horizontal connectivity and very poor vertical connectivity due to good lateral continuity and well developed interbedded claystones, respectively.



Three vertical sections, i.e. in E-AA2 (2969-3015 m), in E-AR1 (2850-2920 m) and in E-BA2 (2770-2866 m), give a good picture of interchannel characteristics in the study area. The two first sections display the bedded characteristics of the interchannel deposits, interpreted as crevasse splay deposits, which have a larger extension than channel-fill reservoirs. Some thicker interbeds, interpreted as small channel-fills, increase the vertical connectivity of the interchannel reservoirs due to sand-on-sand connection favoured by erosion. If small channel-fills are not present, as in E-BA2, this vertical reservoir connectivity will not exist.

7.2.3 Connectivity of reservoirs

Reservoir connectivity seems to be complex within channel belts. This connectivity is obvious where amalgamation is observed, usually at and near channel axes. In several channel complexes intersected by wells, particularly within the 9A and 10A Sequences, stacked amalgamated sandstones are separated by bedded successions. This may give the impression that these stacked sandstones are not connected, which is not true. Individual channel complexes can be connected due to repetitive erosion, which allows sand-on-sand contacts as shown in the channel complex models of Johnson *et al.* (2001), Gardner *et al.* (2003), and Beaubouef, (2004). It is believed that the vertical and lateral migration of channels, especially in base of slope settings, produce very good vertical connectivity between individual channel-fills due to multiple erosion-scours into channel and interchannel deposits. Based on the net-sand interval and facies distribution models, good connectivity of reservoirs may be predicted in 9A Sequence, between the channel-fill reservoirs in E-CA1 and the interchannel reservoirs in E-AA2 or between the channel-fill reservoirs in wells E-AO1 and E-AO2 and the interchannel reservoirs predicted northward (cf. Fig. 6.10). The multiple erosion-fill processes present in 10A Sequence may locally favour good connectivity of both types of reservoirs, for example between E-AD1 and E-BB1 or E-BA1 and E-BA2 (cf. Fig 6.13).

CHAPTER 8

CONCLUSIONS

The basin topography, controlling the Middle Cretaceous deep-water sedimentation in the central part of the Bredasdorp Basin, was broadly controlled by the structural trends inherited from the Permo-Triassic Cape Orogeny and subsequent evolution of the basin through the rift and post-rift stages. The drift succession within the Bredasdorp Basin comprises siliciclastic deep-water deposits that accumulated in its central part due to repetitive allocyclic sequence development controlled by sea level change processes.

For the deep-water sediments, eight distinct facies have been described from cores, based on grain-size, bed thickness trends, bed contacts and primary and secondary sedimentary structures. The massive sandstone facies display a blocky gamma ray shape, and is interpreted as channel-fill sandstones where presenting evidence of amalgamation and erosion at the base or as sheet sands where they are thinner and regularly alternating with shale or siltstone units. Conglomerate facies are essentially observed at the base of channel-fills but occur also as a result of channel-fill grading processes or local renewed phases of deposition within the channel-fills.

Alternating laminated to interbedded sandstone, siltstone and claystone as well as ripple cross-laminated and parallel-laminated sandstones, which display a

serrated gamma ray pattern, commonly occur both below and above massive sandstones and are interpreted as being derived from sedimentation outside channelized areas. One facies, namely clay-rich siltstone, is present between the lower erosional surface (sequence boundary 14At1) and the massive sandstones of a channelized conduit. Its intercalation with laminated to interbedded sandstone, siltstone and claystone, together with soft-sediment deformation features led to interpreting it as by-pass deposits constituting the basal infill of the channel conduit.

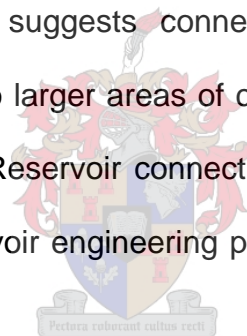
Using gamma ray logs and core description, the association of facies was successfully put into a high-resolution sequence stratigraphic scheme. Units of massive sandstones and underlying clay-rich siltstones and subordinate alternating laminated to interbedded sandstone, siltstone and claystone were assigned to lowstand systems tracts (LST). The latter rest on an erosive or sharp higher-order sequence boundary that separates them from massive claystones, assigned to highstand systems tracts (HST). The gamma ray pattern of highstand deposits displays a roughly prograding trend, whereas that of lowstand deposits exhibits generally a blocky trend but can also exhibit serrated blocky trends when alternating with fines. Deposits of the transgressive systems tract (TST), sandwiched between LST and HST deposits, consist of ripple cross-laminated, parallel-laminated sandstones but also of alternating laminated to interbedded sandstone, siltstone and claystone intervals. Gamma ray patterns of these deposits display a retrograding trend.

Most depositional sequences present a complex organisation of depositional elements including channel-fill, overbanks and sheet sandstones. The large volume of individual stratigraphic units within the 9A and 10A Sequences, but also in the lower 14A sand succession, suggest a high amount of sediment input to the basin during the lowstand phases of deposition. High-energy erosive flows initiated the formation of the sequences and created conduits from slope to basin floor for subsequent flows. Conglomerates and massive sandstones constitute the initial deposits from these flows; the former facies being diagnostic within slope settings. The association of channel-fill sandstone and sheet-like overbank deposits occurs between the middle fan and outer fan settings. This complex organisation passes downdip into thick-bedded to amalgamated sheet sandstones in fan lobes.

Gamma ray logs display the drilled thickness of sequences at the well location and reflect the physical properties of the intersected rocks. Based on this, several maps such as isochore (thickness), net-sand and facies distribution maps were constructed. Both, isochore and net-sand maps reveal the general trend of sediment deposition and the main sand fairway, respectively. From the 9A to 13A Sequence, these two factors reveal a sinuous pattern. Facies distribution maps, however, suggest that channel-fill deposits are frequently associated with overflow deposits, except in 13A Sequence. They reveal also that distal lobes still occur associated with channel-fills. This led to conclude that deposition of the sequences took place in a base-of-slope to lower fan setting. Although not accurate, the maps reveal the influence of basin floor topography on deposition.

This has been evidenced by the change of sequence thickness and the course of flows within the sequences. The constant occupancy of thick parts of overlying sequences on thin parts of underlying sequences, and regular parallel shifting of axial parts of sequences suggest a parallel orientation of topographical highs, which were mainly controlled by erosion along topographical lows.

Distribution of reservoirs reveals that a high proportion of reservoirs occur in the 9A, 10A and 14A Sequences, along the axial parts of flow paths as amalgamated channel-fill complexes. Amalgamation implies good vertical and lateral connectivity in these areas. The high association of overbank reservoirs with channel-fill reservoirs, which suggests connectivity between both types of reservoirs, can perhaps lead to larger areas of connectivity in places, e.g. in the 9A, 10A and 14A reservoirs. Reservoir connectivity should be explored further, with the incorporation of reservoir engineering pressure measurement, reservoir flow and production data.



Application of high-resolution stratigraphy to deep-water deposits delineated fourth-order stratigraphic units, hosting lowstand deposits within each depositional sequence. However, this delineation was limited by the resolution of well logs, and the limited well control and uneven distribution of boreholes. It provided only pathways of channel belts and some clues about the characteristics of deep-water reservoirs, such as channel-fill and associated overflow reservoirs. Focusing on a single depositional sequence, with advanced geophysical, reservoir engineering flow and pressure data can produce more accurate models.

References

- Amy, L.A., Talling, P.J., Peakall, J., Wynn, R.B. and Arzola Thynne, R.G. (2005). Bed geometry used to test recognition criteria of turbidite and (sandy) debrites. *Sedimentary Geology*, **179**, 163-174.
- Beaubouef, R.T. (2004). Deep-water leveed-channel complexes of the Cerro Toro Formation, Upper Cretaceous, southern Chile. *American Association of Petroleum Geologists Bulletin*, **88 (11)**, 1471-1500.
- Beaubouef, R.T., Rossen, C., Zelt, F.B., Sullivan, M.D., Mohrig, D.C. and Jennette, D.C. (1999). Deep-water sandstones, Brushy Canyon Formation, West Texas. American Association of Petroleum Geologists. Hedberg Conference Field Guide. Tulsa. 48pp.
- Boggs, S. Jr. (2001). Principles of sedimentology and stratigraphy. Prentice Hall (eds.). 3rd edition. 726pp.
- Bouma, A.H. (1962). Sedimentology of some flysh deposits, a graphic approach to facies interpretation. Elsevier, Amsterdam. 168pp.
- Bouma, A.H., Normark, W.R. and Barnes, N.E. (1986). Submarine fans and related turbidite systems. Springer Verlag, New York. 351pp.
- Bowen, D.W. and Weimer, P. (2003). Regional sequence stratigraphic setting and reservoir geology of Morrow incised-valley sandstones (lower Pennsylvanian), eastern Colorado and western Kansas. *American Association of Petroleum Geologists Bulletin*, **87 (5)**, 781-815.
- Boyer, J., Duvail, C., Le Strat, P., Gensous, B. and Tesson, M. (2005). High resolution stratigraphy and evolution of the Rhône delta plain during

- Postglacial time, from subsurface drilling data bank. *Marine Geology*, 222-223, 267-298.
- British Antarctic Survey. Natural Environment Research Council. Retrieved on October 27, 2006, from <http://www.antarctica.ac.uk>.
- Brown, Jr.L.F. and Fisher, W.L. (1977). Seismic stratigraphic integration of depositional systems: examples from Brazilian rift and pull-apart basins. In: Payton, C.E. (eds.), *Seismic Stratigraphy – Application to Petroleum Geologists Memoir*, 213-248.
- Brown, Jr.L.F., Benson, J.M., Brink, G.J., Doherty, S., Jollands, A., Jungslager, E.H.A., Keenan, J.H.G., Muntingh, A. and Van Wyk, N.J.S. (1995). Sequence Stratigraphy in offshore South African Divergent Basins. An Atlas on exploration for cretaceous lowstand traps by Soekor (Pty.) Ltd: American Association of Petroleum Geologists, Studies in Geology series, **41**, 184pp.
- Burden, P.L.A. (1992). Soekor, partners explore possibilities in Bredasdorp Basin off South Africa: *Oil and Gas Journal*, 109-115.
- Burden, P.L.A. and Davies, C.P.N. (1997a). Oribi field is South Africa's offshore crude oil production: *Oil and Gas Journal*, **2**, 63-65.
- Burden, P.L.A. and Davies, C.P.N. (1997b). Exploration to first production on block 9 off South Africa: *Oil and Gas Journal*, **1**, 92-98.
- Catuneanu, O. (2002). Sequence Stratigraphy of clastic systems: concept, merits, and pitfalls, *Journal of Earth Sciences*, **35**, 1-43.
- Catuneanu, O., Martins-Neto, M.A. and Erikson, P.G. (2005). Precambrian sequence stratigraphy. *Sedimentary Geology*, **176**, Issues 1-2, 43-65.

- Coe, A.L., Bosence, D.W.J., Church, K.D., Flint, S.S., Howell, J.A. and Wilson, R.C.L. (2003). The sedimentary record of sea-level change. Cambridge University press (eds.). 288pp.
- Cole, D.I. (1992). Evolution and development of the Karoo Basin. *In: de Wit, M.J. and Ransome, I.G.D. (eds.), Inversion tectonics of the Cape Fold Belt, Karoo and Cretaceous Basin of Southern Africa*, Balkema, Rotterdam, 87-100.
- Cronin, B.T., Hurst, A., Celik, H. and Turkmen, I. (2000). Superb exposure of a channel, levee and overbank complex in an ancient deep-water slope environment. *Sedimentary Geology*, **132**, 205-216.
- Danielsen, M., Michelsen, O. and Clausen, O.R. (1997). Oligocene sequence stratigraphy and basin development in the Danish North Sea sector based on log interpretations. *Marine and Petroleum Geology*, **14 (7/8)**, 931-950.
- Dasgupta, P. (2003). Sediment gravity flow – the conceptual problem. *Earth Science Reviews*, **62**, 265-281.
- Davies, C.P.N. (1997). Hydrocarbon evolution of the Bredasdorp Basin, offshore South Africa: From source to reservoir. Unpublished Ph.D. thesis. University of Stellenbosch, South Africa. 286pp.
- De Beer, C.H. (1989). Structure of the Cape Fold Belt in the Ceres Syntaxis. Unpublished MSc. thesis. University of Stellenbosch, South Africa. 134pp.
- De Wit, M.J. and Ransome I.G.D. (1992). Regional inversion tectonics of the Cape Fold Belt, Karoo and Cretaceous Basins of Southern Africa. Balkema, Rotterdam, 15-21.

- Dingle, R.V., Siesser, W.G. and Newton, A.R. (1983). Mesozoic and Tertiary Geology of Southern Africa. A.A. Balkema, Rotterdam, 375pp.
- Du Toit, J. (1976). Mesozoic geology of the Agulhas Bank, South Africa. Unpublished Ph.D. thesis, University of Cape Town. South Africa. 160pp.
- Duerichen, E. (2000). Deep-marine turbidite and conglomerate deposits of the Cretaceous Panoche Group, San Luis Reservoir area, California: Stanford Project on Deep-water Depositional Systems (SPODDS). Annual Review, **8**. Retrieved November 09, 2005, from the World Wide Web: [<http://pangea.stanford.edu/research/SPODDS/Research/>].
- Eschard, R., Albouy, E., Deschamps, R., Euzen, T. and Ayub, A. (2003). Downstream evolution of turbidite channel complexes in the Pab Range outcrops (Maastrichtian, Pakistan). *Marine and Petroleum Geology*, **20**, 691-710.
- Flint, S., Aitken, J. and Hampson, G. (1995). Application of sequence stratigraphy to coal-bearing coastal plain succession: implication for the UK Coal Measures. Whateley, M.K.G and Spears, D.A. (eds.), European Coal Geology, *Geological Society Special Publication*, **82**, 1-16.
- Fouché, J., Bate, K.J. and Van der Merwe, R. (1992). Plate tectonic setting of the Mesozoic Basins, southern offshore, South Africa: A review. In: de Wit, M.J. and Ransome, I.G.D. (eds.), Inversion tectonics of the Cape Fold Belt, Karoo and Cretaceous Basins of southern Africa. 33-45. Balkema, Rotterdam.
- Galloway, W.E. (1989). Genetic stratigraphic sequences in basin analysis I: Architecture and genesis of flooding-surface bounded depositional units. *American Association of Petroleum Geologists Bulletin*, **73 (2)**, 125-142.

- Galloway, W.E. and Hobday, D.K. (1996). Terrigenous clastic depositional system (2nd edition): Heidelberg, Springer-Verlag, 489pp.
- Gardner, M.H., Borer, J.M., Melick, J.J., Mavilla, N., Dechesne, M. and Wild, R.J. (2003). Stratigraphic process-response model for submarine channels and related features from studies of Permian Brushy Canyon outcrop, West Texas. *Marine and Petroleum Geology*, **20**, 757-787.
- Ghosh, B. and Lowe, D.R. (1993). The architecture of deep-water channel complexes, Cretaceous Venado Sandstone Member, Sacramento Valley, California. In: Graham, S.A. and Lowe, D.R. (eds.), *Advances in the Sedimentary Geology of the Great Valley Group, Sacramento Valley, California*. SEPM, Pacific Section, Guidebook, **73**, 51-65.
- Gibbons, K., Hellem, T., Kjemperud, S.D.N. and Veberstad (1993). Sequence architecture, facies development and carbonate-cemented horizons in the Troll Field reservoir, offshore Norway, In Ashton, M. (eds.), *Advances in reservoir Geology, Geological Society Special Publication*, **69**, 1-31.
- Grecula, M. (2000). Stratigraphy and architecture of tectonically controlled turbidite systems: Laingsburg Formation, Karoo Basin, South Africa. Unpublished Ph.D. thesis. University of Liverpool, 291pp.
- Grecula, M., Flint, S.S. and Wickens, H. de V. (2003). Upward-thickening patterns and lateral continuity of Permian sand-rich turbidite channel-fills, Laingsburg Karoo, South Africa. *Sedimentology*, **50**, 831-853
- Habgood, E.L., Kenyon, N.H., Masson, D.G., Akhmetzhanov, A., Weaver, P.P.E., Gardner, J. and Mulder, T. (2003). Deep-water sediment wave fields, bottom current sand channels and gravity flow channel-lobe systems: Gulf of Cadiz, NE Atlantic. *Sedimentology*, **50**, 483-510.

- Hälbich, I.W. (1992). The Cape Fold Belt Orogeny: state of art 1970's – 1980's. In: De Wit, M.J. and Ransome, I.G.D. (eds.), Inversion tectonics of the Cape Fold Belt, Karoo and Cretaceous Basins of Southern Africa. Balkema, Rotterdam, 141-158.
- Hälbich, I.W., Fitch, F.J. and Miller, J.A. (1983). Dating the Cape Orogeny. In: Sohngé, A.P.G. and Hälbich, I.W. (eds.), Geodynamics of the Cape Fold Belt. *Special Publication of the Geological Society of South Africa*, **12**, 149-164.
- Hickson, T. and Lowe, D. (2002). Facies architecture of a submarine fan channel-levee complex: the Juniper Ridge Conglomerate, Coalinga, California, *Sedimentology*, **49**, 335-362.
- Howell, D.G. and Normark, W.R. (1982). Sedimentology of submarine fans. In: Scholle, P.A. and Spreading, D.R. (eds.), Sandstones depositional environments, 31, *American Association of Petroleum Geologists Memoirs*: Tulsa, OK, 365-404.
- Johnson, M.R. (1991). Sandstone petrography, provenance and plate tectonic settings. In: Gondwana context of the southern Cape-Karoo Basin. *South African Journal of Geology*, **94**, 137-154.
- Johnson, S.D., Flint, S., Hinds, D. and Wickens, H. de V. (2001). Anatomy, geometry and sequence stratigraphy of basin floor to slope turbidite systems, Tanqua Karoo, South Africa. *Sedimentology*, **48**, 987-1023.
- Johnston, S.T. (2000). The Cape Fold Belt and Syntaxis and the rotated Falkland Island: dextral transpressional tectonics along the southwest margin of Gondwana. *Journal of African Earth Sciences*, **31 (1)**, 51-63.

- Kendall, C. and Alnaji, N. Sequence Stratigraphy: An overview. Retrieved November 09, 2005, from the World Wide Web:
[<http://strata.geol.sc.edu/index.html>].
- Kneller, B.C. and Branney (1995). Sustained high-density turbidity currents and the deposition of thick massive sands. *Sedimentology*, **42**, 607-616.
- Liro, L.M. and Dawson, W.C. (2000). Reservoir systems of selected basins of the South Atlantic, *in*: Mello M.R. and Katz B.J. (eds.), Petroleum system of South Atlantic margins: *American Association of Petroleum Geologists Memoir*, **73**, 77–92.
- Lock, B.E. (1978). The Cape Fold Belt of South Africa: Tectonic control of sedimentation. *Proceedings of the Geological Association*, **89 (1)**, 263-281.
- Lock, B.E. (1980). Flate plate subduction and the Cape Fold Belt of South Africa. *Geology*, **8**, 35-39.
- Lowe, D.R. (1976). Subaqueous liquefied and fluidized sediment flows and their deposits. *Sedimentology*, **23**, 285-308.
- Lowe, D.R. (1979). Sediment gravity flows. Their classification and some problems of application to natural flows and deposits. In: Doyle, L.J. and Pilkey, O.H. (eds.), *Geology of continental slopes. Society of Economic Palaeontology and Mineral. Special Publication*, **27**, 75-82.
- Lowe, D.R. (1982). Sediment gravity flows II: Depositional models with special reference to the deposits of high density turbidity current. *Journal of Sedimentary Petroleum*, **52**, 279–297

- MacDonald, D.I.M. (1986). Proximal to distal sedimentology variation in a linear turbidite trough: implication for the fan model. *Sedimentology*, **33**, 243-259.
- Marshall, J.E.A. (1994). The Falkland Islands: A key element in Gondwana paleogeography. *Tectonics*, **13 (2)**, 499-514.
- Martini, J.E.J. (1974). On the presence of ash beds and volcanic fragments in graywackes of the Karoo System in the southern Cape Province. *Transactions of the Geological Society of South Africa*, **77**, 113-116.
- McLachlan, I.R. and McMillan, I.K. (1976). Review and stratigraphic significance of southern Cape Mesozoic Palaeontology. *Transactions of the Geologic Society of South Africa*, **79**, 197-212.
- McMillan, I.K., Brink, G.J., Broad, D.S. and Maier, J.J. (1997). Late-Mesozoic sedimentary basins off the south coast of South Africa. In: Selley, R.C. (eds.), *Sedimentary Basins of the World: The African Basins*. 319-376.
- Miall, A. D. (1996). *The Geology of stratigraphic sequences*: New York, Springer-Verlag. 433pp.
- Miall, A.D. (1985). Arcitectural-element analysis: a new method of facies analysis applied to fluvial deposits. *Earth-Science Reviews*, **22**, 216-308.
- Miall, A.D. (1990). *Principle of sedimentary basin analysis*. New York. 668pp.
- Middleton, G.V. (1967). Experiments on density and turbidity currents III. Deposition of sediments. *Canadian Journal of Earth Sciences*, **4 (3)**, 475-505.

- Middleton, G.V. and Hampton, M.A. (1976). Subaqueous sediment transport and deposition by sediment gravity flows, in: Stanley, D.J. and Swift, D.J.P. (eds.), *Marine Sediment transport and environmental management*. John Wiley, New York, 197-218.
- Mitchum, R.M.Jr., Sangree, J.B., Vail, P.R. and Wornardt, W.W. (1993). Recognizing sequence and systems tracts from well logs, seismic data, and biostratigraphy: examen from the late Cenozoic, *In: Posamentier, H.W. and Weimer, P. (eds.), Siliciclastic sequence stratigraphy: recent developments and applications: American Association of Petroleum Geologists Memoir, 58*, 163-198.
- Mitchum, R.M.Jr., Vail, P.R., Todd, R.G., Widmier, J.M., Thompson, S., Sangree, J.B., Bubb, J.N. and Hatlelid, W.G. (1977). Seismic stratigraphy and changes of sea-level, Part 1: Glossary of terms used in seismic stratigraphy. *In: Payton, C.E. (eds.), Seismic stratigraphy and application to hydrocarbon exploration. American Association of Petroleum Geologists Memoir, 26*, 205-212.
- Mutti, E. (1985). Turbidite systems and their relations to depositional sequences. *In: Zuffa, G.G. (eds.), Provenance of Arenites. NATO ASI Ser. C, 148*, Reidel Publishing. Dordrecht. 65-93.
- Mutti, E. (1992). Turbidite sandstones. Agip and Instituto di Geologia Università di Parma, Italy. 275pp.
- Mutti, E. and Normark, W.R. (1987). Comparing example from ancient and modern turbidite systems: problems and concepts. *In: Leggett, J.L. and Zuffa, G.G. (eds.), Marine Clastic Sedimentology. Concepts and case studies*, Graham and Trotman, London, 1-38.

- Mutti, E. and Normark, W.R. (1991). An integrated approach to the study of turbidite system. In: Weimer, P. and Link, M.H. (eds.), *Seismic facies sedimentary processes of submarine fans and turbidite system*: New York, Springer- Verlag, 75-106.
- Mutti, E. and Ricci Lucchi, F. (1972). Turbidites of the Northern Apennines: Introduction to Facies Analysis. *International Geology Review*, **20**, 125-166.
- Mutti, E. and Ricci Lucchi, F. (1975). Turbidite facies and facies associations. *In* Example of turbidite facies and associations fro selected formations in the northern Apennines. In: Mutti, E. (eds.), IX International Congress of Sedimentology, Nice-75, Field Trip A11. 21-36.
- National Geophysic Data Center (2006). National Geophysic Data Center, NOAA Satellite and Information Service. Retrieved August 2, 2006, from the World Wide Web: [[http:// www.ngdc.noaa.gov/mgg/image](http://www.ngdc.noaa.gov/mgg/image)].
- Normark, W.R. (1970). Growth pattern of deep sea fans. *American Association of Petroleum Geologists*, **54**, 2170-2195.
- Normark, W.R. (1978). Fan valleys, channels and depositional lobes on modern submarine fans: character for the recognition of sandy turbidite environments. *American Association of Petroleum Geologists*, **62**, 912-931.
- Paola, C., Wiele, S.M. and Reinhart, M.A. (1989). Upper regime parallel lamination as the result of turbulent sediment transport and low-amplitude bed forms. *Sedimentology*, **36**, 47-59.
- Pettijohn, F.J. (1975). *Sedimentary rocks*. (3rd edition). Harper and Row, New York (eds.). 628pp.

- Pickering, K., Stow, D., Watson, M. and Hiscott, R. (1986). Deep-facies, processes and models: a review and classification scheme for modern and ancient sediments. *Earth-Sciences Review*, **23**, 75-174.
- Posamentier, H.W. and Allen, G.P. (1999). Siliciclastic sequence stratigraphy-concept and applications: SEPM Concepts in Sedimentology and Palaeontology, **7**, 210pp.
- Posamentier, H.W., Erskine, R.D. and Mitchum, R.M. (1991). Models for submarine fan deposition within a sequence stratigraphic framework. *In*: Weimer, P. and Link, M. (eds.), *Seismic facies and sedimentary processes of modern and ancient submarine fans and turbidite systems*. Springer-Verlag, New York. 127-136.
- Posamentier, H.W., Jersey, M.T. and Vail, P.R. (1988). Eustatic controls on clastic deposition I. Conceptual framework. *In*: Wilgus, C.K., Hastings, B.S., Kendall, C.G.S.C., Posamentier, H.W., Ross, C.A. and Van Wagoner, J.C. (eds.), *Sea-level changes – An integrated approach*, SEPM Special Publication, **42**, 110-124.
- Reading, H.G. and Richards, M.T., (1994). Turbidite systems in deep-water basin margins classified by grain size and feeder system: *American Association of Petroleum Geologists Bulletin*, **78**, 792-822.
- Rhodes, R. C. (1974). Discussion on an author's reply to "tectonostratigraphy as applied to analysis of south African Phanerozoic Basins" by Winter, H. de la R. *Transactions of the Geological Society of South Africa*, **89**, 427 - 429.
- Richards, M.T., Reading, H.G. and Bowman, M. (1998). Submarine fans and related depositional systems II: Variability in reservoir architecture and wireline log character. *Marine and Petroleum Geology*, **15 (8)**, 821-839.

- Rider, M.H. (1986). The Geological interpretation of well logs. London, New York, 171pp.
- Saito, T. and Ito, M. (2002). Deposition of sheet-like turbidite packets and migration of channel-overbank systems on a sandy submarine fan: an example from the late Miocene-Early Pliocene fore arc basin, Boso Peninsula, Japan. *Sedimentary Geology*, **149**, 265-277.
- Seilacher, A. (2001). Concretion morphologies reflecting diagenetic and epigenetic pathways. *Sedimentary Geology*, **143**, 41-57.
- Serra, O. and Sulpice, L. (1975). Sedimentology analysis of shale-sand series from well logs. SPWLA sixteenth annual logging symposium, 1-23.
- Shanmugam, G. (1997). The Bouma Sequence and the turbidite mind set, *Earth-Science Reviews*, **42**, 201-229.
- Shanmugam, G. (2000). 50 year of the turbidite paradigm (1850s-1990s): deep-water processes and facies models – a critical perspective. *Marine and Petroleum Geology*, **17**, 285-342.
- Shanmugam, G. and Moiola, R.J. (1985). Reinterpretation of depositional process in a classic flysch sequence (Pennsylvanian Jackforth Group) Ouachita Mountain and Oklahoma. *American Association of Petroleum Geologists Bulletin*, **79**, 672-695.
- Shanmugam, G. and Moiola, R.J. (1988). Submarine fans: characteristics, models, classification, reservoir potential. *Earth Science Reviews*, **24**, 383-428.
- Shanmugam, G., Lehtonen, L.R., Straume, T., Sylvertsen, S.E., Hodgkinson, R.J. and Skibeli, M. (1994). Slump and debris-flow dominated Upper slope

- facies in the Cretaceous of the Norwegian and northern North Seas (61-670N): Implication of for sand distribution. *American Association of Petroleum Geologists Bulletin*, **78 (6)**, 910-937.
- Sixsmith, P.J. (2000). Stratigraphic development of a Permian turbidite system on a deforming basin floor: Laingsburg Formation, Karoo Basin, South Africa, Unpublished Ph.D. thesis. University of Liverpool. 229 pp.
- Smellie, J. L. (1981). A complete arc-trench system recognized in the Gondwana sequences of the Antarctic Peninsula region. *Geological Magazine*, **11**, 139-159.
- Stelting, C.E., Bouma, A.H., and Stone, C.G. (2000). Fine-grained turbidite systems: overview, *In: Bouma, A.H. and Stone, C.G. (eds.), Fine-grained turbidite systems. American Association of Petroleum Geologists Memoir. 72/SEPM Special Publication*, **68**, 1-8.
- Stow, D.A.V. and Johansson, M. (2000). Deep-water massive sands: nature, origin and hydrocarbon implication. *Marine and Petroleum Geology*, **17**, (2), 125-135.
- Stow, D.A.V. and Shanmugam, G. (1980). Sequence of structures in fine-grained turbidites: comparison of recent deep-sea and ancient flysch sediments. *Sedimentary Geology*, **25**, 23-42.
- Stow, D.A.V., and Tabrez, A.R. (1998). Hemipelagites: processes, facies and models. *In: Stoker, M.S. and Evans, D. and Cramp, A. (eds.). Geological processes on continental margins, Geological Society of London, Special Publication*, **129**, 317-337.
- Stow, D.A.V., Huc, A.Y. and Bertrand, P. (2001). Depositional processes of black shales in deep water. *Marine and Petroleum Geology*, **18**, 491-498.

- Tearpock, D.J. and Bischke, R.E. (2003). Applied subsurface geological mapping with structural methods. Walker, L.G. (eds.). New Jersey. 864pp.
- Thomson, K, (1998). When did the Falklands rotate? *Marine and Petroleum Geology*, **15**, 723-736.
- Turner, J. (2006). 9A to 13A Isochron. Unpublished map from the Petroleum Oil and Gas Corporation of South Africa (Pty) Ltd.
- Turner, P., Pilling, D., Walker, D., Exton, J., Binnie, J. and Sabaou, N. (2001). Sequence Stratigraphy and Sedimentology of the late Triassic TAG-I (Blocks 401/402, Bekine Basin, Algeria). *Marine and Petroleum Geology*, **18**, 959-981.
- Tye, R.S., Bhattacharya, J.P., Lorsong, J.A., Sindelar, S.T., Knock, D.G., Puls, D.D. and Levinson, R.A. (1999). Geology and stratigraphy of fluvio-deltaic deposits in the Ivishak Formation: Applications for development of Prudhoe Bay Field, Alaska. *American Association of Petroleum Geologists Bulletin*, **83 (10)**, 1588-1623.
- Vail, P.R. (1987). Seismic stratigraphy interpretation procedure. *In*: Bally, A.W. (eds.), Atlas of seismic stratigraphy. American Association of Petroleum Geologists Studies in Geology, **27**, 1-10
- Vail, P.R., Audremard, F., Bowman, S., Eisner, P. and Perez-Cruz, G. (1991). The stratigraphic signatures of tectonics, eustasy and sedimentation: an overview. *In*: Einsele, G., Ricken, W. and Seilacher, A. (eds.), Cycles and events in stratigraphy: Berlin. Springer-Verlag. 617-659.
- Vail, P.R., Mitchum, R.M., Campion, K.M. and Rahmanian, V.D. (1977). Seismic stratigraphy and global changes in sea-level: Part 3. Relative changes of sea-level from coastal onlap. *In*: Payton, C.E. (eds.), Seismic stratigraphy

- Applications to hydrocarbon exploration, *American Association of Petroleum Geologists Memoir*, **26**, 63-81.
- Van der Merwe, W.C. (2005). Stratigraphy and facies architecture of the uppermost fan system in the Tanqua sub-basin, Permian Ecca Group, South Africa. Unpublished MSc. thesis. University of Stellenbosch. South Africa. 197pp.
- Van der Spuy, D. (2003). Aptian source rocks in some South African cretaceous basins. *In*: Arthur, T.J., MacGregor, D.S. and Cameron, N.R. (eds.), *Petroleum Geology of South Africa: New themes and developing technologies. Geological Society of London. Special publication*, **207**, 185-202.
- Van Wagoner, J.C. (1995). Overview of sequence stratigraphy of foreland basin deposits: terminology, summary of papers, and glossary of sequence stratigraphy. *In*: Van Wagoner, J.C., Bertram, G.T. (eds.), *Sequence Stratigraphy of foreland basin deposits. American Association of Petroleum Geologists Memoir*, **64**, 9-21.
- Van Wagoner, J.C., Mitchum, R.M., Campion, K.M. and Rahmanian, V.D. (1990). Siliciclastic sequence stratigraphic in well logs, cores and outcrops: Concept for high-resolution, correlation of time and facies. *American Association of Petroleum Geologists Methods in exploration Series*, **7**. Oklahoma, 55pp.
- Van Wagoner, J.C., Posamentier, H.W., Mitchum, R.M., Vail, P.R, Sarg, J.F., Louitit, T.S. and Hardenbol, J. (1988). An overview of the fundamentals of sequence stratigraphy and key definitions. *In* Sea-level changes: an integrated approach (eds.), *SEPM Special Publication*, **42**, 40-45.

Visser, J.N.J. (1995). Post-glacial Permian stratigraphy and geography of southern and central Africa: boundary conditions for climatic modelling. *Palaeogeography, Palaeoclimatology, Palaeoecology*, **118**, 213 - 243.

Walker, R.G. (1978). Deep-water sandstone facies and ancient submarine fans: models for exploration and stratigraphic traps: *American Association of Petroleum Geologists Bulletin*, **62**, 932-966.

Wickens, H. de V. and Mclachlan, I.R. (1990). The stratigraphy and sedimentology of the reservoir interval of the Kudu 9A-2 and 9A-3 boreholes. *Communications of the geological survey of Namibia: The Kudu offshore drilling project*, **6**, 9-22.

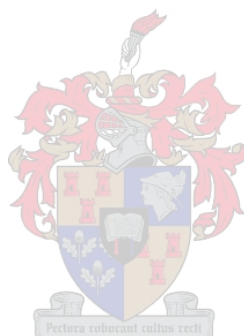
Wikipedia. The Free Encyclopedia. Retrieved October 27, 2006, from the World Wide Web: [<http://www.en.wikipedia.org/wiki/Gondwana>].

Ziegler P.A. and Cloetingh, S. (2004). Dynamic processes controlling the evolution of rifted basins. *Earth Science reviews*, **64**, 1-50.

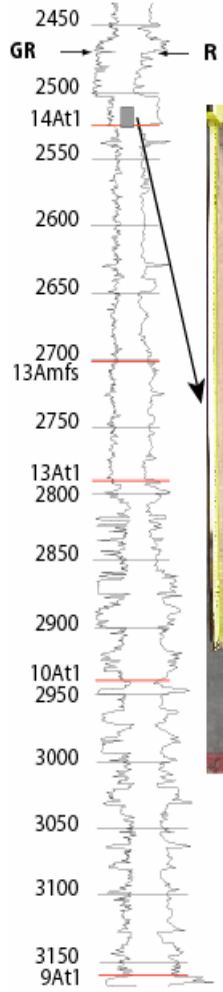


Appendix

Whole core photographs and their stratigraphic positions in the wells.



E-AA1



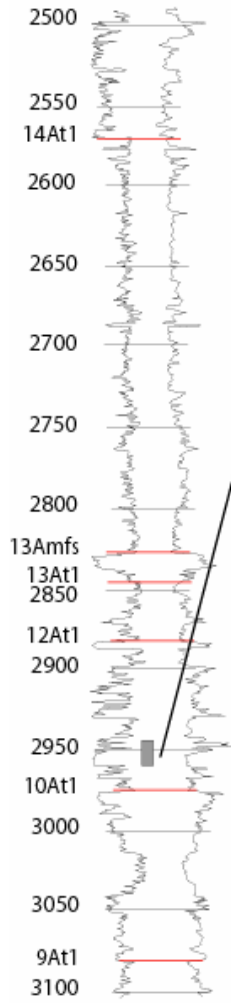
Core photograph of core 1 (2509-2524 m). The 14At1 unconformity is shown near the base of the core.



Core photograph of core 4 (3013-3031 m)



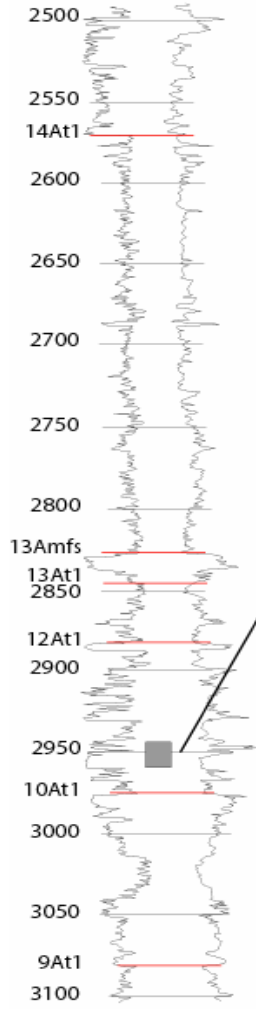
E-AD1



Core photograph of core 6 (2945-2959 m)



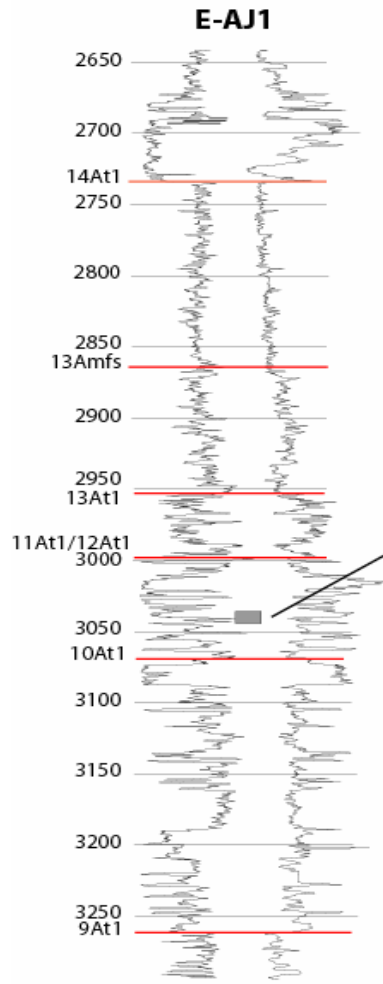
E-AD1



Core photograph of core 6 (2945-2959 m)



Core photograph of core 4 (3037-3043 m)

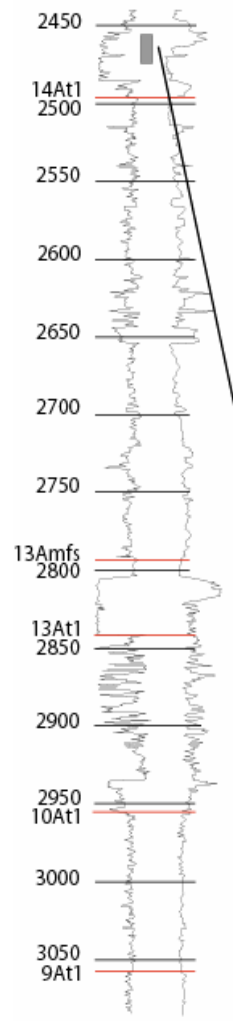


E-A01

Core photograph of core 2 (3000-3028.5 m)



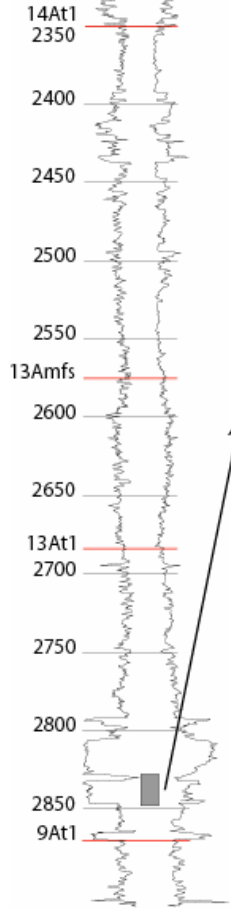
E-AR1



Core photograph of core 1 (2455-2473.5 m)



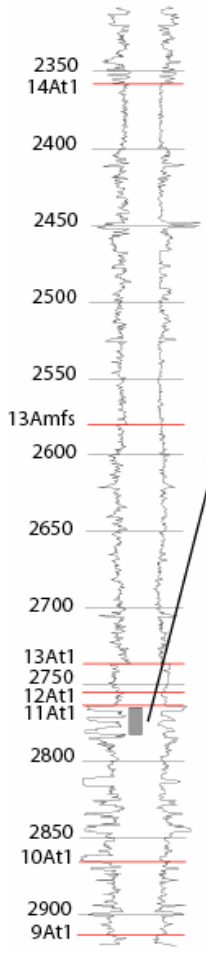
E-BA1



Core photograph of core 2 (2828-2848 m)



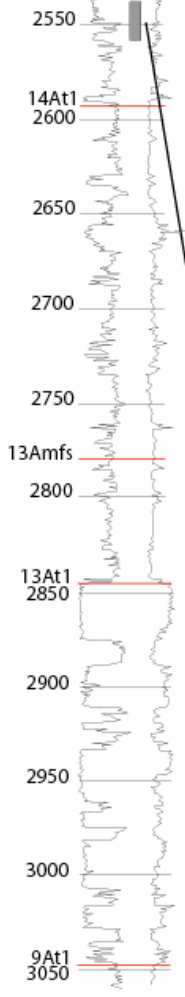
E-BA2



Core photograph of core 1 (2755-2783 m)



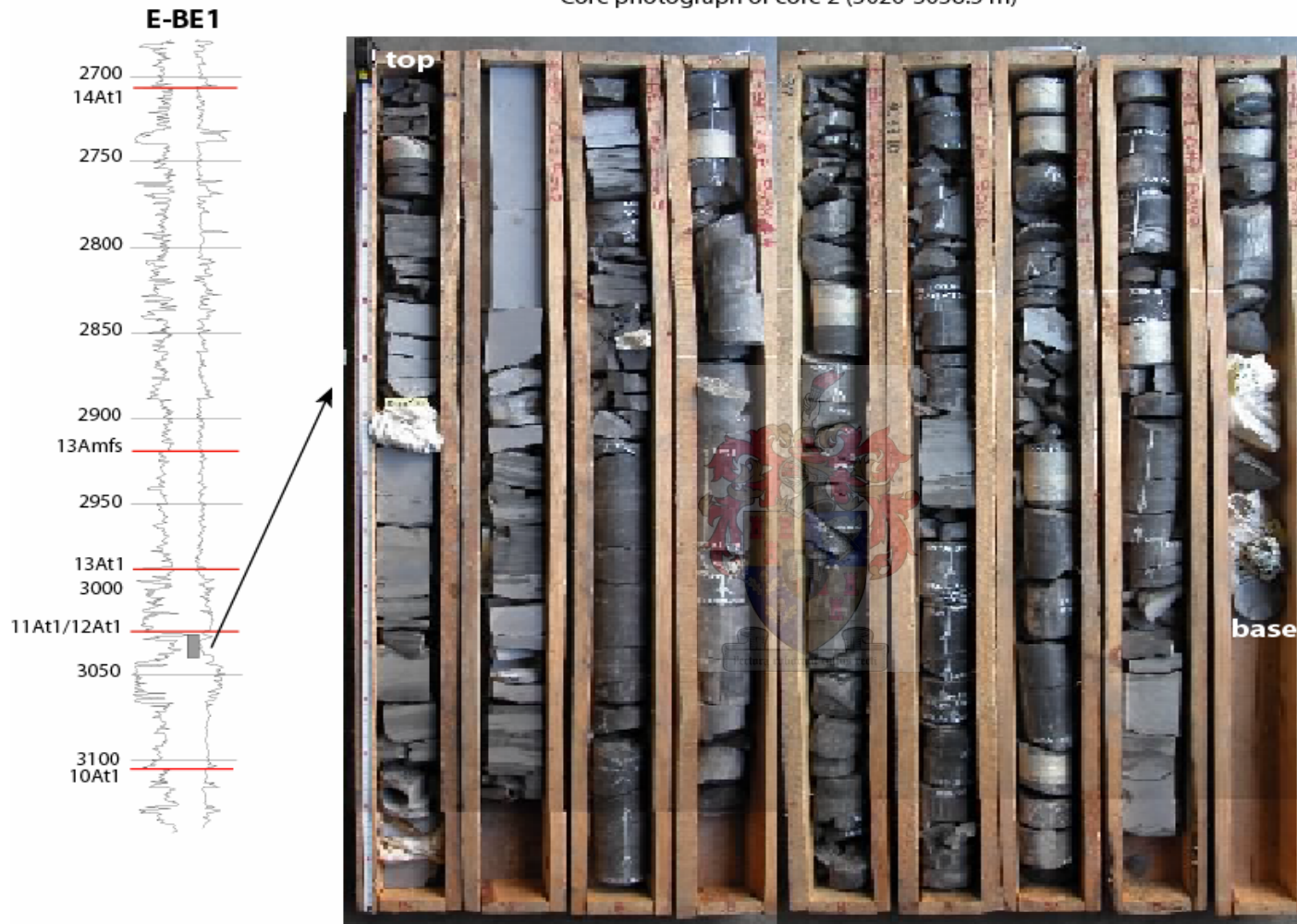
E-BB1



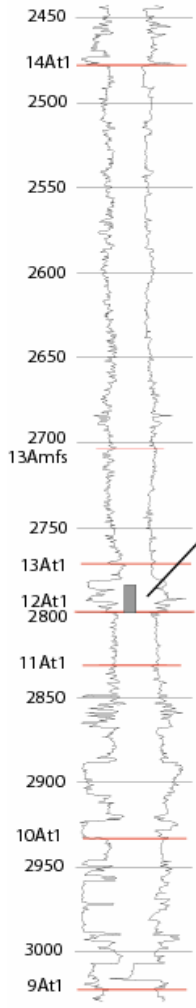
Core photograph of core 2 (2537.5-2556.42 m)



Core photograph of core 2 (3026-3038.5 m)



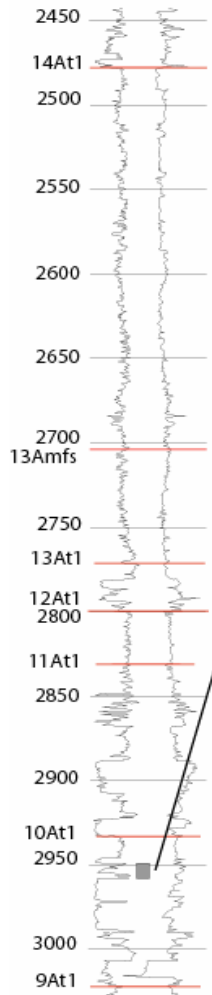
E-CA1



Core photograph of core 1 (2784-2802 m)



E-CA1



Core photograph of core 5 (2949-2961 m)

